Self-Consolidating Concrete (SCC) for Infrastructure Elements
Report A – Shear

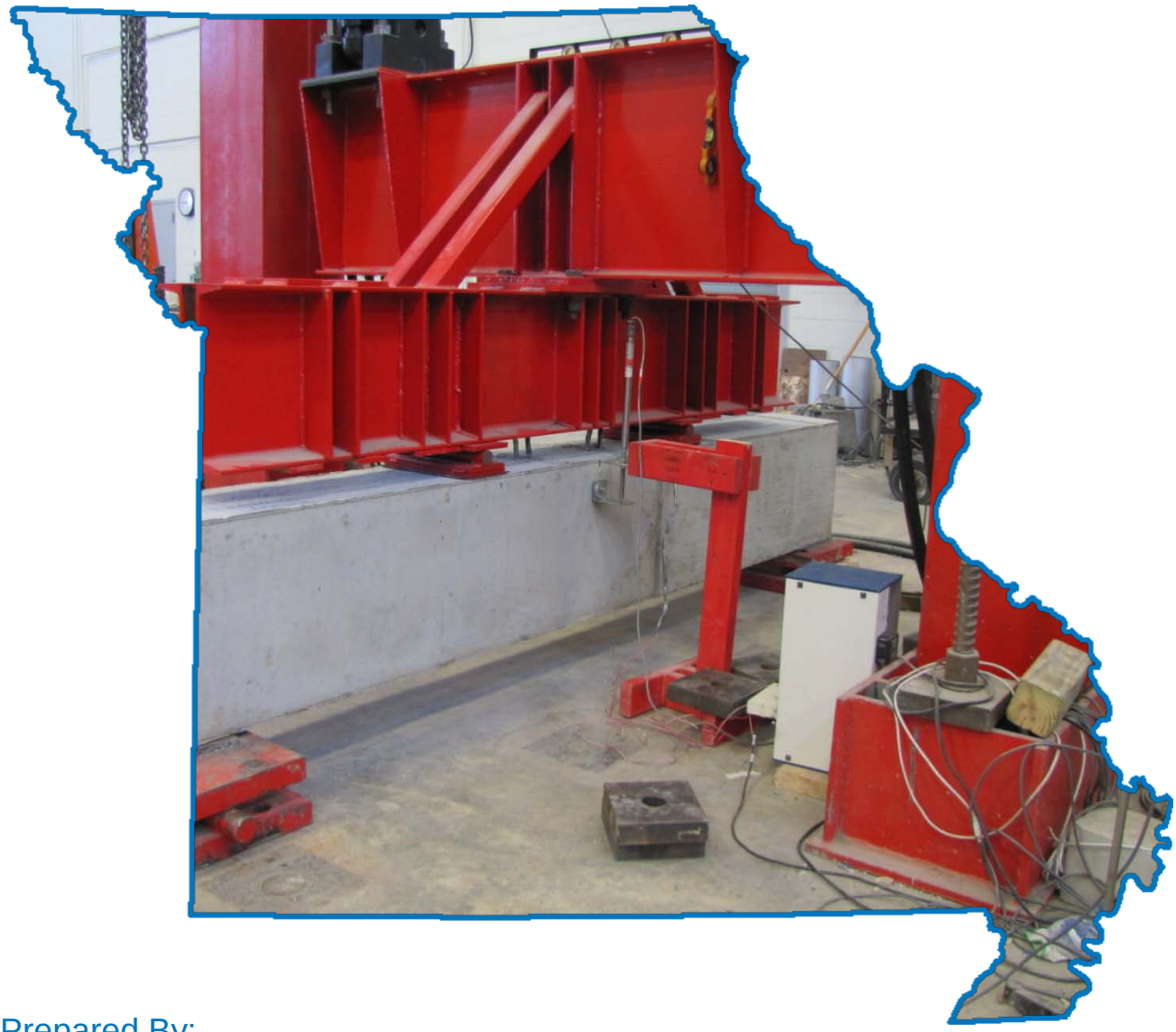

Prepared By:

Missouri University of Science and Technology

Final Report Prepared for Missouri Department of Transportation
2012 August Project TRyy1103 Report cmr 13-003

FINAL Report A

TRyy1103

Project Title: Self-Consolidating Concrete (SCC) for Infrastructure Elements

Report A: Self-Consolidating Concrete (SCC) for Infrastructure Elements: Shear Characteristics

Prepared for
Missouri Department of Transportation
Construction and Materials

Missouri University of Science and Technology, Rolla, Missouri

July 2012

ABSTRACT

Because of its unique ability to maintain high flow-ability and remain homogeneous, self-consolidating concrete (SCC) has the potential to significantly reduce the costs associated with civil infrastructure; however, the use of higher paste and lower coarse aggregate volumes than non-SCC concretes raises concerns about the structural implications of using SCC. Of particular concern is the effect of concrete compressive strength, and aggregate type, shape, and content level on shear strength of SCC mixes. This research focused on the components that contribute to the concrete's ability to provide shear resistance, in particular, shear provided by aggregate interlock. Variables investigated by push-off tests to determine the shear contribution from aggregate interlock included concrete compressive strength (6 and 10 ksi [41.3 and 68.9 MPa] target), coarse aggregate type (limestone and river gravel), and volumetric content level of the coarse aggregate portion (36%, 48%, 58%, and 60%). Post-failure digital imaging software was used to confirm fresh concrete parameters in the hardened state as well as check for variability and the impact on shear. Additional attention was given to the global contributions of shear by the concrete in larger scaled tests of pre-stressed beam members. The results were used to assess the appropriateness of designing Missouri Infrastructure elements using the current *AASHTO LRFD Bridge Design Specification* for shear and while using typical Missouri SCC batch proportions and materials.

The research suggests that SCC has advanced to the level that robust mix designs can, and have been, utilized for Civil infrastructure. Aggregate interlock results agree with previous researchers that increased concrete compressive strength and the use of river gravel rather than limestone aggregate improves shear resistance. A distinguishable trend was not identifiable for shear resistance with C.A. fraction. Digital imaging confirmed non-segregating mixtures and that the actual C.A. bisecting a shear plane closely matched calculated values. The precrack and push-off testing itself was analyzed and suggestions for future researchers were proposed. Precast prestressed concrete beam tests indicate distinct behavior of SCC relative to control conventional concrete (CC) of similar strengths. The SCC shear beams exhibited increased deflections, higher ultimate loads, and even different failure modes. Given the distinguishable member behavior, additional research is advisable. Future

research should focus on full-scale members with practical geometries and reinforcing configurations.

TABLE OF CONTENTS

Page

LIST OF FIGURES

Page

LIST OF TABLES

Page

NOTATIONS

a	Maximum aggregate size
d_v	Effective shear depth (per AASHTO)
f'_c	Unconfined compressive strength of concrete
f_{ci}	Normal stress on the shear plane on the cracked concrete imposed by crack dilation
f_{ct}	Tensile strength of concrete, as measures by a splitting tensile strength (STS) test fixed
f_r	Modulus of rupture, MOR
s_x	Crack spacing parameter, from member and reinforcement geometry
s_{xe}	Effective crack spacing parameter
v_{ci}	Limiting value of maximum shear stress on the shear plane on the cracked concrete
$\overline{A}_x$	The unit area of contact between the aggregate and paste in the x-direction (in the direction of crack slip)
$\overline{A}_y$	The unit area of contact between the aggregate and paste in the y-direction (in the direction of crack opening).
E_c	Young's Modulus (modulus of elasticity) of concrete, MOE
P	Precrack load
P_k	Ratio of aggregate volume to total concrete volume
R^2	Coefficient of determination
V_a	Shear contribution due to aggregate interlock

V_c	Shear strength of concrete
V_{cy}	Shear contribution due to concrete in the uncracked compression zone
V_d	Shear contribution due to dowel action of longitudinal reinforcement
V_s	Shear contribution due to lateral shear reinforcement
β	Factor of tensile stress in the concrete
δ	Crack slip length
δ'	Crack slip limit
ε_1	The principle tensile strain in the concrete
ε_x	Longitudinal tensile strain in the web
θ	Angle of principle compressive stress in the web
μ	Friction coefficient
σ	Normal stres
τ	Shear stress
w	Crack opening width
AASHTO	American Association of State Highway and Transportation Officials
ACI	American Concrete Institute
AEA	Air entraining admixture
SCC	Self-consolidating concrete
CC	Conventional concrete
C.A.	Coarse aggregate
CFT	Compression field theory (of shear)
DAS	Data Acquisition System
F.A.	Fine aggregate

FEM	Finite element model
HRWRA	High range water reducing admixture
HSC	High strength concrete
LVDT	Linear voltage displacement transducer
MCFT	Modified compression field theory (of shear)
NCHRP	National Cooperative Highway Research Program
SCOH	Standing Committee on Highways, an AASHTO committee
SOM	Subcommittee on Materials, an AASHTO subcommittee
VMA	Viscosity modifying admixture
W/CM	Water to cementitious material ratio

1. INTRODUCTION

1.1 GENERAL

Self-consolidating concrete (SCC) is highly flowable, non-segregating concrete that can be placed with no mechanical consolidation. SCC has the potential for numerous advantages over conventional concrete (CC) which include, but are not limited to:

-Reduced labor, equipment, and associated cost

-Is cast with desired mechanical properties, independent of placement crew skill

-Accelerated construction

-Enables filling of complex formwork or members with congested reinforcement

-Decrease employee injuries

-Permits more flexible reinforcement detailing and design

-Creates smooth, aesthetically appealing surfaces

All of the benefits can be accomplished through the use of conventional concrete materials and admixtures. There are, in fact, three recognized mixture-proportioning approaches for making SCC; using high powder content and High Range Water Reducing Admixtures (HRWRA), low powder contents with HRWRA and viscosity modifying admixtures (VMA), and lastly by using moderate amounts of powder content, HRWRA, VMA and controlling stability through other mechanisms such as blending aggregates and lowering water content (ACI 237 2007). This investigation achieved SCC flowability and stability through the first method, by using HRWRA paired with increased ratios of fine aggregate (F.A.) to coarse aggregate (C.A.) and

large cement contents. The first method of achieving SCC was seen to be common practice by Missouri precast concrete providers at the time of this study, and was therefore the method pursued. Details of the batch proportions used will be discussed later, in section 3 of this report.

1.2 OBJECTIVE AND SCOPE

The primary objective of this research was to examine the variables that contribute to aggregate interlock, and their affect on the overall shear behavior of both CC and SCC in a precast, prestressed beam application using locally available materials to reflect current Missouri Precaster practices. The first step was to develop mixtures that were representative of the concrete batch proportions currently being used by Missouri Precasters. Next, plastic properties of the concrete were recorded for an evaluation of behavior and robustness using standard and non-standard test methods. Mechanical properties of compressive strength (f'_c), Young's Modulus also known as modulus of elasticity (E_c), and splitting tensile strength (f_{sp}) were collected for comparison between CC and SCC. To investigate shear, a non-standard, but widely recognized test known as a push-off test was utilized to investigate variables affecting the aggregate interlock component of shear; these results were then compared to test results collected from the testing of precast, prestressed beams.

In the state of Missouri, SCC is not currently permitted by the Missouri Department of Transportation (MoDOT) for use in structural applications without MoDOT oversight, trial batching, and independent laboratory testing, but is used for non-structural precast application because of the many advantages of the material with

respect to CC (MoDOT 2012). This research began with contacting, and collecting survey information from, precast concrete companies in and around the state of Missouri. The intent of the survey was to determine how widespread the use of SCC is in Missouri, establish the sophistication and robustness of the batch proportions used, and to develop a baseline SCC mix design for this research. MoDOT was consulted to establish the CC or control batch proportions. This collected information was then paired with the Principal Investigator's previous work with high strength concrete (HSC) to develop two additional baseline batch proportions for SCC and CC HSC.

The plastic state concrete properties were not the focus of this research; however, standard and non-standard tests were performed in order to develop an understanding of the rheology of the SCC mixes. One important aspect to note would be the achievement of SCC by using HRWRA with an increased F.A. to C.A. ratio for stability as opposed to using a conventional batch proportion with a large HRWRA dosage and VMA for stability. The increase in F.A. volume at the expense of C.A. volume is the explanation some have proposed for why SCC may have reduced aggregate interlock potential as compared to CC.

Mechanical properties of concrete compressive strength, Young's Modulus, and splitting tensile strength were also collected. These mechanical properties are essential to the design and analysis of civil structures. Young's Modulus is used to predict load response of structures, splitting tensile stress can be used to determine cracking behavior and capacity, and strength is used to develop member capacity by several mechanisms as well as being correlated to the other mechanical properties tested. Test results were used to evaluate CC and SCC compared to each other as well as standard prediction equations.

Finally, the main focus of this research is shear capacity and behavior of SCC. Specifically the aggregate interlock component of concrete shear was investigated in detail. The push-off test is a non-standard test, but has been used by researchers since the late 1960's as far as this author could determine, and is widely recognized by concrete shear researchers. A significant benefit of the push-off test is the ability to test many variables at a low cost, given the size of the specimen. Previous research, results, and models will be discussed in section 2 as part of the literature review. The goal with this study was to determine whether current models can be used to predict aggregate interlock while using Missouri aggregates within currently used Missouri precast SCC mixtures. The models were then also compared to the precast prestressed beam test results to determine if predicted behavior was exhibited.

1.3 ORGANIZATION OF REPORT

This report contains eight sections, four appendices, and a list of references. Information regarding each section and appendix is explained below.

Section 1 provides an introduction to this report. A brief background is given as to what self-consolidating concrete is, the potential benefits from using it, and the reason for the reluctance of widespread use. This section also describes the scope of work for this project, and outlines the information contained herein.

The second section conveys detailed information provided by other researchers that is important to this investigation. The literature review was conducted to gather information regarding fresh and hardened concrete properties, as well as shear in hardened concrete. Specific aspects of concrete shear were examined which include

aggregate interlock as a component of shear, the push-off test as an investigation of aggregate interlock, shear models based on aggregate interlock and overall shear behavior, and lastly shear in beams.

Section 3 provides the means by which concrete batch proportions were determined. This section describes the use of a survey that was distributed to Missouri precast concrete plants, Missouri ready mix suppliers, and to American Association of State Highway and Transportation Officials (AASHTO) members across the nation. Section 3 discusses the results of the survey, and how that information was used. MoDOT was also consulted in order to determine the control batch proportions.

The material and fresh concrete properties are presented in section 4. The specific tests and their associated standard for each of the material properties and fresh properties are described, along with the number of each test conducted. The results of the material and fresh concrete properties tests are shown, and briefly discussed.

Section 5 surveys the hardened properties investigated. The test setup and procedures are described. The hardened properties test results are shown and discussed.

The push-off test is presented in section 6. The pre-crack and push-off tests are described in detail. The test setup, procedure, specimen design and fabrication, and all of the difficulties encountered are detailed. Results from the investigation are represented along with a detailed analysis. A forensic investigation of the failed cross-sections of the push-off specimens was also undertaken and is presented in section 6.

Section 7 presents the shear beam test. As in section 6, the test setup, procedure, design, and fabrication are shown, along with difficulties overcome. The member

behavior is evaluated and compared for CC and SCC beams. The analysis and comparison with accepted shear models is also shown.

In section 8, the whole of this report is summarized. Conclusions about this investigation are made when possible, and recommendations are made accordingly.

2. LITERATURE REVIEW

2.1 GENERAL

The widespread use of SCC has developed from the initial conception in Japan where the material was developed in 1989 to ensure proper consolidation with a small skilled labor workforce in applications where concrete durability and service life were of concern (ACI 237 2007; FHWA 2005). The level of sophistication in relation to SCC has risen substantially in the last twenty years; advanced material proportioning has led to studies investigating the effects of fine-to-coarse aggregate ratio, coarse and fine aggregate characteristics, water-to-cementitious material, binder, and paste ratios, HRWRA, VMA, air entraining admixtures (AEA), mineral admixtures, inert filler fines to replace cement, and more on fresh rheological and hardened mechanical behavior (Khayat and Assaad 2002; Ghezel and Khayat 2002; NCHRP 2009). It can be beneficial to take advantage of the ever-improving material.

Advancements in understanding and chemical admixtures have led to the distinct material behavior that now defines SCC, "…highly flowable, nonsegregating concrete that can spread into place, fill the formwork, and encapsulate the reinforcement without any mechanical consolidation." (ACI 237 2007). The performance of SCC has led to advantages over conventional concrete in many ways including: reduced cost, higher rate of placement, enables filling of highly reinforced sections, provides placement logistics flexibility, reduced noise for urban areas and worker health, decreased laborer injury, and more. SCC in the hardened state can also demonstrate benefits that include the superior surface quality, reduced surface permeability, and more homogeneous mechanical

properties that are developed independent of laborer skill (ACI 237 2007). With all of the advantages of SCC, more and more interested parties are getting involved and encouraging more widespread use.

The material cost of SCC is usually greater than CC because of the large demand of cementitious material and admixtures; however, overall project costs may be reduced because of labor, equipment, and time savings (Ghezal and Khayat 2002; FHWA 2005). It is the multitude of potential advantages that is driving the spreading use of SCC. In the decades since invention, Japan has increasingly used SCC, even on such large-scale projects as the Akashi-Kaikyo bridge (the longest central span suspension bridge in the world) where SCC was used for the anchorages (Nowak et al. 2007). European entities have formed to increase usage of SCC for infrastructure. In 1994, the European Project Group was formed from five organizations dedicated to the promotion of advanced materials and systems for the supply and use of concrete. Since the group was founded, they have developed several state of the art documents (the latest in 2005) addressed to specifiers, designers, purchasers, producers, and users of SCC; they draw their information from the ever burgeoning supply of case studies and research projects from 12 European countries and the UK concrete society. There is, to date, no European Standard (EN) for SCC (EFNARC 2005). The United States is taking similar action to Europe. Interested transportation departments, research universities, societies, and specifying organizations are taking active roles in increasing the U.S. knowledge and use of SCC. Many case studies have been conducted across the country from New York to Virginia, Nebraska, and beyond (FHWA 2005). A project interested in advising the nation in regard to SCC was undertaken and a report was presented that recommended

guidelines for the use of SCC in precast, prestressed concrete bridge elements (NCHRP 2009). The National Cooperative Highway Research Program (NCHRP) report is full of useful information, but has not led to any national specification adoption.

Given the vast number of projects and case studies, there are still no widely accepted specifications for the use of SCC, only guidelines. The complexity of the numerous material interactions that take place in high performance concretes such as SCC make systematic, well designed research essential. Some seemingly contradictory research findings make specifiers and designers reluctant to use this advanced material (FHWA 2005; Kim 2008; Lachemi 2005; Naito et al. 2006; NCHRP 2009). An aspect of concrete that is already not well understood, shear failure, is given even greater scrutiny because of reduced C.A. in SCC.

2.2 FRESH CHARACTERISTICS

The definition of SCC encompasses a great deal of information about the material in the fresh state that may not be readily obvious. The words used to describe SCC; flowable, nonsegregating, and fill are referring to tests with definable quantitative measurements and suggested ranges. Standardized tests have been developed to test filling ability, passing ability, filling capacity, and segregation resistance (static stability); **Figure 2.1** shows a table taken from an NCHRP report that summarizes the fresh property of interest, the associated test methods (standard and non-standard), suggested test result targets, and whether the tests should be conducted as part of an SCC mix design program or for routine quality control (NCHRP 2009). An important feature of the suggested SCC fresh concrete quality control tests is that they can be fulfilled by the

ASTM standardized tests of only slump flow, J-ring flow, and the already utilized air content tests. It is also important to know that the slump flow and J-ring tests are simple, demonstrate repeatability, and fast; the two tests must be conducted within 6 minutes to be in conformance with the standard (ASTM C 1621 2009).

Property	**Test Method**	**Target values**	**Design**	**QC**
Filling ability	Slump flow T-50 (ASTM C1611)	23.5-29 in. (600-735 mm) 1.5-6 s	√	√
Passing ability	J-Ring flow (ASTM C1621)	21.5-26 in. (545-660 mm)	√	√
	L-Box blocking ratio (h_2/h_1)	0.5-1.0	√	√
Filling capacity	Filling capacity	70%-100%	√	
	Slump flow and J-Ring flow tests			√
	Slump flow and L-Box tests			√
Static stability	Surface settlement	Rate of settlement, 25-30 min (value can decrease to 10-15 min) -MSA of 3/8 and 1/2 in. (9.5 and 12.5 mm) ≤ 0.27%/h (Max. Settlement ≤ 0.5%) -MSA of 3/4 in. (19 mm) ≤ 0.12%/h (Max. settlement of 0.3%)	√	
	Column segregation (ASTM C 1610)	Column segregation index (C.O.V.) ≤ 5% Percent static segregation (S) ≤ 15%	√	
	VSI (ASTM C 1611)	0-1 (0 for deep elements)	√	√
Air volume	AASHTO T 152	4%-7% depending on exposure conditions, MSA, and type of HRWRA. Ensure stable and uniform distribution of	√	√

Figure 2.1 – Suggested Fresh Property Tests (Mix Design and Quality Control)
(NCHRP 2009)

Because SCC is placed with no external compaction effort, the fresh properties control the quality of placement and the hardened properties; therefore, it is important to develop an SCC with sufficient robustness. Most concrete constituent variability can be equated to water demand, whether it is changes in moisture content, material gradation, or specific surface for example. A well designed SCC should lend acceptable tolerance to daily fluctuations in the materials during production and should withstand a change of 8.5 - 17 lb/yd^3 (5 - 10 L/m^3) in water content without falling outside performance specifications (EFNARC 2005; NCHRP 2009). Newer VMA chemical admixtures can help to reduce the impact of material variability and enhance the robustness of well designed SCC. However, VMA should not be viewed as a way of avoiding the need for a good mix design, ongoing quality assurance, and careful selection of constituent materials (EFNARC 2006). NCHRP has recommended slump flow and slump flow minus J-ring flow values based on intended use, **Figure 2.2** presents the recommendations which are consistent with other guidelines (EFNARC 2005; NCHRP 2009). It is again worth noting the fresh characteristics are being described by the two simple tests with the benefits described earlier. Also, it has been concluded from other researchers that filling capacity is best described by a combination of passing ability and non-restricted deformability tests such as the two shown below (Hwang, S. et al. 2006).

Relative Values		Slump flow, in.			Slump flow - J-Ring flow, in.		
		23.5-25	25-27.5	27.5-29	3-4	2-3	≤ 2
Low	Reinforce-ment density	■				■	
Medium			■			■	
High				■			■
Small	Shape intricacy	■				■	
Moderate			■			■	
Congested				■			■
Shallow	Depth	■			■		
Moderate			■			■	
Deep			■				■
Short	Length	■				■	
Moderate			■			■	
Long			■				■
Thin	Thickness		■				■
Moderate			■			■	
Thick		■				■	
Low	Coarse aggregate content			■			■
Medium				■		■	
High		■			■		

Figure 2.2 – Suggested Fresh Consistency by Application (NCHRP 2009)

It is the need for consistent quality control, the large impact of small material variability, and the more readily controlled environment of the precasting plant that has enabled the more widespread use of SCC by precasters, while leaving the ready mixed concrete industry in its infancy (ACI 237 2007; EFNARC 2006; NDOR 2007). If a good quality SCC mix design is implemented well, superior hardened properties can result. There are also important trade-offs of SCC in the hardened state that should be considered.

2.3 HARDENED CHARACTERISTICS

The hardened mechanical properties of compressive strength, tensile strength, and modulus of elasticity will be discussed because of their importance to a designer and/or a specifier. Other hardened characteristics such as creep, shrinkage, durability, and bond are not of interest to this researcher's investigation.

Concrete compressive strength (f'_c) is very important to the design of concrete structures as it is a measure of the strength of the construction material. Compressive strength is also highly correlated to elastic stiffness and tensile strength and should be evaluated to predict the structural response to loading. Compressive strength is highly dependent on the water to cementitious material (W/CM) ratio, age, powder content (cement and supplementary cementitious materials), curing conditions, admixtures used, and aggregate gradation and surface texture (Mindess et al. 2003). It has been widely recognized that for a given W/CM, SCC can develop higher compressive strength as compared to CC. The improved compressive strength is a result from the lack of vibration and reduction in bleeding and segregation that promotes a more uniform and improved interfacial transition zone between the aggregate and paste (ACI 237 2007; EFNARC 2005). During a scientific investigation, the impact of the effects of curing conditions, age, powder content, and aggregate gradation and surface texture can be mitigated by controlling these variables.

The tensile strength of concrete is described by two separate tests, but the two are often considered together. The modulus of rupture (MOR, f_r) is tested by loading a small concrete beam into flexure and is set equal to the extreme tension fiber stress at failure. The splitting tensile strength (STS, f_{ct}) is tested by placing a concrete cylinder on its side

and applying a line load along the length, the splitting tensile strength is then computed from the failure load and geometry of the specimen. There have been mixed results when comparing the tensile strength of SCC to CC. Some report that the tensile strength of SCC is comparable to CC because the volume of paste has no significant effect on tensile strength (EFNARC 2005). Some purport that SCC may have a higher MOR than CC with similar proportions (ACI 237 2007). Lastly, some researchers have found that MOR for SCC may be reduced, while STS for SCC appeared improved; the explanation was that MOR is a more direct test of the SCC's volumetrically increased and weaker paste tension surface, while STS tests a larger cylinder core surface that encompasses the properties of the aggregate, paste, and the interfacial transition zone (Kim 2008). The confusion over the tensile properties of SCC is a potential area for more research to improve estimates.

Modulus of elasticity (MOE, E_c) is the linear, elastic straining of a material in response to loading over an area. It is readily agreed by researchers that SCC generally has a decrease in MOE because of the typical practice of removing hard C.A. volumes and replacing them with softer paste volumes. Various reports suggest that SCC can have reduced MOE from 4 - 15%, but SCC has been shown to be well predicted by AASHTO prediction equations and should be adequately covered by the safe assumptions on which the formula are based (ACI 237 2007; EFNARC 2005; Kim 2008, NCHRP 2009). The reduction of MOE for high strength concrete may not be as drastic because the concrete stiffness already relies more on the stiffness of the paste. Because MOE controls the response of concrete members to load as well as the member camber, creep, and shrinkage, the reduction in MOE should be fully understood for the SCC mixtures in use.

For hardened SCC, there appear to be benefits and disadvantages when compared to CC. Compressive strength of SCC can be increased over CC of similar batch proportions. Tensile strength of SCC may be improved relative to CC, but may also exhibit greater variability. Elastic stiffness of SCC is decreased from similar CC, leading to increased camber, shrinkage, creep, and prestress loss potential. The shear characteristics and behavior should also be discussed.

2.4 SHEAR CHARACTERISTICS

As already discussed, the constituent material proportions of SCC differ from those traditionally used in CC. With such drastic changes to mixture proportions, an investigation into important failure modes, including shear, should be undertaken.

2.4.1 General The shear capacity of concrete can be of great concern, especially in certain shear-critical applications and given the extremely brittle and not well understood mechanisms of failure. The common practice of reducing coarse aggregate volume to increase paste and fine aggregate fractions in SCC mixtures has raised concerns about the possible reduction of shear capacity due to loss of aggregate interlock. The shear strength provided by concrete, V_c, is taken equal to the failure capacity of a beam without stirrups usually said to be the inclined cracking shear or concrete contribution to shear. **Figure 2.3** shows the relative contributions to inclinded cracking shear of the resisting mechanisms of shear in the compression zone, V_{cy}, the vertical component of shear transferred across the crack by aggregate interlock, V_a, the dowel action of the longitudinal reinforcement, V_d, and the shear reinforcing steel, V_s (ACI – ASCE 426 1973). It can be seen from **Figure 2.3** that aggregate interlock is the primary

mechanism of resistance to shear failure at the time of inclined cracking or member failure without shear reinforcement. So, it can be understood that a significant reduction in aggregate interlock from C.A. replacement can have a significant reduction in total concrete shear resistance.

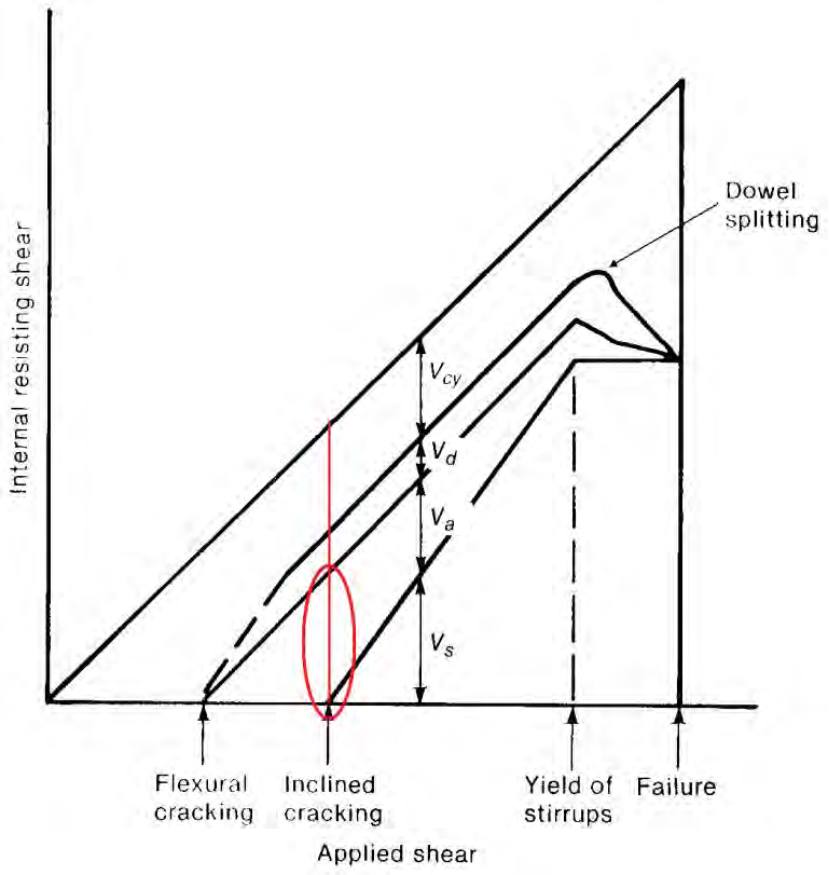

Figure 2.3 – Traditional Shear Resistance Mechanisms (ACI – ASCE 426 1973)

To date, there are few studies available that have directly investigated the impact of the reduction of C.A. volume in SCC mixtures on aggregate interlock. One study did look at SCC in particular, and conducted "push-off" tests to directly investigate the impact of concrete compressive strength, aggregate type, and aggregate volume on

aggregate interlock. The results show what would traditionally be shown by theory; aggregate interlock decreases with increased concrete compressive strength, aggregate interlock decreases with reduced C.A. volumes, and that aggregate interlock is affected by the aggregate type (Kim 2008). It is worth continuing to investigate these variables for SCC so that the findings can be verified and models can be more reasonably proposed.

There have been more studies where full scale precast, prestressed SCC and CC beams have been comparatively tested in shear. Some researchers have found that SCC has similar shear capacity to comparison CC beams (FHWA 2005; Kim 2008; Naito et al. 2006). Other projects have found that precast, prestressed SCC girders may fail in shear slightly below comparison CC, but that SCC still exhibited adequate safety margins when compared to predicted capacity from existing design equations (Lachemi 2005; NCHRP 2009). It appears that SCC consistently performs well in full-scale shear members, but additional investigation is warranted given the brittle and unpredictable nature of shear failures.

2.4.2 Aggregate Interlock The shear resistance mechanism known as aggregate interlock is developed from the interlocking of aggregate particles on the two faces of a crack in a concrete member. In normal strength concrete, the weak link of the two phase concrete system of aggregate and paste is the interfacial transition zone between, thus, fracture usually develops in the paste, along the surface of the aggregate leaving a roughened crack surface (Walraven 1981). **Figure 2.4** shows the mechanism of aggregate interlock being activated by aggregates of maximum size, a, along a crack of width, ω, and generating shearing and normal stresses of v_{ci} and f_{ci} respectively (Vecchio and Collins 1986).

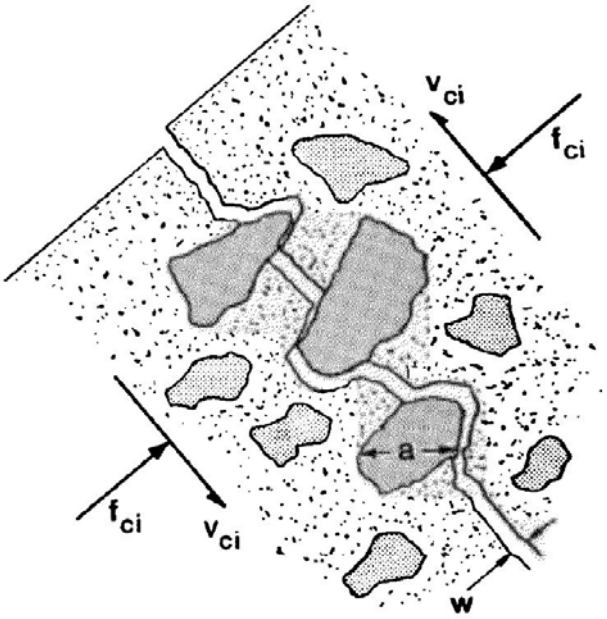

Figure 2.4 – Aggregate Interlock (Vecchio and Collins 1986)

The theoretical aggregate interlock model proposed by Walraven and Reinhardt was confirmed by the push-off tests they performed which also enabled the derivation of the limiting value of v_{ci}. The model assumes that rigid spherical aggregate protruding from a flat crack interact with rigid, perfectly plastic paste. The aggregate of varying size, based on gradation, contact the deformable paste in a predicable way, this contact area can be computed in the crack opening and sliding directions. The aggregate sliding against the paste causes shearing and normal stresses caused by friction and plastic deformation, and crack dilation respectively (Walraven 1981). It is believed that high strength concrete with higher paste strength causes the crack plane to bisect a number of aggregate particles, effectively reducing aggregate interlock potential; this was confirmed by Walraven, who reported as much as a 65% reduction in aggregate interlock when

testing high strength concretes (Walraven and Stroband 1994). This theory helped to enhance the original compression field theory (CFT) proposed by Collins and Mitchell to form the modified compression field theory (MCFT) from Vecchio and Collins, and the later simplified modified compression field theory (simplified MCFT); that has since been adopted by specifying organizations such as the AASHTO LRFD Bridge Design Specifications and Canadian Standards Association.

The early push-off testing performed by Walraven was done on normal strength concrete, f'_c = 2900 – 8200 psi (20 – 57 MPa) with river gravel aggregate. The simplified MCFT limits the contribution of aggregate for high strength concrete by taking the aggregate size equal to zero (Wight and MacGregor 2009). A researcher has proposed modification to the current equations for high strength concrete to account for the reduced contribution of aggregate interlock, and for SCC mixtures (Kim 2008). It can be beneficial to investigate the applicability of new proposed equations for normal and high strength SCC for locally available materials.

2.4.3 Push-off Test The push-off test has been around in various forms since as early as 1969 (Mattock 1969) as far as this researcher could determine. The test has varied in size, instrumentation, reinforcement detail, and overall restraint. The general test specimen geometry and orientation used in this study can be seen in **Figure 2.5** below, but will be presented in more detail in section 6 below. The size and instrumentation has varied by all researchers, but generally information is collected about the applied load (both ultimate precrack load and the shearing push-off load throughout the test), normal force, and the crack opening and slipping response to load. Internal restraining bars (extending through the shear interface) as well as external restraint

systems, such as the one shown in **Figure 2.5** have been used (Albajar 2008; Barragan et al. 2006; Mattock et al. 1969; Mattock and Hawkins 1972; Walraven and Reinhardt 1981; Walraven and Stroband 1994).

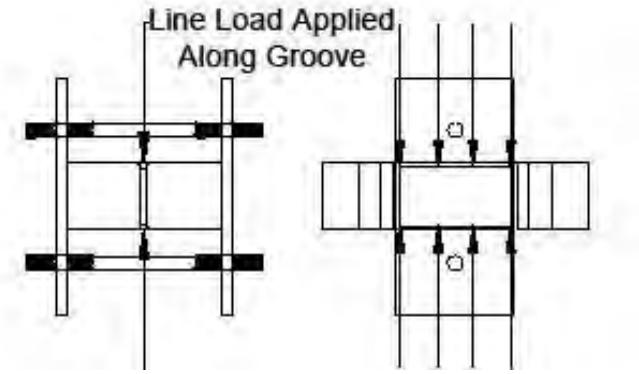

(a) Precrack Test

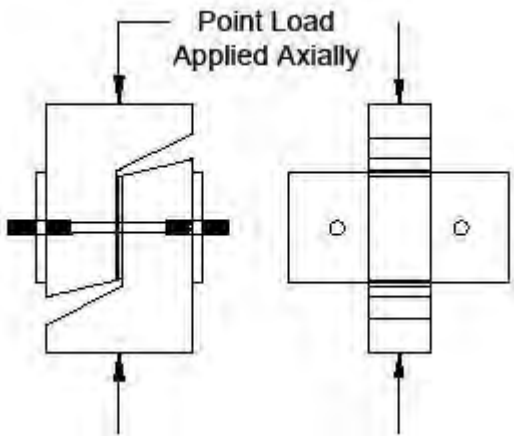

(b) Push-off Test

Figure 2.5 – Push-Off Test Geometry and Orientations

The relationships of interest to this study that were developed by Walraven (1981) resulted from the externally restrained push-off specimen. The results from his investigation, and the analysis of Vecchio and Collins (1986) enabled the prediction of

the maximum shear stress acting on a given crack and formed the foundation of the MCFT.

2.4.4 Shear Models According to Walraven (1981), the aggregate sliding against the paste causes shearing and normal stresses from friction and crack dilation respectively; this behavior is developed in a predictable way as described by **Eq. 2.1 – 2.12**.

$$\sigma = \sigma_{pu}(\overline{A}_x - \mu\overline{A}_y) \tag{2.1a}$$

$$\tau = \sigma_{pu}(\overline{A}_y + \mu\overline{A}_x) \tag{2.1b}$$

where σ is stress normal to the direction of the crack, τ is shear stress along the direction of the crack, σ_{pu} is the paste strength taken as **Eq. 2.2** by Walraven, μ is a friction factor determined as 0.4 by Walraven's study, $\overline{A}_x$ is the unit area of contact between the aggregate and paste in the x-direction (in the direction of crack slip), and $\overline{A}_y$ is the unit area of contact between the aggregate and paste in the y-direction (in the direction of crack opening). Basically, the normal stress is reduced by friction resulting from dilation whereas shear stress resistance is enhanced by frictional action developed from crack slipping.

$$\sigma_{pu} = 56.7 f'^{.56}_c \text{ (psi)} \quad \text{or} \quad \left[\sigma_{pu} = 6.39 f'^{.56}_c\right] \text{(MPa)} \tag{2.2}$$

The unit contact areas can be determined by **Eq. 2.3 – 2.6** which are the result of the full derivation performed by Walraven. It is shown that the contact area of the aggregate with the paste depends upon the crack width ω, embedment depth, u, of the aggregate into the paste, aggregate size, a, the crack slip length, δ, and the ratio of aggregate volume to total concrete volume, p_k.

$$A_y = \int_{\frac{\varpi^2+\delta^2}{\delta}}^{D_{\max}} p_k \cdot \frac{4}{\pi} \cdot F\left(\frac{D}{D_{\max}}\right) \cdot G_1(\delta, \varpi, D) \cdot dD \tag{2.3}$$

$$A_x = \int_{\frac{\varpi^2+\delta^2}{\delta}}^{D_{\max}} p_k \cdot \frac{4}{\pi} \cdot F\left(\frac{D}{D_{\max}}\right) \cdot G_2(\delta, \varpi, D) \cdot dD \tag{2.4}$$

Eqs. 2.3 and **2.4** where the crack slip, δ, is less than the crack opening, ω (δ<ω).

$$\begin{aligned} A_y = & \int_{2\varpi}^{\frac{\varpi^2+\delta^2}{\varpi}} p_k \cdot \frac{4}{\pi} \cdot F\left(\frac{D}{D_{\max}}\right) \cdot G_3(\delta, \varpi, D) \cdot dD \\ & + \int_{\frac{\varpi^2+\delta^2}{\varpi}}^{D_{\max}} p_k \cdot \frac{4}{\pi} \cdot F\left(\frac{D}{D_{\max}}\right) \cdot G_1(\delta, \varpi, D) \cdot dD \end{aligned} \tag{2.5}$$

$$A_x = \int_{2\varpi}^{\frac{\varpi^2+\delta^2}{\varpi}} p_k \cdot \frac{4}{\pi} \cdot F\left(\frac{D}{D_{\max}}\right) \cdot G_4(\delta,\varpi,D) \cdot dD + \int_{\frac{\varpi^2+\delta^2}{\varpi}}^{D_{\max}} p_k \cdot \frac{4}{\pi} \cdot F\left(\frac{D}{D_{\max}}\right) \cdot G_1(\delta,\varpi,D) \cdot dD \quad (2.6)$$

Eqs. 2.5 and **2.6** where the crack slip, δ, is more than the crack opening, ω (δ>ω).Where the variables G1, G2, G3, G4, and F are given by **Eq. 2.7 – 2.11**. These variables consider the slip condition of the crack, variability in crack width, aggregate size fractions, and aggregate embedment conditions.

$$G_1(\delta,\varpi,D) = D^{-3}\left(\sqrt{D^2-\left(\varpi^2+\delta^2\right)}\frac{\delta}{\sqrt{\varpi^2+\delta^2}}u_{\max} - \varpi\cdot u_{\max} - u_{\max}^2\right) \quad (2.7)$$

$$G_2(\delta,\varpi,D) = D^{-3}\left\{\delta - \sqrt{D^2-\left(\varpi^2+\delta^2\right)}\frac{\varpi}{\sqrt{\varpi^2+\delta^2}}u_{\max} + \left(u_{\max}+\varpi\right)\right.$$
$$\sqrt{\tfrac{1}{4}D^2-\left(\varpi+u_{\max}\right)^2} - \varpi\sqrt{\tfrac{1}{4}D^2-\varpi^2} + \tfrac{1}{4}D^2\arcsin\frac{\varpi+u_{\max}}{\frac{1}{2}D} \quad (2.8)$$
$$\left. - \frac{D^2}{4}\arcsin\frac{2\varpi}{D}\right\}dD$$

$$G_3(\delta,\varpi,D) = D^{-3}\left(\tfrac{1}{2}D-\varpi\right)^2 \quad (2.9)$$

$$G_4(\delta,\varpi,D) = D^{-3}\left(\frac{\pi}{8}D^2 - \varpi\sqrt{\tfrac{1}{4}D^2-\varpi^2} - \frac{D^2}{4}\arcsin\frac{2\varpi}{D}\right) \quad (2.10)$$

$$F\left(\frac{D}{D_{\max}}\right) = 0.532\left(\frac{D}{D_{\max}}\right)^{0.5} - 0.212\left(\frac{D}{D_{\max}}\right)^{4} - 0.072\left(\frac{D}{D_{\max}}\right)^{6} - 0.036\left(\frac{D}{D_{\max}}\right)^{8} - 0.025\left(\frac{D}{D_{\max}}\right)^{10} \quad (2.11)$$

And where u_{max}, the maximum aggregate embedment depth for which contact of the paste is still possible, is determined from **Eq. 2.12**.

$$u_{\max} = \frac{-\frac{1}{2}\varpi\left(\varpi^2+\delta^2\right)+\frac{1}{2}\sqrt{\varpi^2\left(\varpi^2+\delta^2\right)^2-\left(\varpi^2+\delta^2\right)\left\{\left(\varpi^2+\delta^2\right)^2-\delta^2D^2\right\}}}{\left(\varpi^2+\delta^2\right)} \quad (2.12)$$

All of these theoretical equations were confirmed from experimental tests performed by Walraven and Reinhardt (1981) where the results were fit to **Eq. 2.1** when setting $\mu = 0.4$ and σ_{pu} to **Eq. 2.2**. Walraven then continued to demonstrate the effect of various material and aggregate characteristics such as friction factor, cyclic loading, the contribution from various aggregate fractions, maximum aggregate size, and aggregate gradation to evaluate the sensitivity of aggregate interlock to these variables. **Figure 2.6** shows the effect of aggregate gradation; the two gradations are for the same maximum size aggregate, but conform to the upper bound (smaller aggregate) and lower bound (larger aggregate) gradation limits as set by the Netherlands Code of Practice at the time of the evaluation (Walraven 1981).

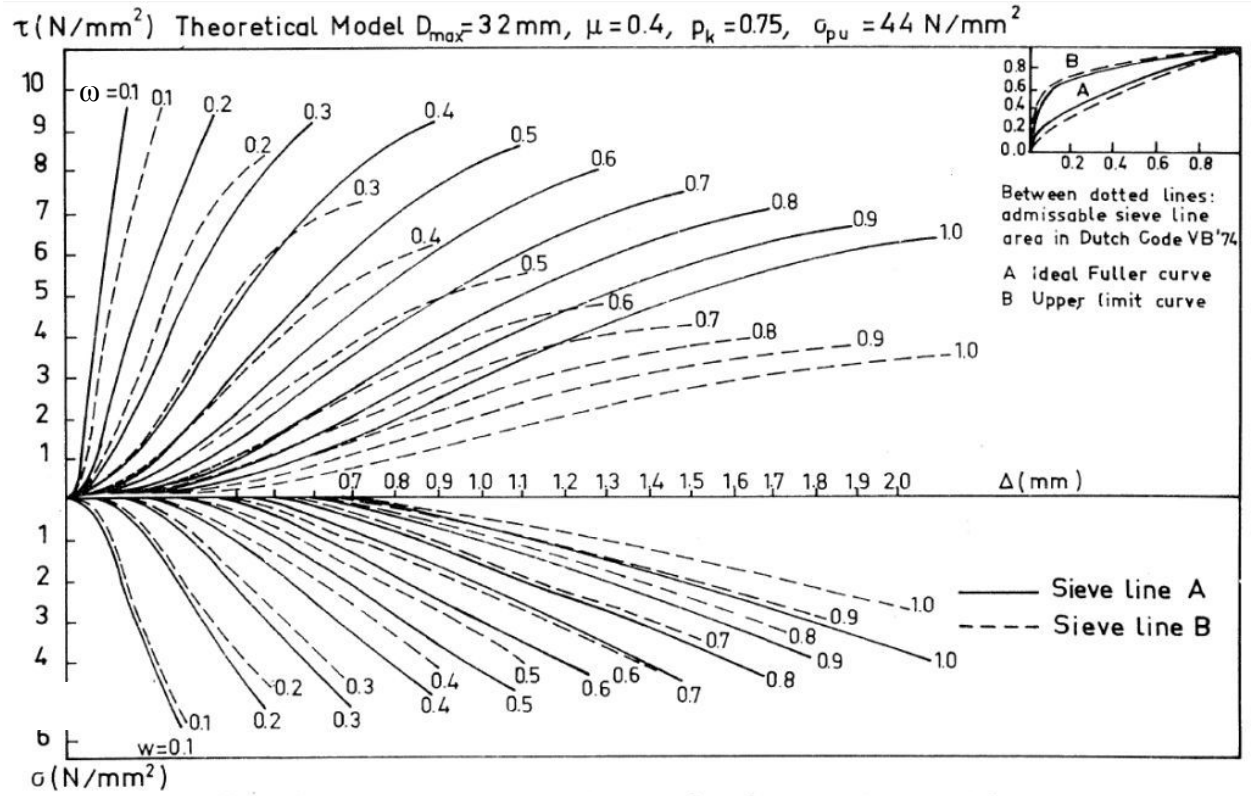

The effect of the grading curve on the transfer of stresses in a crack for two comparable mixes, confirming to different grading curves ($D_{max} = 32$ mm, $p_k = 0.75$, $\sigma_{pu} = 44$ N/mm^2, $f_{cc} \approx 32$ N/mm^2)

Conversion: 1 inch = 25.4 mm
1 ksi = 6.89 MPa (N/mm^2)

Figure 2.6 – Effect of Gradation Variability (Walraven 1981)

So, the investigation by Walraven and Reinhardt was very useful for understanding the mechanics of aggregate interlock and predicted the behavior closely. It was also made clear from Walraven's study that reducing the maximum aggregate size, reducing the amount of aggregate, or using a sandier gradation as in **Figure 2.6** all had similar effects, which was to reduce shear resistance. As has been discussed, all of these actions are taken either separately or together to achieve stable and robust SCC mixtures;

Walraven's model demonstrates the fundamental concern associated with aggregate interlock and overall shear behavior in SCC.

Vecchio and Collins were then interested in developing a shear model to explain member response to load, and did so in the form of the Modified Compression Field Theory (MCFT). The MCFT had assumptions and models of its own expanding on previous work from Collins and Mitchell to predict stress-strain interaction behavior while also deriving expressions from Walraven and Reinhardt's (1981) experimental work as they presented in **Figure 2.7** to determine **Eq. 2.13 and 2.14** (Vecchio and Collins 1986). The physical tests used to develop stress-strain theory behind the MCFT consisted of flat panels loaded in the x and y direction, at varying ratios. The focus of the panel study was to model concrete as an orthotropic material wherein equilibrium and compatibility are explained in terms of average stresses and strains. The panels were extensively studied in determining the response of cracked concrete to compression and tension, but little attention was given to crack shear behavior. Subsequent to the original panel study, another researcher has reviewed the data for crack shear behavior and determined that existing crack-slip models (such as that described by Walraven) correlate well with the panel data, even though the models were developed from drastically different test setups and mechanistic theories (Vecchio and Lai 2004). Further details of the MCFT will be presented in **Section 2.4.5** below because of the applicability to overall member behavior and the adaptation by specifications such as the AASHTO LRFD Bridge Design Specifications and Canadian Standard Association Design of Concrete Structures (CSA).

$$v_{ci} = 0.18 v_{ci,\max} + 1.64 f_{ci} - 0.82 \frac{f_{ci}^{\ 2}}{v_{ci}} \qquad (2.13)$$

$$v_{ci,\max} = \frac{12\sqrt{f'_c}}{.31 + 24\frac{w}{a+.63}} \text{ (psi, in)} \quad \text{or} \quad \left[v_{ci,\max} = \frac{\sqrt{f'_c}}{.31 + 24\frac{w}{a+16}} \right] \text{ (MPa, mm)} \qquad (2.14)$$

where v_{ci} is the shear across the crack, limited by $v_{ci,max,}$ the maximum shear a crack of width, ω, containing aggregate of maximum size, a, can resist. The compressive stress on the crack surface is f_{ci} and f'_c is concrete compressive strength.

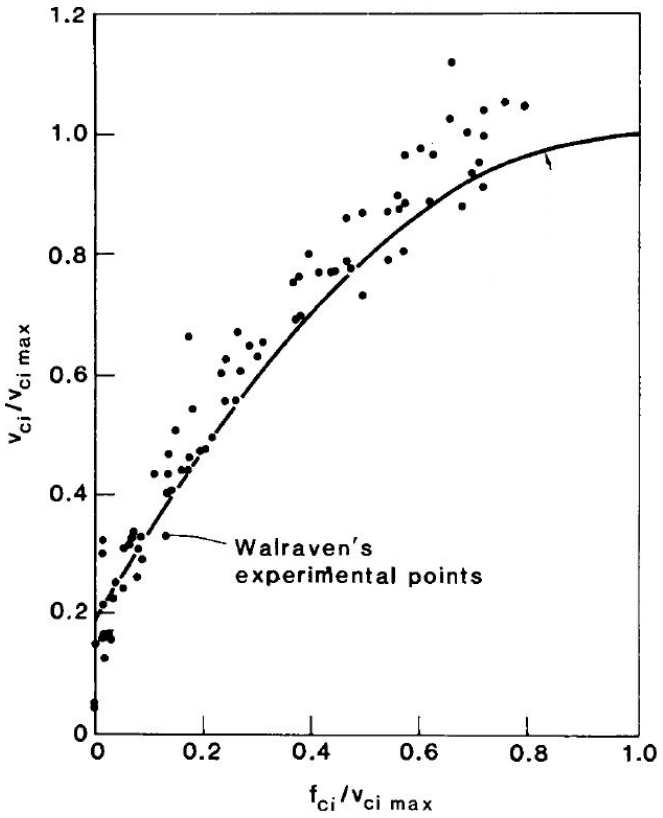

Figure 2.7 – Determination of Expression for Shear Across Cracks, Equation 2.13

(Vecchio and Collins 1986)

From the models discussed, it can be seen that maximum shear stress development can be predicted as a function of crack widths, aggregate size, and concrete compressive strength. Furthermore, shear can be influenced by normal stresses acting upon cracks as well. It is also worth noting that the most sophisticated models for expressing shear behavior in concrete are determined from both theoretical mechanics as well as empirical fitting of data. Given that the models are fitted for CC of normal strength concrete using river gravel aggregate, additional work with SCC of all strength levels and for high strength concrete in particular is still warranted. Even though researchers have reviewed the models for SCC over a range of strength levels, additional research is justified for SCC using locally available materials because of the increased volatility of SCC behavior with respect to material variability.

2.4.5 Shear in Beams To begin, a brief background on the MCFT assumptions and models is worth presenting to provide deeper understanding. Vecchio and Collins (1986) begin with a few simplifying assumptions:

- For each strain state, there corresponds only one stress state
- Stresses and strains can be taken as average when taken over large enough lengths or areas to include several cracks
- There is no overall slip of the reinforcement within the test element
- The reinforcing bars are uniformly distributed

These assumptions are important in defining equilibrium conditions, compatibility equations, and enabling averaging or “smearing” of stresses and strains. Of note was the determination that stress and strain principal axis are roughly equal, meaning cracks

develop in directions orthogonal to principal tensile strains. One important result of the analysis is the understanding of stress transmission across cracks; **Figure 2.8** from Vecchio and Collins demonstrates this concept. The calculated average shear stress of plane 1 is zero, because it is a principle plane; however, there are actually local variations from the average and this is demonstrated at the cracked plane 2 where shear across the crack, v_{ci}, and the compressive stress on the crack, f_{ci} act. The evaluation of the local crack stresses has already been shown in **Eq. 2.13** (Vecchio and Collins 1986).

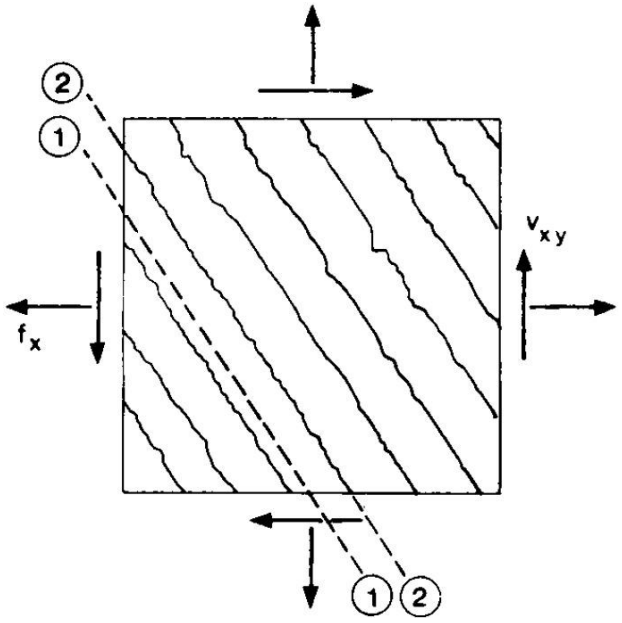

(a) Cracked concrete stress element

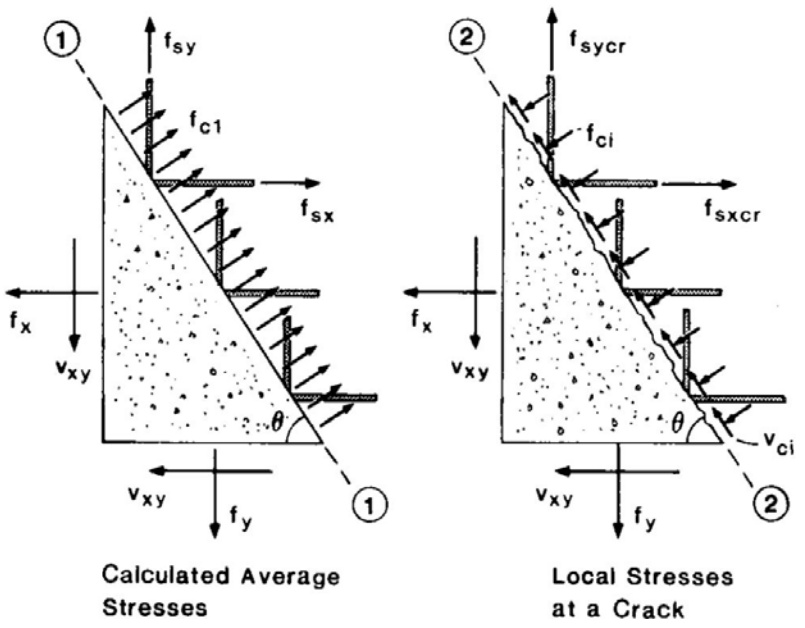

(b) Varying ways of viewing stress element

Figure 2.8 – Distinguishing Average Versus Local Stresses in Cracked Members

(Vecchio and Collins 1986)

Another important finding from the study was the understanding of cracked concrete response to compressive stress. The maximum compressive stress that concrete can withstand is reduced when the concrete is cracked, and is reduced further if a tensile stress acts orthogonal to the compressive stress. **Eq 2.15** was proposed to describe the diminishing compressive strength of concrete when exposed to increasing tensile stress (Vecchio and Collins 1981).

$$f_{c2} = f_{c2,\max}\left[2\left(\frac{\varepsilon_2}{\varepsilon'_c}\right) - \left(\frac{\varepsilon_2}{\varepsilon'_c}\right)^2\right] \qquad (2.15a)$$

Where $$\frac{f_{c2,\max}}{f'_c} = \frac{1}{.8 - .34\frac{\varepsilon_1}{\varepsilon'_c}} \leq 1.0 \qquad (2.15b)$$

Where f_{c2} is the principal compressive stress in the concrete, ε_2 is the principal compressive strain, ε_1 is the coexisting principal tensile strain, and ε'_c, taken as negative, is the concrete strain at peak stress f'_c. This can explain a host of observed behavior such as reduced shear resistance in high moment regions where large tensile strains may exist, decreased and increased shear resistance with applied tensile and compressive loads respectively, as well as deep beam effects where strains are amplified by the depth of the member and overall shear resistance appears reduced (Sherwood et al. 2006; Vecchio and Collins 1986; Wight and MacGregor 2009). Their analysis formed the foundation of developing strain and size effect components to modern shear models.

Over time, the MCFT has evolved to include new research findings and has attempted to simplify the procedure for finding shear capacity. It has evolved such that shear capacity is computed per **Eq. 2.16 – 2.19** (AASHTO 2007; Sherwood et al. 2006).

$$V = V_C + V_S = 0.0316\beta\sqrt{f'_c}\,b_v d_v + \frac{A_v f_y}{s} d_v \cot\theta \qquad \text{(ksi)}$$

$$\left[V = V_C + V_S = 0.083\beta\sqrt{f'_c}\,b_v d_v + \frac{A_v f_y}{s} d_v \cot\theta \right] \qquad \text{(MPa)} \qquad (2.16)$$

Where V_c and V_s are the shear contributions from the concrete and shear reinforcement respectively, b_v is the width of the web of the member, d_v is the shear depth of the

member, f'_c is the concrete compressive strength, A_v is the area of shear reinforcement over a stirrup spacing, s, f_y is the shear reinforcement yield strength, θ is the inclination of the crack, and β is the factor for tensile stress in the cracked concrete (AASHTO 2007). The coefficient would be 1 if using psi, and the metric equation then being one twelfth as in **Eq. 2.14**, so the concrete resistance to shear is derived from this equation. The β factor has been expressed by **Eq. 2.17**, slightly modified from the source to account for the way of expressing **Eq. 2.16**, and this closely approximates the values found in the look-up tables available in the AASHTO LRFD **(**Sherwood et al. 2006). The β factor is comprised of a strain effect term and a size effect term.

$$\beta = \frac{4.82}{(1+1500\varepsilon_x)} * \frac{51}{(39+s_{xe})} \text{ (in.)} \quad \left[\beta = \frac{4.82}{(1+1500\varepsilon_x)} * \frac{1300}{(1000+s_{xe})} \right] \text{ (mm)} \qquad (2.17)$$

Where ε_x is the mid-height strain of the member in the longitudinal direction and s_{xe} is the effective crack spacing parameter occurring at the mid-height of the member. The ε_x and s_{xe} terms are determined from member geometry and loading conditions and from the maximum aggregate size respectively. For the case of not providing adequate lateral reinforcement (as may be done for research to produce shear failures), ε_x can be expressed as **Eq. 2.18** and s_{xe} is always determined from **Eq. 2.19** (AASHTO 2007).

$$\varepsilon_x = \frac{(\frac{M_u}{d_v} + 0.5N_u + 0.5(V_u - V_p)\cot\theta - A_{ps}f_{po})}{E_s A_s + E_p A_{ps}} \qquad (2.18)$$

$$s_{xe} = \frac{1.38 s_x}{a + 0.63} \leq 80 \text{ (in.)} \qquad \left[s_{xe} = \frac{35 s_x}{a + 16} \leq 2000 \right] \text{ (mm)} \qquad (2.19)$$

Where s_x, the crack spacing parameter, can be taken as d_v, as defined above, for beams with concentrated reinforcement in the bottom flange, but is defined differently for members with well distributed longitudinal reinforcement (AASHTO 2007). The form of **Eq. 2.19** should look familiar, as it was derived from the aggregate size effect portion of **Eq. 2.14**. These variables have also been proposed to be used to determine the other objective variable of θ as in **Eq. 2.20**, but are found in look-up tables in practice (Sherwood et al. 2007).

$$\theta = (29 + 7000\varepsilon_x)(0.88 + \frac{s_{xe}}{100}) \text{ (in)} \quad \left[\theta = (29 + 7000\varepsilon_x)(0.88 + \frac{s_{xe}}{2500}) \right] \text{ (mm)} \qquad (2.20)$$

The simplifications of determining the objective functions of β and θ are helpful for designers, and have been shown to accurately (on a level similar to the un-simplified MCFT) predict member response to loading. So again, the method for determining member shear failure is a blend of theoretical mechanics and empirical test data fitting. Members tested can be monitored to compare observed behavior next to the predictions of the model. SCC and CC batch proportions can be developed to ensure similar mechanical properties and then can be fabricated into members to be tested in shear. The shear behavior of SCC can be compared to that of CC and against the predictive models just described.

As mentioned previously, some researchers have found that SCC behaves similar to CC in shear, while others have found inferior performance of SCC; however, all that this researcher could find concluded that the predictive models were conservative for both SCC and CC. To begin, some of the more harsh conclusions will be presented. A national SCC study found that the two SCC girders tested had similar cracking shears when compared to the two CC girders tested; however, the SCC girders had inferior post-crack behavior with decreased ductility and lower failure loads, likely due to decreased aggregate interlock from C.A. replacement with binder. All tested girders exceeded 2007 AASHTO LRFD predicted nominal shear resistances (NCHRP 2009). Another researcher found very similar behavior; Lachemi found that the prestressed SCC and CC beams in his study showed similar pre-cracking behavior, but the SCC beams had diminishing post-cracking capacity and increased deflections; all beams were conservative by the 1994 CSA model (Lachemi et al. 2005). Other researchers provide more positive results for SCC beams tested in shear. In 2003, VDOT reported that prestressed SCC girders were tested and that shear behavior was “as predicted”, this researcher assumes that to mean relative to shear models used, presumably then modern AASHTO equations (FHWA 2005). Another concludes that prestressed SCC and CC beams exceed nominal strength in all failure modes including shear, that progression of damage was consistent from SCC to CC, and that SCC exhibited increased ductility over CC in all cases (Naito et al. 2006). A different researcher tested his prestressed members in flexure and bond. Upon member failure he measured values of crack opening and shear crack angle for input into the AASHTO LRFD model to predict shear failure loads if the prestressed beams were not constructed to be bond critical. He showed that the AASHTO LRFD

models were conservative overall, but especially for the concrete contribution to shear resistance, even for SCC mixtures (Kim 2008). The numerous researchers found to be investigating SCC seem to be finding the general consensus that SCC may have a slight reduction in shear capacity, but that SCC is still conservatively estimated by prediction equations.

2.5 SUMMARY

SCC has been around for over twenty years, and engineers being an understandably conservative group have not yet written specifications for the widespread use of SCC in the U.S.; however, given the fiscal advantages of the advanced material, it appears to only be gaining in popularity. The rheological characteristics of SCC are well understood today. Fresh property tests have been developed and several have been standardized for testing the unique behavior of plastic SCC. Useful guidelines have been developed for establishing fresh property test result ranges based on the placement application, guidelines for establishing QC/QA testing programs have also been given (**Figures 2.1 and 2.2**). Hardened mechanical properties of SCC are at least partially established. Modulus of elasticity is consistently lower for SCC, but is still conservatively estimated by common models. Concrete compressive strength of SCC is often improved over a CC of a similar batch proportion, while tensile strength is similar. Research has shown SCC as well as high strength concrete to have a diminished shear resistance contribution from aggregate interlock, as demonstrated by studies focused around the push-off test.

Push-off tests can be a useful tool in determining the impact of several variables on the mechanism of aggregate interlock, as it is a small test that can be performed relatively easily and at low cost. Push-off test results have been incorporated into advanced shear models that not only describe shear friction, but also predict compatibility of stresses and strains, and equilibrium conditions. The modern shear models have been shown to accurately predict shear behavior over a wide variety of loading conditions and member geometries. Shear behavior of SCC prestressed beams and girders seems to be similar to CC; at worst, researchers consistently find that SCC shear resistance may be reduced, but is conservatively estimated by current models. Continued research should be undertaken to investigate more fully the variations of SCC and how they affect behavior. More experience with SCC can only lead to increased understanding, improved model fitting, and enhanced use of the benefits that SCC offers.

3. MIX DESIGN

3.1 INTRODUCTION

This section describes the process by which the concrete batch proportions were selected to create four basic mixtures: a 6 ksi (41.4 MPa) 28 day target strength CC, a 6 ksi (41.4 MPa) 28 day target strength SCC, a 10 ksi (68.9 MPa) 28 day target strength HSC, and a 10 ksi (68.9 MPa) 28 day target strength HS-SCC. To distinguish between the HSC and HS-SCC, the reporting and naming convention of just CC and SCC were maintained. In this thesis, the difference between CC and SCC refers to the mixture constituents; whereas, the distinction of the target strength will differentiate the normal and high strength concrete batch proportions. The objective of the mix development process was to replicate as closely as possible the kinds of concrete mixtures that would be used by Missouri precast and ready mix concrete suppliers, and toward that end, a survey was created and distributed to numerous Missouri concrete suppliers. The batch proportions were then selected based on the survey results, along with guidance from the project liaison from the Missouri Department of Transportation (MoDOT). The two higher strength (10 ksi [68.9 MPa] 28 day target strength) mixtures were also refined using the knowledge, and previously published work, of the project's Principal Investigator who has worked extensively with high strength concrete (HSC) (Myers and Carrasquillo 1999). This method of mix development was less rigorous than a detailed investigation of several trial batches of varying batch proportions; however, the resultant mixtures should reflect the current state of practice in making SCC from Missouri concrete suppliers using locally available materials. Additionally, material data sheets can

be found for the chemical and mineral admixtures used throughout this investigation in **Appendix A** attached below.

3.2 SCC PRECAST PRODUCER SURVEY

A questionnaire was created and distributed to numerous parties so that the research team could have an understanding of the current state of practice regarding SCC use in the state of Missouri and elsewhere. The questionnaire was distributed through email, using online survey software. A Microsoft Word formatted version showing the specific questions asked on the survey can be found below in **Appendix B**. The survey was distributed to 27 Missouri ready mix concrete suppliers, 13 Missouri precast concrete suppliers, and 51 Department of Transportation (DOT) officials who are AASHTO members across the country. Participation in the survey was completely voluntary and contributors were assured that no proprietary mixture information would be disclosed from this investigation.

Unfortunately, no ready mix concrete suppliers replied to our solicitations. It is known from the personal experience of the project Principal Investigator that some ready mix producers in Missouri have made SCC, but it remains unknown to what extent or level of sophistication.

Positive results were gathered from the Missouri precast concrete suppliers; 6 out of 13 solicited precast suppliers replied with valuable responses, several even provided multiple mix designs in use at their facilities. **Table 3.1** details the compiled survey results from the precast suppliers. Due to confidentiality agreements, the actual mix designs from the survey responses cannot be shared. The low, high, and average for each

category are shown. The low and high columns represent the lowest and highest values for a given category and are not representative of a particular concrete batch proportion.

Table 3.1 – Compiled Survey Results from Responding Precast Suppliers

Respondent	Low	High	Average
Nominal Max. Agg. Size	1/2"	3/4"	5/8"
Reported Release Strength (psi)	3000	6000	4400
Reported Design Strength (28day unless noted, psi)	5000	10000	7400
Cement (pcy)	580	780	689
Add'l Cementitious Mt'l (pcy)	0	200	54
W/Cm ratio	.28	.46	0.37
Calculated Percent C.A. by weight of Agg. Portion (%)	.30	.53	.48
WR/HRWRA (oz/cy)	8	112	63
Retarder (oz/cy)	0	30	5
VMA (oz/cy)	0	23	3
Air Entrainment (oz/cy)	0	90	20

Indicates Omitted, Presumably Zero Data
Indicates Calculated Data, not Directly Given

Conversions: 1 inch = 25.4 mm
1 lb/in2 (psi) = 6.89 kPa
1 oz/yd3 = 38.7 mL/m3
1 lb/yd3 (pcy) = 0.59 kg/m^3

Several observations were made from these survey results and key variables in the batch proportions used throughout this study were decided. The survey results were averaged, and the decisions made from these averaged values. Beginning at the top of the average column, the first item of interest is the nominal maximum aggregate size (NMS) of 5/8 inches (16mm), which lies between 1/2 - 3/4 inches (13 - 19 mm) or somewhere between MoDOT's Gradation D and Gradation E. Because some precasters use the larger Gradation D, and because ready mix suppliers would likely use the larger Gradation D,

aggregates used for this study conformed to the gradation requirements of MoDOT Gradation D and will be discussed in full detail in **Section 4.2** below. Next, the average reported design strength was 7400 psi (51.0 MPa) and is near the lower target strength of 6000 psi (41.4 MPa) indicating mixtures that would be of interest to this study. Next, the total average cementitious material of 744lb (337 kg) comprised of 689 lb (313 kg) cement plus 54 lb (24 kg) supplementary cementitious material was used. The average water to cementitious material ratio (W/CM) was calculated at 0.37. The last major point of interest was an average coarse aggregate to total aggregate weight ratio of about 0.48. The specific gravity of these materials is unknown, but typical aggregates have similar densities, so the coarse aggregate was expected to take up about 48% of the aggregate volume. Finally, the average mixture contained water reducers or high range water reducers and air entraining admixtures, but rarely used retarders or viscosity modifying admixtures. **Table 3.2** summarizes the important average variables from the survey below.

Table 3.2 – Important Averages from Survey Results

Nominal max. agg. size (inches)	5/8
Compressive strength (lb/in^2)	7400
Cement (lb/yd^3)	744
Water to cementitious material (W/CM)	0.37
Coarse aggregate volume fraction (%)	48

Conversion: 1 inch = 25.4 mm
1 lb/in^2 = 6.89 kPa
1 lb/ yd^3 = 0.59 kg/m^3

The national DOT survey also had good results with 29 replying out of the 51 petitioned. It should also be noted that the national survey participants were selected through the use of the January, 2011 AASHTO online member directory of the Standing Committee on Highways (SCOH) and the Subcommittee on Materials (SOM) by selecting one candidate from each state, with preference for voting members (AASHTO 2011). The purpose of the national survey was to assess the sense of familiarity that industrial leaders have with SCC, to evaluate the relative robustness of their understanding, discover trends, identify potential geographic "hot spots" where use is common, and to recognize where MoDOT's knowledge base lies relative to others. **Figure 3.1** visually represents some of the insights gained from the national SCC survey using a color coded map from an online source (DIYMAPS 2011).

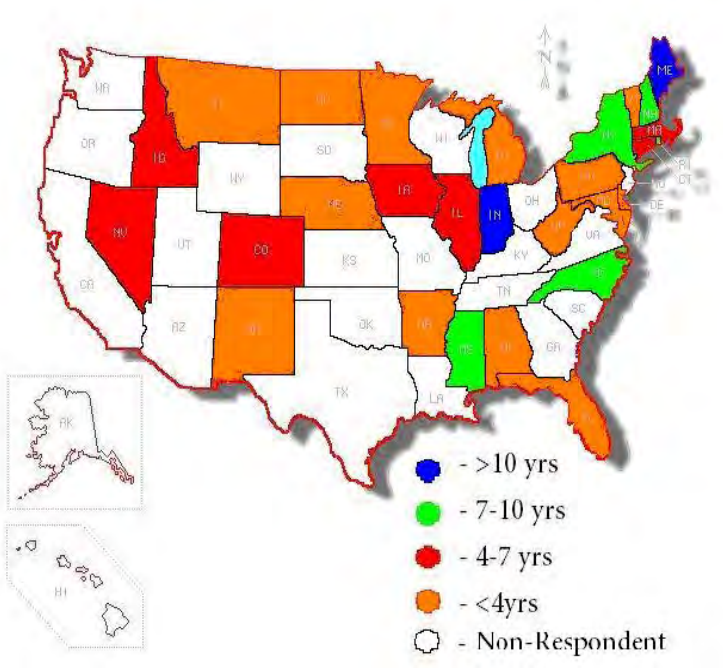

(a) Years of SCC Use

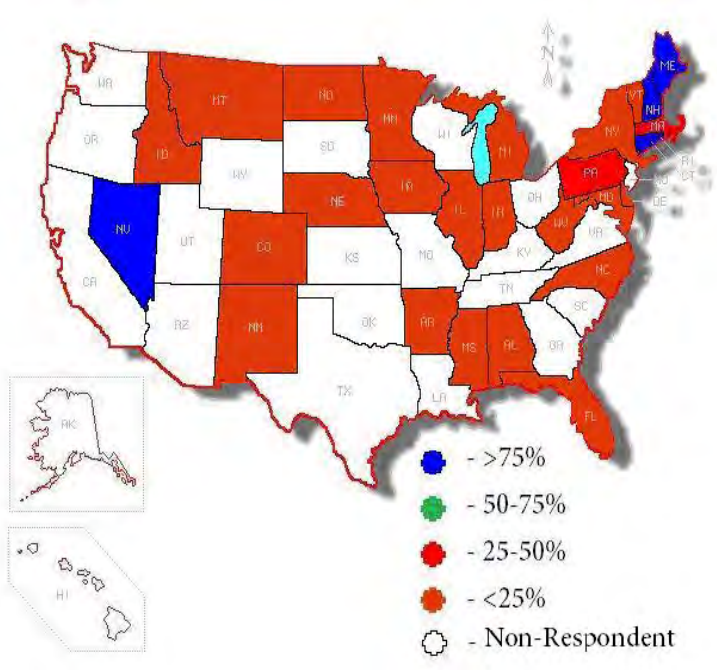

(b) Estimated Percent of Projects Using SCC

Figure 3.1 – National DOT Survey Results

From the responses shown in **Figure 3.1** one can easily see that the North East U.S. generally has more experience with SCC. It can also be seen that as states use SCC for longer periods of time, they generally have a higher percentage of their projects using SCC; this increased usage with time would reflect not only the fiscal advantages of using SCC, but also that positive results are being experienced. It should be noted that the longest reported experience with SCC was 16 years, only now verging on long enough field use durations to have experienced long term durability.

Along with the information conveyed in **Figure 3.1** other trends were identified from the survey responses. Most respondents clearly differentiated the use of SCC between ready mix and precast concrete suppliers; the trend was always a more advanced

knowledge, more common use, and longer use among precasters. SCC was used in all applications, not only aesthetic or low stress drainage structures; reportedly, the most common use for SCC is in structural beams and girders. Aggregates used for SCC seem to be as diverse as the local geology; river gravel and limestone is used approximately equally, and other materials such as granite, trap rock, and quartz are used to a lesser extent, as would be typical of conventional concrete. As was reflected in the precast survey responses, the most common nominal maximum aggregate size was 3/4 inches (19mm) with 1/2 inches (13mm) also being commonly reported. Unlike Missouri precasters, numerous responders reported mix designs used VMA's for stability; this also seemed to be more prevalent among more experienced DOT's.

3.3 MoDOT GUIDENCE AND SPECIFICATIONS

The MoDOT concrete materials expert liaison provided this investigation with the baseline batch proportions. The baseline batch proportions were determined by the liaison by examining submitted mix designs used for state projects where CC was used. The CC baseline mixture was expected to develop minimum 28 day strength of 6 ksi (41.4 MPa). The specified batch proportions can be seen in **Table 3.3**.

Table 3.3 – 6 ksi (41.4 MPa) Target Strength CC Batch Proportions

Class A-1 Concrete	
Cement (lb/yd^3)	750
W/CM	0.37
Coarse aggregate volume fraction (%)	58
Design air content (%)	6.0

Conversion: 1 lb/ yd^3 = 0.59 kg/m^3

Conveniently, the Missouri precast survey responses summarized in **Table 3.2** closely matched the baseline mixture given by MoDOT in **Table 3.3** in two important ways; the cement dosage and water to cement ratio were virtually the same. Because the survey results were so similar to the given MoDOT batch proportions, they were slightly adjusted to match those of **Table 3.3** except the coarse aggregate volume fraction was held down to the 48% resulting from the survey. The adopted 6 ksi (41.4 MPa) target strength SCC mixture is shown in **Table 3.4** below.

Table 3.4 – 6 ksi (41.4 MPa) Target Strength SCC Batch Proportions

Cement (lb/yd^3)	750
W/CM	0.37
Coarse aggregate volume fraction (%)	48
Design air content (%)	6.0

Conversion: 1 lb/ yd^3 = 0.59 kg/m^3

The next step was to develop the 10 ksi (68.9 MPa) target strength batch proportions. It was decided to increase cementitious material and reduce water to cementitious material ratio in order to increase the compressive strength. A decrease in the design air content to 3% was justified because higher strength concretes result in a disconnected capillary structure due to the lower w/cm ratios used and are therefore less vulnerable to freeze-thaw damage requiring less entrained air content (Myers and Carrasquillo 1999; Mindess 2003). Bridge girders are also inherently protected from critical saturation level to produce freeze-thaw by the deck system coverage. Maintaining the coarse to fine aggregate ratio was done to reflect the survey results and the batch

proportions given by MoDOT. The project Principle Investigator (PI) had worked extensively with high strength concrete throughout his dissertation and so trial batches were made from mixtures familiar to the PI that were used in actual field bridge projects, while maintaining the coarse to fine aggregate ratio, and while attempting to achieve desirable rheology. The resultant batch proportions are shown in **Table 3.5** below.

Table 3.5 – 10 ksi (68.9MPa) Target Strength CC and SCC Batch Proportions

	Conventional Concrete	Self-Consolidating Concrete
Cement (lb/yd^3)	840	840
Class C Fly Ash (lb/yd^3)	210	210
W/CM	0.30	0.30
Coarse aggregate volume fraction (%)	58	48
Design air content (%)	3.0	3.0

Conversion: 1 lb/ yd^3 = 0.59 kg/m^3

Increasing the paste volume and using 20% ASTM class C fly ash helped to maintain workability with a water-to-cementitious material ratio as low as 0.30. Again, the fly ash mill certification can be found in **Appendix A** below.

3.4 SUMMARY

From reviewing **Tables 3.2 – 3.5** above for the four basic mixtures, the only difference in batch proportions from CC to SCC at each strength level (6 and 10 ksi [41.4 and 68.9 MPa]) is the coarse aggregate volume fraction, with the SCC having decreased amounts of coarse aggregate. **Table 3.6** summarizes the four basic mixtures. The

difference between the strength levels is the paste volume, water to cementitious material ratio, and the air content while maintaining the coarse aggregate volume fraction.

Table 3.6 – Four Basic Mixtures to the SCC Project

		Cement, lb	Fly Ash, lb	Water, lb	Fine Aggregate, lb	Coarse Aggregate, lb	MB-AE-90, oz (oz/cwt)	Glenium 7700, oz (oz/cwt)
6ksi	MoDOT A-1 (CC)	750	0	278	1166	1611	11.3 (1.5)	29.3 (3.9)
	SCC	750	0	278	1444	1333	11.3 (1.5)	46.5 (6.2)
10ksi	HSC (CC)	840	210	315	1043	1440	13.7 (1.3)	52.5 (5.0)
	HSC SCC	840	210	315	1291	1192	10.5 (1.0)	75.6 (7.2)

Notes: Aggregate weights based on SSD condition
Cement – Type III
Fly Ash – Class C
HRWRA – BASF Glenium 7700
AEA – BASF MB-AE-90

Conversion: 1 lb = 0.45 kg
1 oz = 29.6 mL
1 oz/cwt = 0.66 mL/kg

It was also necessary to develop additional SCC batch proportions for testing aggregate interlock. As discussed above, the precaster survey results were used to determine an average 6 ksi (41.4 MPa) SCC mixture for comparison to the 6 ksi (41.4 MPa) CC mixture given by MoDOT; the difference between the SCC and CC mixtures was the coarse aggregate volume fraction. Two additional SCC mixtures were determined from the precaster survey by taking the most outlying coarse aggregate data. The lowest two coarse aggregate volume fractions were most outlying in the data set and averaged to approximately 36%; this was the batch proportion used for the second SCC

mixture. Taking the difference between the baseline and most outlying SCC data, 48% - 36%, of 12% and creating a third SCC mixture equally outlying from the average made a mixture of 48% + 12% = 60%. The high coarse SCC was not reportedly used by any survey respondents, and is more indicative of conventional concrete proportions (58% C.A. was used for the CC mixture) and could be viewed as an upper bound to usable SCC batch proportions. The high coarse SCC can be useful in determining the role of C.A. in aggregate interlock as well as identifying if there is variance in behavior between two similar batch proportions just because one was CC and the other SCC. This was repeated for the 10 ksi (68.9 MPa) target high strength concrete. This entire matrix was then repeated again for a second common type of Missouri aggregate, river gravel. An additional batch proportion was tested from another study being conducted concurrently on the Missouri S&T campus. Lastly, a few additional 4 ksi (27.6 MPa) target strength batch proportions were developed toward the end of the study because all of the mixtures achieved higher than target strengths. A complete test matrix for the aggregate interlock test will be discussed further below and is shown in **Table 4.1**.

4. MATERIAL AND FRESH CONCRETE PROPERTIES

4.1 GENERAL

This section delineates the actions executed to carry out the material and fresh concrete properties testing for this research investigation. The tasks performed, the information gathered, and the associated testing standards with each task, if any, are reported. To begin with, **Figure 4.1** below defines the way in which the various mixtures were identified, with an example mixture shown. **Table 4.1** below represents a concise resource to see all the concrete batch proportions tested throughout this investigation.

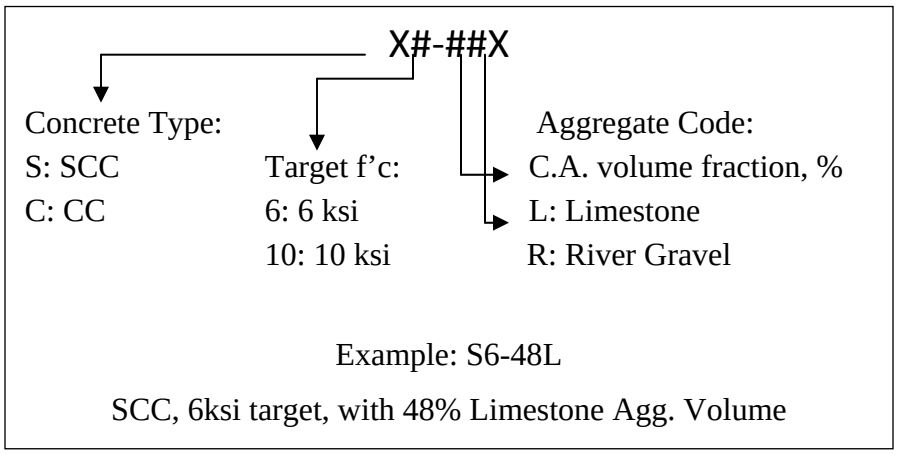

Conversion: 1 ksi = 6.89 MPa

Figure 4.1 – Designation Key

Table 4.1 – Concrete Batch Proportions Tested

	C.A. Type	Concrete Type	C.A. Volume, %	Designation
4 ksi Target	Limestone	Conventional	58	C4-58L
		Self-Consolidating	36	S4-36L
		Self-Consolidating	60	S4-60L
9 ksi Target*	River Gravel (Pea Gravel)	Self-Consolidating	57	S9-57R
6 ksi Target	Limestone	Conventional	58	C6-58L
		Self-Consolidating	36	S6-36L
		Self-Consolidating	48	S6-48L
		Self-Consolidating	60	S6-60L
	River Gravel	Conventional	58	C6-58R
		Self-Consolidating	36	S6-36R
		Self-Consolidating	48	S6-48R
		Self-Consolidating	60	S6-60R
10 ksi Target	Limestone	Conventional	58	C10-58L
		Self-Consolidating	36	S10-36L
		Self-Consolidating	48	S10-48L
		Self-Consolidating	60	S10-60L
	River Gravel	Conventional	58	C10-58R
		Self-Consolidating	36	S10-36R
		Self-Consolidating	48	S10-48R
		Self-Consolidating	60	S10-60R

* Actual field mix used in hybrid composite beam bridge field demonstrations project, bridge #B0439 Mountain Grove, MO

Conversion: 1 ksi = 6.89 MPa

The specific tests performed during this study are described. To begin, tests to characterize the materials being used were executed. Properties were then determined for freshly mixed concrete through testing. These actions prepared the investigator to then form hardened concrete specimens and enabled the characterization of the mechanical properties and shear behavior.

4.2 MATERIAL PROPERTIES

In order to develop concrete batch proportions that actually match the mix designs determined for use, several tests need to be performed on the materials to be used. Specific gravity, absorption, and moisture content are all necessary to determine batch weights through the absolute volume method. Additionally, dry sieve gradation tests were also performed on the coarse aggregate samples.

Bulk specific gravity is the link between volume and weight and was tested for the coarse and fine aggregate. Absorption values are measured to determine the change in mass of an aggregate when free water is absorbed into the pore spaces; absorption was determined for the coarse and fine aggregates used. Both the limestone and river gravel coarse aggregates were tested in accordance with ASTM C 127 – 2007, Standard Test Method for Density, Relative Density (Specific Gravity), and Absorption of Coarse Aggregate (ASTM C 127 2007). The fine aggregate was tested in accordance with ASTM C 128 – 2007, Standard Test Method for Density, Relative Density (Specific Gravity), and Absorption of Fine Aggregate (ASTM C 128 2007). **Table 4.2** below summarizes the relative density and absorption values determined for the aggregates used.

Table 4.2 – Bulk Specific Gravity (Oven Dry Basis) and Absorption of Aggregate

	Bulk Specific Gravity (Oven-dry, unit-less)	Absorption (%)
Limestone	2.56	3.00
River Gravel	2.59	4.03
Sand	2.60	0.70

Just as absorption of the aggregate material is necessary in determining batch weights, so is moisture content. The total evaporable moisture content measures how much moisture is actually present on the aggregate and should be tracked and measured at the time of use. The total moisture may exceed the aggregate absorption value indicating a saturated aggregate with surface moisture, or total moisture may be below absorption indicating an unsaturated partially dry aggregate particle. Total moisture was determined so that an accurate amount of water could be added to a mixture such that the water to cement ratio was equal to that required of the mix design; total moisture was found by following ASTM C 566 – 2004, Standard Test Method for Total Evaporable Moisture Content of Aggregate by Drying (ASTM C 566 2004).

Next, it should be mentioned that aggregate gradation tests were also performed. Because previous researchers have found that the aggregate interlock mechanism of shear is dependent upon the coarse aggregate nominal maximum size (NMS) as well as gradation (Walraven 1981), it was necessary to find a river gravel and limestone with these properties in common. Additionally, the river gravel was collected and stored in 55 gallon (210 L) drums because of lack of available space to create a stock pile in the lab. Inherent in most methods of transporting aggregate, and the method used in particular, the potential for segregation is high. Gradation testing was performed to help monitor the gradation consistency, and make adjustments if necessary, for the samples used to produce specimens. **Figure 4.2** below shows the gradation curves for the limestone and river gravel coarse aggregates. Observe from **Figure 4.2** that the NMS for both aggregates was 3/4 inch (19mm) and that the relative percent passing for each sieve was fairly consistent between each aggregate type and for each river gravel test. We also

see from the figure that each of these aggregates consistently fall within the boundary lines corresponding to the MoDOT “Gradation D” and ASTM “#67”. The ASTM #67 gradation as well as the procedure performed to sieve the aggregate is found within ASTM C 136 – 2006, Standard Test Method for Sieve Analysis of Fine and Coarse Aggregates (ASTM C 136 2006). Furthermore, coarse aggregates conforming to Gradation D is to be used in structural concrete according to MoDOT (MoDOT 2012).

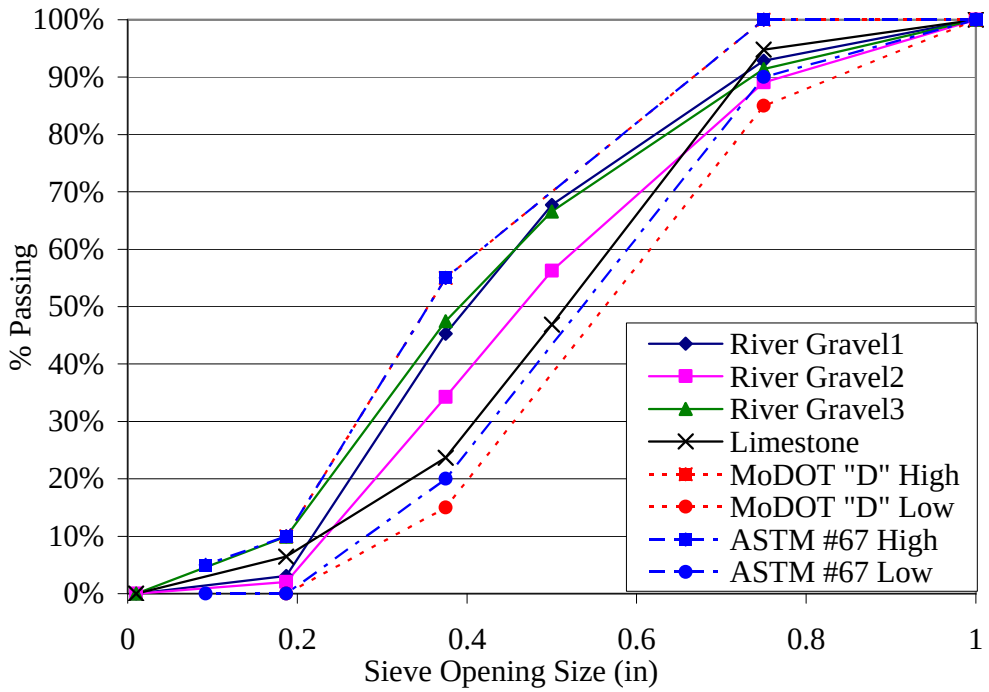

Conversion: 1 inch = 25.4 mm

Figure 4.2 – Coarse Aggregate Sieve Analysis

All of the collected material parameters were gathered, and consistently tracked over time for variables that may change such as moisture content. The material properties were paired with the batch proportions determined for use in each of the mix designs. A spreadsheet was used to determine the appropriate material batch weights, based on the material absolute volumes. A sample of the batch weight spreadsheet can be found in

Appendix C below, along with the spreadsheets used to collect the appropriate fresh concrete properties.

4.3 FRESH PROPERTIES

All laboratory mixtures were tested for the same fresh properties, with field mixtures being tested for only part of the test regimen. SCC laboratory mixtures were tested to measure passing ability, consistency and filling ability, stability, unit weight, and air content. SCC field mixtures only measured filling ability, unit weight, and air content. All CC mixtures were measured for consistency (slump), unit weight, and air content. **Figure 4.3** below shows the $6ft^3$ ($0.17\ m^3$) mixer used for all laboratory batching.

Figure 4.3 – 6 Cubic Foot Mixing Drum

The slump flow test was used to assess consistency and filling ability of all SCC mixtures following ASTM C 1611 – 2009, Standard Test Method for Slump Flow of Self-Consolidating Concrete (ASTM C 1611 2009). The metrics of slump flow, T_{50}

(Sometimes T_{20} as in 20 inches rather than 50 centimeters), and VSI are all measured using ASTM C 1611 – 2009. Slump flow is the average of the maximum and perpendicular diameters of the concrete disc resulting from a slump cone being filled with SCC and then lifted; this researcher used the inverted slump cone procedure. T_{50} is the time required for the slump flow concrete disc to grow to 50 cm (Sometimes called T_{20} for 20 inches) in the largest diametrical dimension, and indicates viscosity. Finally VSI, or Visual Stability Index, is a subjective visual indication of the stability of the resultant slump flow disc represented as a number from 0-3. A VSI of 0 indicates a stable SCC and 3 is unstable, as evident by a concentration of coarse aggregate in the center of the disc, and a mortar halo around the perimeter of the disc. Guidance is given in the ASTM C 1611 – 2009 document for determining VSI. **Figure 4.4(a) – Figure 4.4(c)** below shows the slump flow test.

(a) Place SCC into inverted slump cone

(b) Lift cone and allow SCC to flow (slump flow of 23.5 inches [595 mm] pictured)

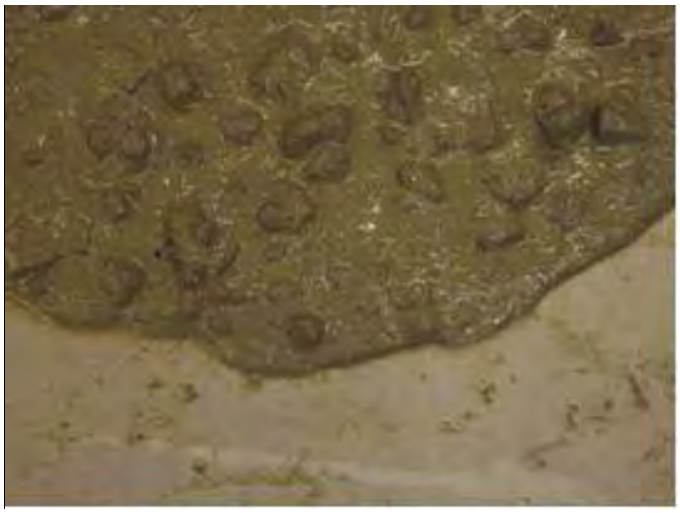

(c) Close-up for Determining VSI (VSI=1; No Mortar Halo, but Surface Sheen)

Figure 4.4 – Slump Flow Test

Passing ability was evaluated using two test methods. The non-standard, but widely known, “L-box” test was performed, along with the standardized “J-Ring” in the form of ASTM C 1621 – 2009, Standard Test Method for Passing Ability of Self-Consolidating Concrete by J-Ring (ASTM C 1621 2009). The J-ring test is essentially the slump-flow test, with a ring of vertical bars surrounding the inverted slump cone prior to

lifting. The maximum and perpendicular diameters of the concrete disc are averaged, and compared to the slump flow average diameter; passing ability is then determined from the magnitude of the difference. Guidance is given by Table 1 in ASTM C 1621 – 2009 for evaluating passing ability by use of blocking assessment. The L-box test also measures passing ability, but using a different setup. To view the J-ring and L-box setup, see **Figure 4.5** below. The L-box consists of a bottom trough with a vertical box attached, creating an L shape. The vertical box is gated at the bottom, with vertical bars beyond the gate. The vertical box is filled, the gate opened, and the SCC is allowed to flow through the bars and down the trough. The depth of SCC at the end of the trough is measured and divided by the depth of the SCC at the gate; this ratio of depth is used as the parameter to assess passing ability. An L-box test result of 0.85-1.00 can generally be regarded as having adequate passing ability.

Figure 4.5 – J-ring (left) (J-ring of 22.5 inches [570 mm] pictured) **and L-box (Right)**

Next, stability for the laboratory SCC mixture was measured using ASTM C 1610 – 2010, Standard Test Method for Static Segregation of Self-Consolidating Concrete

Using Column Technique (ASTM C 1610 2010). In **Figure 4.6** below, you see the 26 inch (660 mm) tall column used in the segregation column test. The column is filled with SCC and allowed to sit, undisturbed for 15 minutes. The top and bottom fourths are then retained and washed over a #4 (4.75mm) sieve. This researcher then oven-dried the resulting aggregate and performed the calculations prescribed in ASTM C 1610 – 2010 to determine the static segregation of the SCC mixtures, this indicates stability of the mixture.

Figure 4.6 – Segregation Column

For all concrete mixtures, except one set of field specimens, the unit weight was determined as in ASTM C 138 – 2010, Standard Test Method for Density (Unit Weight), Yield, and Air Content (Gravimetric) of Concrete (ASTM C 138 2010). The container used to measure unit weight was the base used in measuring air content by the pressure method; **Figure 4.7** below shows the pressure meter and base. For all concrete mixtures,

the air content was measured per the procedure in ASTM C 231 – 2010, Standard Test Method for Air Content of Freshly Mixed Concrete by the Pressure Method (ASTM C 231 2010). Because this standard is for conventional concrete, this researcher should note that no tamping or striking with a mallet was performed for the SCC mixtures during placement into the test apparatus; only the final strike with a mallet while releasing the pressure valve was performed to obtain an accurate reading from the pressure meter.

Figure 4.7 – Pressure Meter and Base Used for Unit Weight and Air Content

Lastly for the fresh property tests, for CC mixtures, slump was used to measure consistency and was performed in accordance with ASTM C 143 – 2010, Standard Test Method for Slump of Hydraulic-Cement Concrete (ASTM C 143 2010).

Manual consolidation through tamping was performed for CC mixtures when placing. All specimens were covered for approximately 1 day with plastic sheeting and then transported to a moist cure room. Placement and curing was performed to a standard consistent with ASTM C 192 – 2007, Standard Practice for Making and Curing Concrete

Test Specimens in the Laboratory (ASTM C 192 2007). It should again be noted that SCC mixtures were not manually consolidated, only placed and allowed to self-consolidate.

The fresh concrete properties were measured throughout the execution of this investigation, and therefore will be reported. **Tables 4.3** and **Table 4.4** below concisely organize the experimental program for fresh properties, and their results. The test results were gathered in this study for acceptance of concrete for forming mechanical and shear test specimens; therefore, the results are shown without a thorough analysis.

Table 4.3 – Fresh Property Tests and Results for Limestone Mixtures

	ASTM (if standard) test method and test description							
Name	C143 Slump (in)	C138 Unit Weight (lb/ft^3)	C231 Air Content (%)	C1610 Segregation (%)	C1611 Slump Flow (in)	VSI	C1621 J-Ring (in)	L-box (in/in)
C4-58L	6.5	145.6	5.3	---	---	---	---	---
S4-36L	---	139.2	8.5	---	24.5	1	23.5	---
S4-60L	---	138.8	6.9	---	22.5	1	19.5	---
C6-58L	8.5	144.7	5.5	---	---	---	---	---
S6-36L	---	142.7	7.0	3.5	21.0	0	20	.43
S6-48L	---	139.6	7.3	12.3	25.5	1	25.0	.66
S6-60L	---	144.9	5.0	4.0	26	1	25.5	0
C10-58L	9	148.4	2.8	---	---	---	---	---
S10-36L	---	143.5	3.4	101.7	29	3	30	.96
S10-48L	---	146.4	2.2	31.2	28.5	2	28.5	.94
S10-60L	---	150.0	1.6	**	28.5	1	28	.67
S6-36L*	---	145.6	4.4	---	28.5	1	27	---
S6-60L*	---	143.2	1.6	---	29	2	28.5	---

***** Indicates replicate batch, for supplementing shear test information for bad test results.

** Indicates lost specimen from failure of the segregation column from leaking

Conversion: 1 inch = 25.4 mm
1 lb/ ft^3 = 16.02 kg/m^3

Table 4.4 – Fresh Property Tests and Results for River Gravel Mixtures

	ASTM (if standard) test method and test description							
Name	C143 Slump in	C138 Unit Weight lb/ft^3	C231 Air Content %	C1610 Segregation %	C1611 Slump Flow in	VSI	C1621 J-Ring in	L-box in/in
C6-58R	6.5	145.5	3.3	---	---	---	---	---
S6-36R	---	141.3	6.5	5.1	25	1	24	.87
S6-48R	---	143.9	3.0	10.4	27	1	26.5	0
S6-60R	---	141.5	5.8	1.6	22.5	1	21.5	0
C10-58R	2	145.6	2.6	---	---	---	---	---
S10-36R	---	144.3	3.0	1.0	29	0	29	.96
S10-48R	---	143.9	2	1.6	27.5	1	27.5	.95
S10-60R	---	145.9	1.5	5.5	27.5	1	26	.82
S9-57R	---	---	2.8	---	27.5	---	---	---

Conversion: 1 inch = 25.4 mm
1 lb/ ft^3 = 16.02 kg/m^3

The acceptance criteria for shear testing were broad. With the batch proportions used, the slump of the concrete was approximately 0 to 0.5 inches (0 to 13 mm) before the addition of HRWRA, and the final slump or slump flow was achieved almost entirely through HRWRA addition. While batch proportions were established through surveys and not through trial batches, large fresh property variation was experienced; however, the fresh properties do not affect shear behavior and the large variation is of little concern for this investigation. For the baseline concrete mixtures also used by researchers investigating shrinkage, creep, and durability, additional trial batching was conducted and tighter tolerances were enforced. Overall, the SCC fresh concrete mixtures used exhibited high filling ability with moderate passing ability and therefore moderate filling capacity.

5. HARDENED PROPERTIES

5.1 INTRODUCTION

Tests were conducted to investigate the hardened concrete mechanical properties of modulus of elasticity (MOE, E_c), unconfined compressive strength (f'_c), and splitting tensile strength (STS, f_{sp}). The tested properties will impact concrete behavior and are therefore important for analyzing companion shear specimens discussed later. These hardened properties were tested for all concrete batch proportions, but not necessarily at all test ages. **Table 5.1** shows the tests performed at various ages of the specimens; there was some variation from **Table 5.1** due to scheduling, particularly for the specimens formed while at Coreslab Structures, Inc. in Marshall, MO.

Table 5.1 – Target Test Ages for Hardened Properties

Specimen Age	Compressive Strength	Modulus of Elasticity	Splitting Tensile Stress
1 day	X	---	---
7 day	X	---	---
28 day	X	---	---
56 day*	X	X	X

***** Some specimens were not tested through the full 56 day period, only through 28 days. These would have MOE and STS results at 28 days.

Concrete compressive strength, f'_c, is used extensively when working with concrete. Numerous models that describe behavior, from those as rudimentary as empirical relationships to the most complex of theories, use concrete compressive strength as a key variable. There are even models correlating concrete compressive

strength to other design variables like those investigated in this study of MOE and STS. Modulus of Elasticity (MOE) is a measure of a material's elastic deformation under load. MOE is used in calculations such as deformations, deflections, and in determining the stiffness of members.

Of interest to this study is also the splitting tensile strength (STS). The STS is an indirect measure of the tensile strength of the concrete. The concept is that a cross-section of a concrete cylinder, when loaded in compression on one diameter, acts as a principally loaded stress element. The loaded concrete cross section results in principal tensile stresses being produced in the perpendicular diameter, which causes cracking when the stress exceed the tensile strength of the concrete. **Figure 5.1** below shows the concept behind the STS test as well as the theoretical stress distribution developed in the cross section of the specimen. The theoretical maximum tensile stress is $2P/\pi LD$, where P is the applied compressive load, L the cylinder length, and D the cylinder diameter (Mindess 2003).

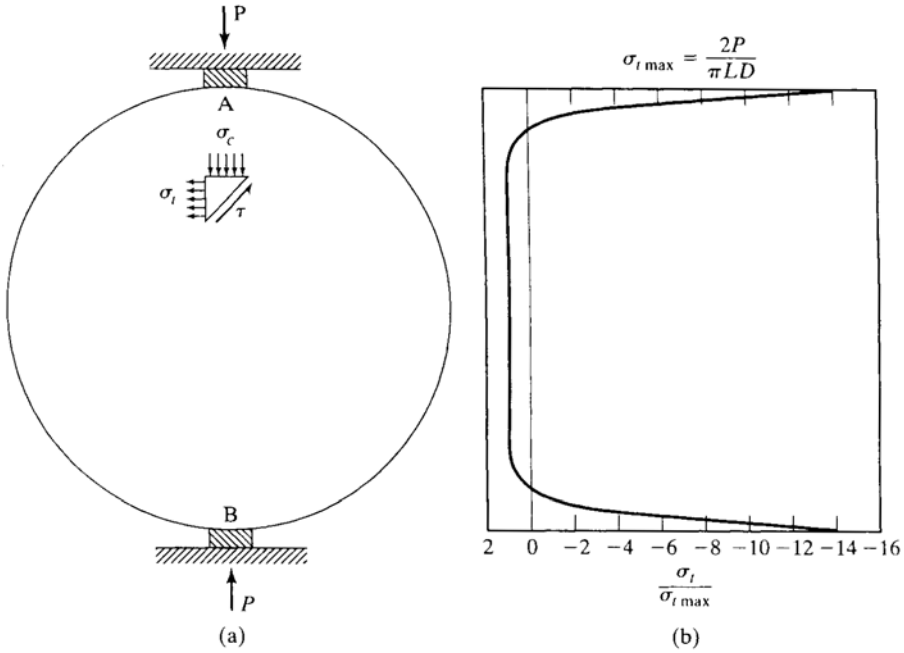

Figure 5.1 – STS Diagram (Mindess 2003)

From the figure, it is seen that the majority of the cross-section is loaded in uniform tension; when this tensile stress exceeds the tensile strength of the concrete, the specimen will fail and split along the vertical diameter.

5.2 TEST SETUP AND PROCEDURE

With the understanding that concrete compressive strength is an important variable to determine, we must test it accurately, with repeatability. ASTM C 1231 – 2010, Standard Practice for Use of Unbonded Caps in Determination of Compressive Strength of Concrete Cylinders, was used for determining concrete compressive strength (ASTM C 1231 2010). While ASTM C 1231 2010 requires qualification testing for use of neoprene pads with concrete equal to or greater than 12 ksi (82.7 MPa), this action was

not performed. Each specimen was tested on a 600,000 lb (2670 kN.) capacity Forney compression machine until failure. **Figure 5.2** below shows the execution and resultant failure of an unconfined compressive strength test.

MOE was determined using ASTM C 469 – 2010, Standard Test Method for Static Modulus of Elasticity and Poisson's Ratio of Concrete in Compression (ASTM C 469 2010). Several modifications to the standard were made:

- The load was removed abruptly, not at the same rate of loading
- The concrete compressive strengths and MOE were not measured on the same loading
- Companion specimens to determine compressive strength were not used prior to MOE testing, only 1 specimen, then subsequent MOE specimens

To clarify the last deviation, ASTM C 469 2010 requires a set of companion cylinders be used to determine compressive strength such that the 40% stress level can be used for MOE specimen loading; this researcher performed 1 strength test, using the determined value as the compressive strength for the first MOE test. The first MOE specimen was subsequently loaded to failure to make a second determination of compressive strength, which was averaged with the first specimen, and provided the 40% stress level for the second MOE test, and so on. **Figure 5.2** below also shows the MOE test being performed on a cylinder that will then be stressed to failure for testing of compressive strength, f'_c.

(a) Modulus of elasticity (MOE) test and gage

The same specimen is used for compressive strength:

(b) During test (c) Test specimen after failure

Figure 5.2 – MOE and Compressive Strength Test

The STS investigation followed ASTM C 496 – 2011, Standard Test Method for Splitting Tensile Strength of Cylindrical Concrete Specimens (ASTM C 496 2011). Two modifications to the standard test procedure were made. The specification calls for

supplementary bearing bars when the test specimen exceeds the length of the loading machine's bearing plate, of a thickness equal to the excess length of the specimen. The large thickness of the supplementary bearing bar is intended to ensure uniform loading along the entire length of the specimen. In this study, the excess length of the specimen was about 2 inches (51 mm), while the supplementary bearing bar was only about 1inch (25 mm) thick, resulting in a modification to the standard test. A small percentage of specimens fractured laterally (through the diameter), directly under the bearing plate, indicating that perhaps the supplementary bearing bar was not thick enough; however, this mode of failure was noted for these specimens. The next modification is in regard to the specified plywood bearing strips. The standard prohibits reuse of plywood bearing strips; however, this researcher used small strips of more durable particle board and continued reuse until imperfections were detected. See **Figure 5.3** for a picture of a STS specimen being tested.

Figure 5.3 – Splitting Tensile Strength (STS) Test

5.3 TEST RESULTS

The results from the compressive strength, MOE, and STS tests are presented in **Tables 5.2 – 5.6** below. The values listed in the tables are the average of individual test results.

Table 5.2 – Compressive Strength Test Results for Limestone Mixtures

	Compressive Strength, f'_c (psi)			
Designation	1 day	7 day	28 day	56 day
C4-58L	2560	5290	6130	---
S4-36L	2790	4910	5850	---
S4-60L	1870	4150	4900	---
C6-58L	4450	6190	7600	---
S6-36L	5530	7350	9460	---
S6-48L	4270	6390	8140	8410
S6-60L	5240	7530	9400	---
C10-58L	5330	8690	10,820	11,210
S10-36L	6390	10,780	13,010	12,580
S10-48L	7380	11,100	13,450	13,740
S10-60L	6850	11,330	13,450	13,880
S6-36L*	6550	9450	10,770	---
S6-60L*	5770	9840	11,050	---

***** Indicates replicate batch, for replacing poor shear test information

Conversion: 1000 psi = 6.89 MPa

Table 5.3 – Compressive Strength Test Results for River Gravel Mixtures

	Compressive Strength, f'_c (psi)			
Designation	1 day	7 day	28 day	56 day
C6-58R	6990	10,050	10,180	10,750
S6-36R	6150	9270	10,070	10,640
S6-48R	6410	9860	10,380	10,530
S6-60R	5550	7770	8440	8710
C10-58R	5630	8120	9450	---
S10-36R	8360	12,210	13,940	14,510
S10-48R	7970	12,030	13,650	14,420
S10-60R	7680	11,320	13,570	13,920
*S9-57R	3440	6630	8410	9190

* Supplementary mixture from another research project on MS&T campus

Conversion: 1000 psi = 6.89 MPa

Table 5.4 – Compressive Strength Test Results for Coreslab Specimens

	Compressive Strength, f'_c (psi)				
Designation	1 day	4 day	8 day	14 day	28 day
C6-58L	4810	5110	5620	5630	5730
S6-48L	5660	5840	6690	6910	6950
C10-58L	5670	7890	7950	8360	8480
S10-48L	6330	8300	8600	9100	9250

Conversion: 1000 psi = 6.89 MPa

Table 5.5 –MOE, STS, and Coefficients Test Results for Limestone Mixtures

	(psi)		Unit-less Coefficient	
Designation	MOE	STS	MOE	STS
C4-58L	3,837,000	385	54,800	5.5
S4-36L	3,683,000	445	53,600	6.5
S4-60L	3,141,000	380	49,800	6.0
C6-58L	4,614,000	370	52,900	4.3
S6-36L	5,111,000	565	52,600	5.8
S6-48L	4,435,000	460	48,400	5.1
S6-60L	4,855,000	520	50,100	5.4
C10-58L	5,243,000	550	49,500	5.2
S10-36L	5,880,000	580	52,400	5.2
S10-48L	6,046,000	760	51,600	6.5
S10-60L	5,586,000	800	47,400	6.8
S6-36L*	5,188,000	575	54,000	6.1
S6-60L*	5,020,000	570	51,700	5.9

***** Indicates replicate batch, for supplementing shear test information for bad test results.

Conversion: 1000 psi = 6.89 MPa

Table 5.6 –MOE, STS, and Coefficients Test Results for River Gravel Mixtures

	(psi)		Unit-less Coefficient	
Designation	MOE	STS	MOE	STS
C6-58R	5,892,000	680	56,800	6.6
S6-36R	5,602,000	725	54,300	7.0
S6-48R	5,812,000	690	56,600	6.7
S6-60R	4,845,000	580	51,900	6.2
C10-58R	5,349,000	550	55,000	5.6
S10-36R	6,767,000	790	56,200	6.5
S10-48R	6,515,000	730	54,300	6.1
S10-60R	6,338,000	745	53,700	6.3
S9-57R	5,009,000	680	52,300	7.1

Conversion: 1000 psi = 6.89 MPa

The initial test program intended to test strength only through 28 days and conducting MOE, STS, and the shear tests of precracking and push-off at the “Ultimate” age of 28 days. Some issues arose when performing the shear tests on the first mixtures to reach 28 days, so subsequently cast mixtures were allowed to continue curing through 56 days while the issues were resolved. The shear test results on the mixtures where the issues were noticed were thrown out, and re-batching was conducted to generate new specimens; these subsequent specimens were only cured for 28 days. The testing of shear properties at 28 days as compared to 56 days was not considered to be an issue. Concrete is sufficiently mature, especially concrete made with type III cement, within 28 days, that additional curing to 56 days does not significantly alter the concrete micro structure or pore water distribution.

The following section discusses in more depth the results presented above. Conclusions are presented regarding the hardened concrete properties and why they are important to this study.

5.4 DATA ANALYSIS AND CONCLUSIONS

The results from above are compiled and presented visually in **Figures 5.4 – 5.8**. The strength development of the various mixtures throughout this investigation is plotted in **Figure 5.4**. It is beneficial for both MOE and STS to be normalized with respect to the square root of the compressive strength ($\sqrt{f'_c}$) for comparison to values suggested by the American Concrete Institute (ACI). The MOE, STS, and their coefficients are shown below in **Figure 5.5 – 5.8**.

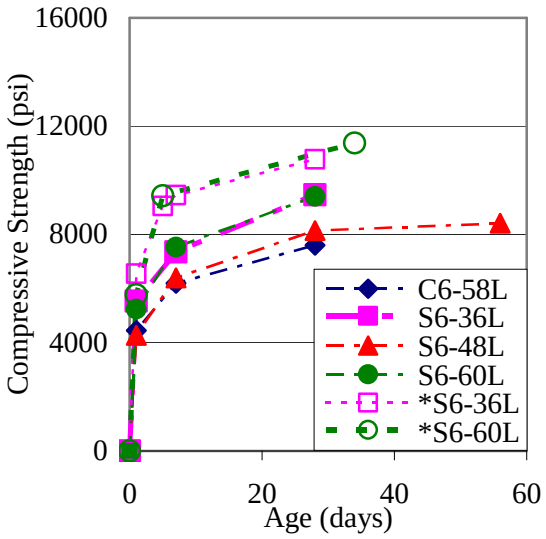

(a) 6ksi target limestone mixtures

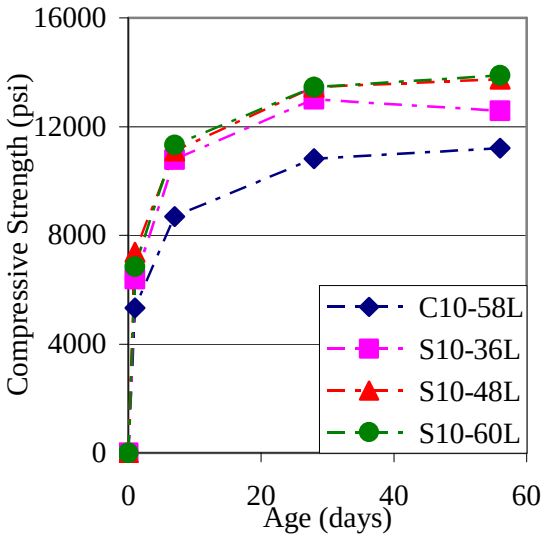

(b) 10ksi target limestone mixtures

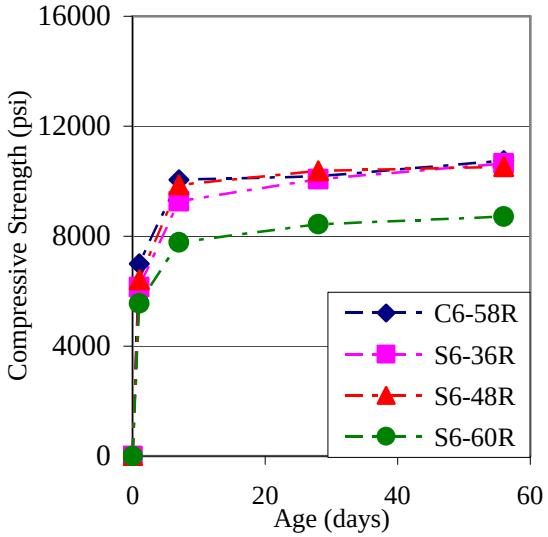

(c) 6ksi target river gravel mixtures

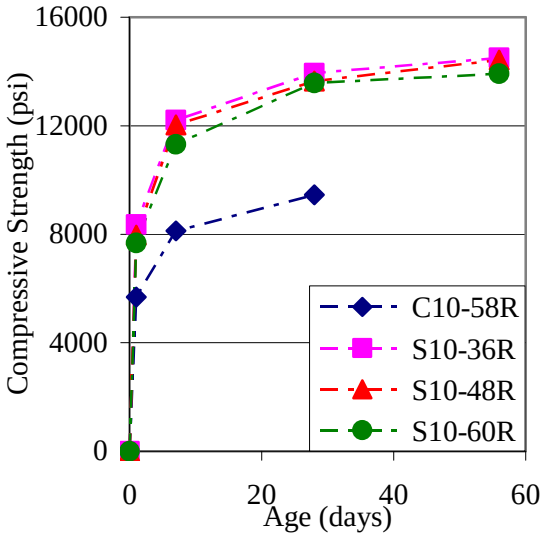

(d) 10ksi target river gravel mixtures

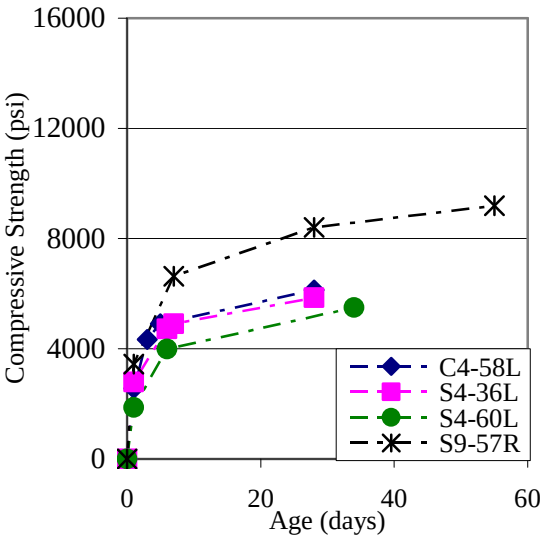

(e) Additional mixtures; 4 ksi limestone and 9 ksi pea gravel

Conversion: 1000 psi = 1 ksi = 6.89 MPa

Figure 5.4 – Compressive Strength Development over Time

Observe from the strength development curves of **Figure 5.4** a very high rate of strength development at early ages, with a rapid depletion of additional strength gain; this is the type of curve expected for concrete mixtures with type III cement as was used in this investigation, and is also typical of precast concrete suppliers. Some HRWRA's can also contribute to higher early strengths. The manufacturer's product data sheet for the HRWRA used throughout this project (in **Appendix A**), Glenium 7700, indicates potential for higher early strengths (BASF 2010).

Besides the general shape of the strength development curves, the "ultimate" strengths achieved at the time that the shear tests commenced were all higher than the target strengths. The higher-than-target strengths should not be surprising given the mix development process described in **Section 3** where survey results were the primary factors considered in material proportioning. Also observe that the strengths achieved at the time of shear testing are fairly consistent for each group of curves that kept aggregate type and w/c ratio constant.

Next, review the results for the MOE and STS tests performed. Note that **Figure 5.5** and **Figure 5.6** show the test results for MOE and STS respectively and that **Figure 5.7** and **Figure 5.8** show the test results normalized with respect to $\sqrt{f'_c}$ for comparison to typically expected values according to ACI.

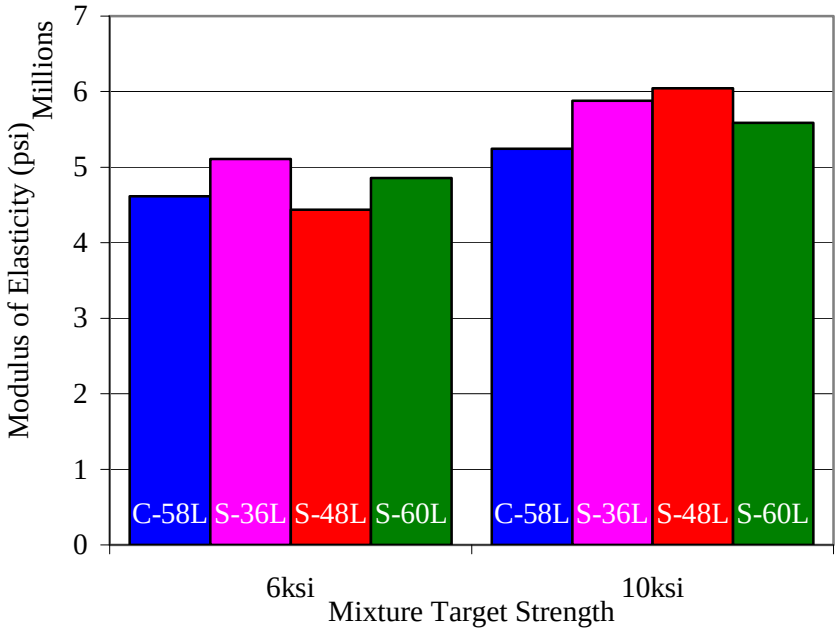

(a) Limestone mixtures

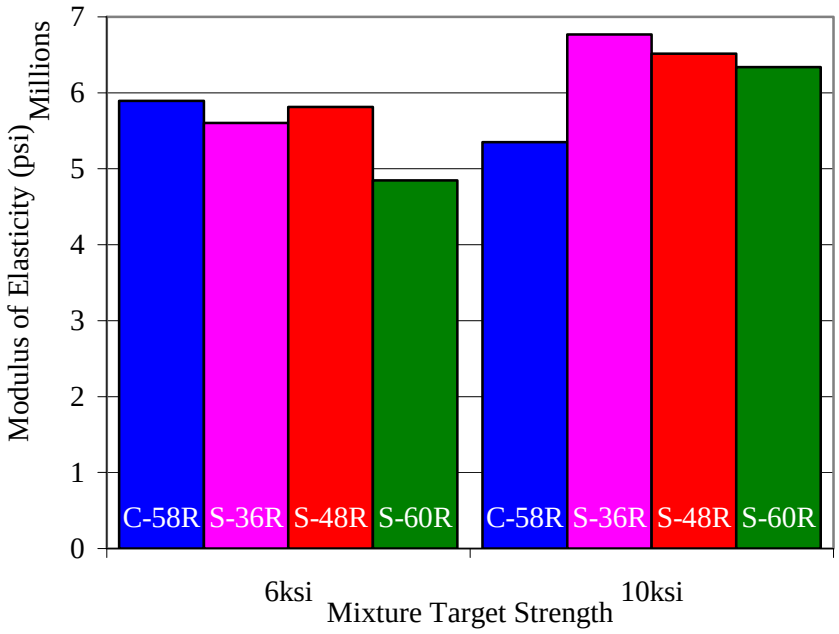

(b) River gravel mixtures

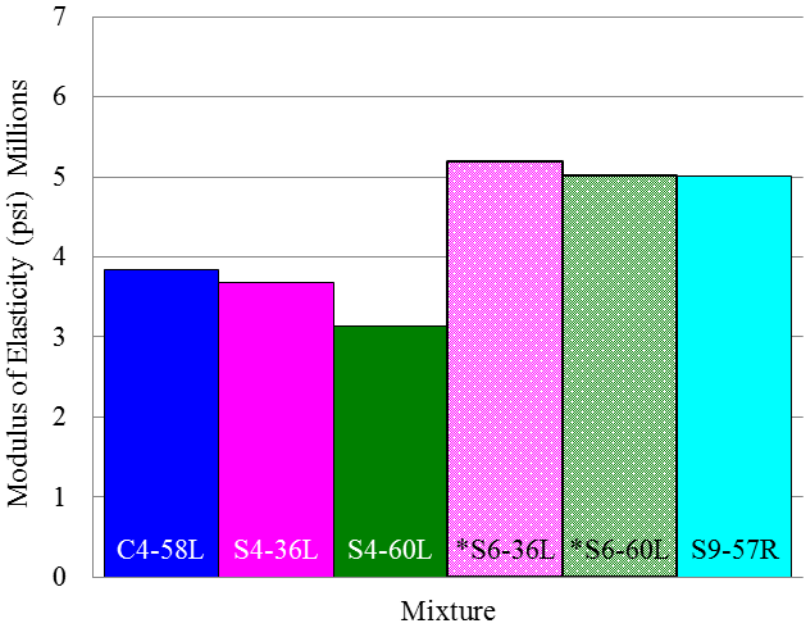

(c) Additional Mixtures; 4 ksi limestone, 6 ksi re-batch, and 9 ksi pea gravel

Conversion: 1 ksi = 6.89 MPa

Figure 5.5 – "Ultimate" MOE for All Mixtures

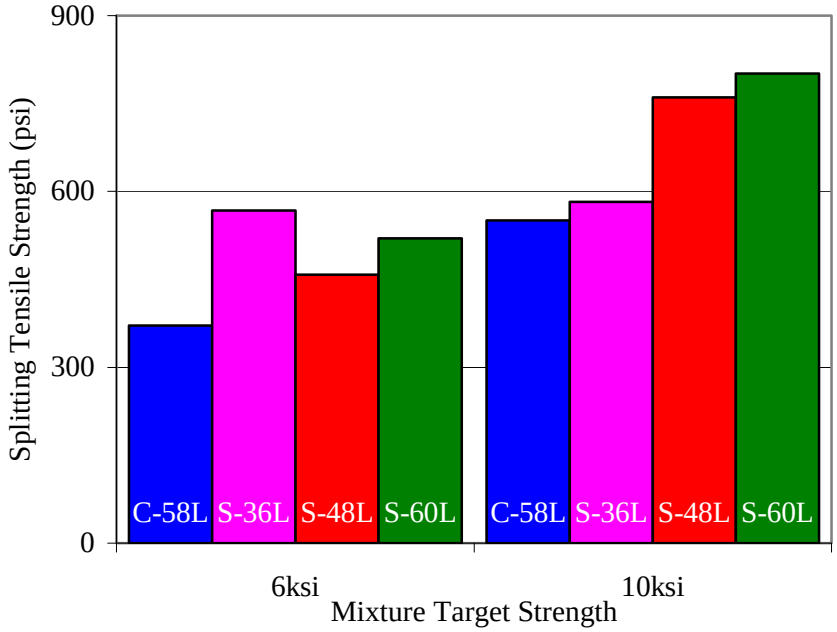

(a) Limestone mixtures

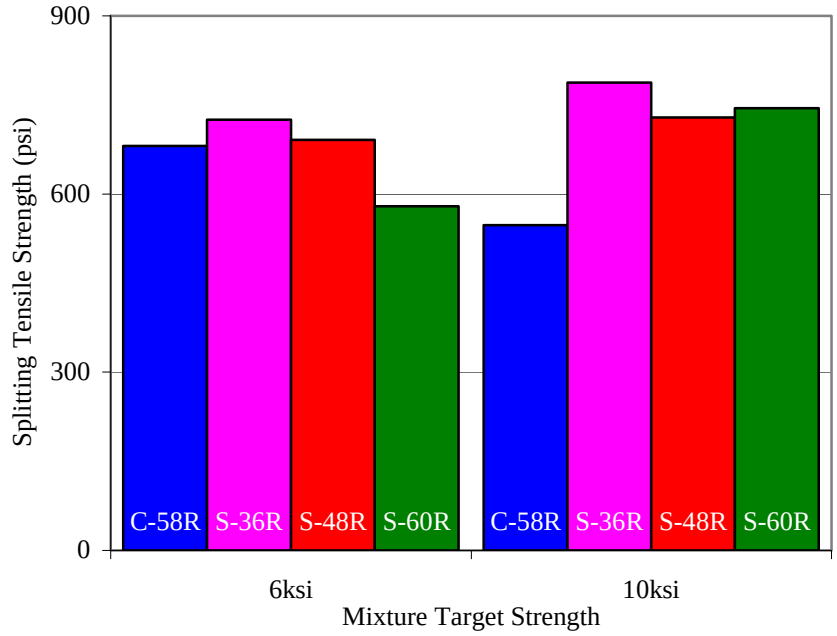

(b) River gravel mixtures

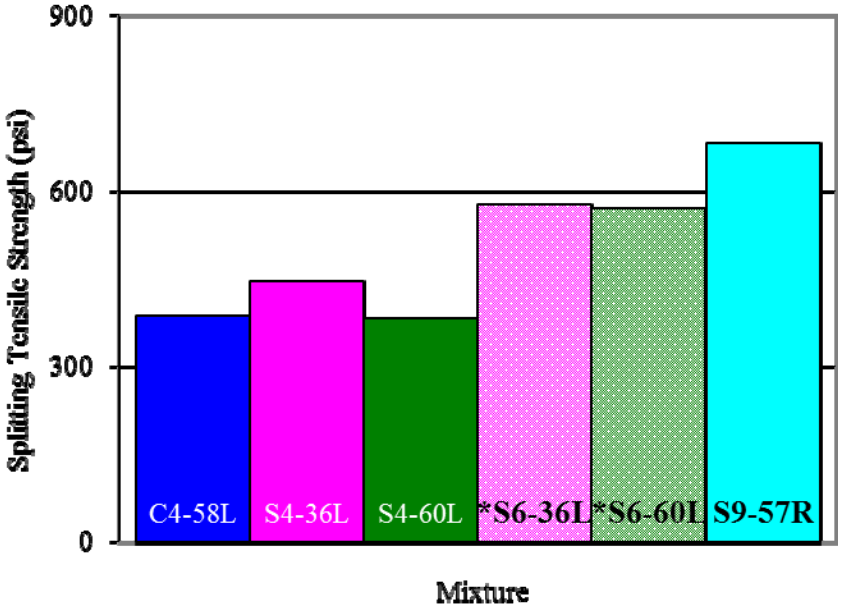

(c) Additional Mixtures; 4 ksi limestone, 6 ksi re-batch, and 9 ksi pea gravel

Conversion: 1000 psi = 1 ksi = 6.89 kPa

Figure 5.6 – "Ultimate" STS for all Mixtures

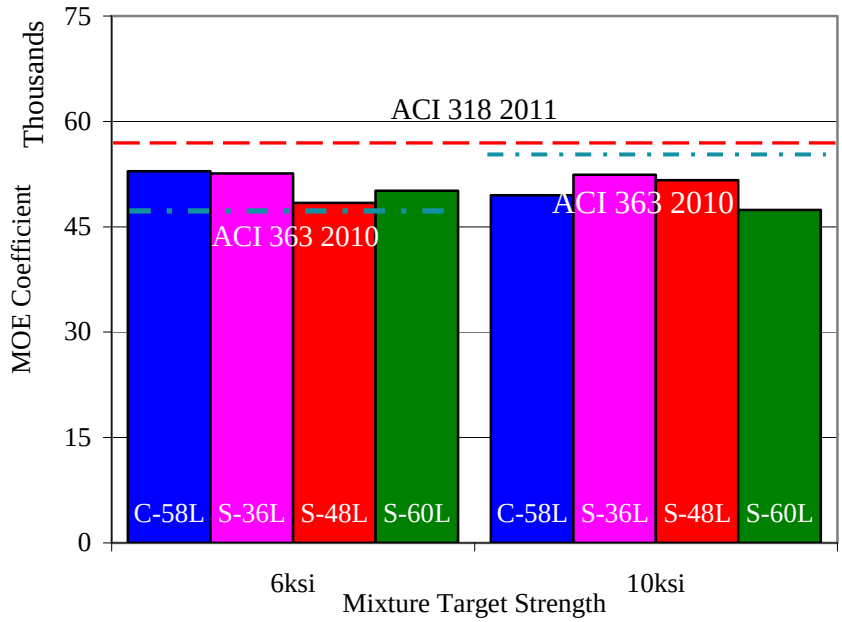

(a) Limestone mixtures

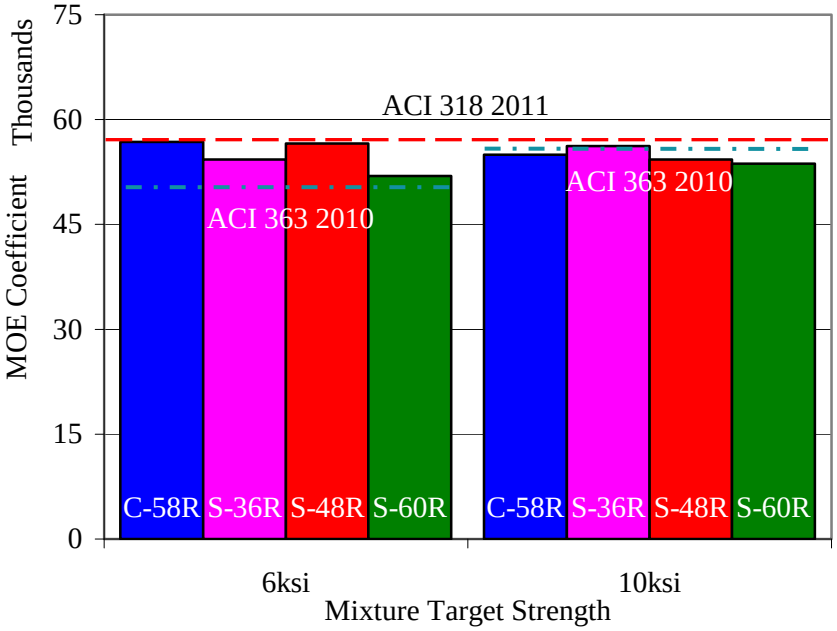

(b) River gravel mixtures

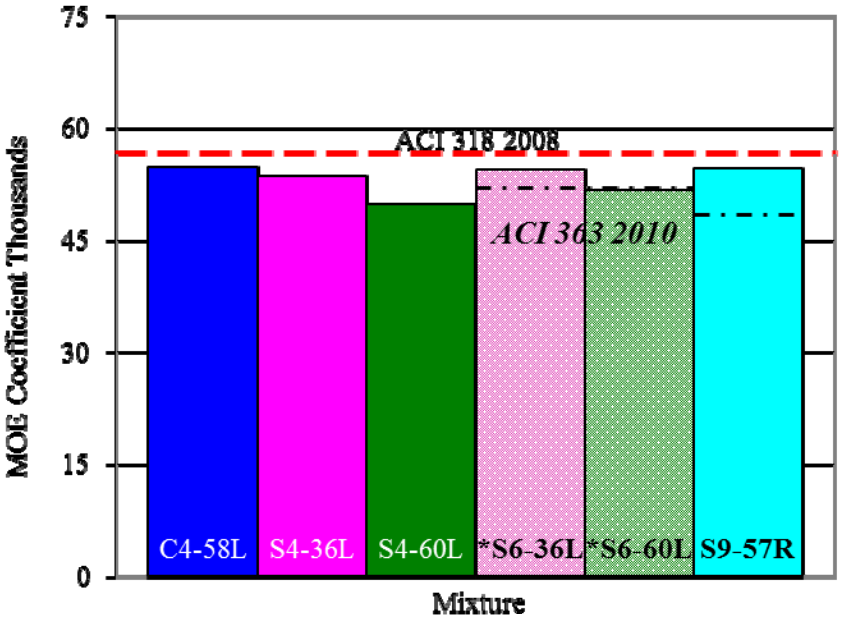

(c) Additional Mixtures; 4 ksi limestone, 6 ksi re-batch, and 9 ksi pea gravel

Conversion: 1 ksi = 6.89 MPa

Figure 5.7 – Normalized "Ultimate" MOE

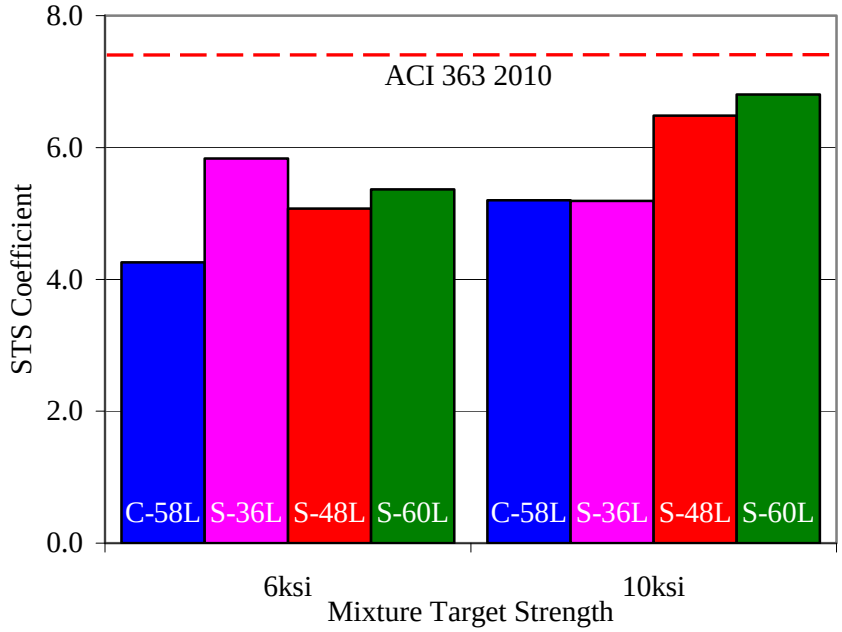

(a) Limestone mixtures

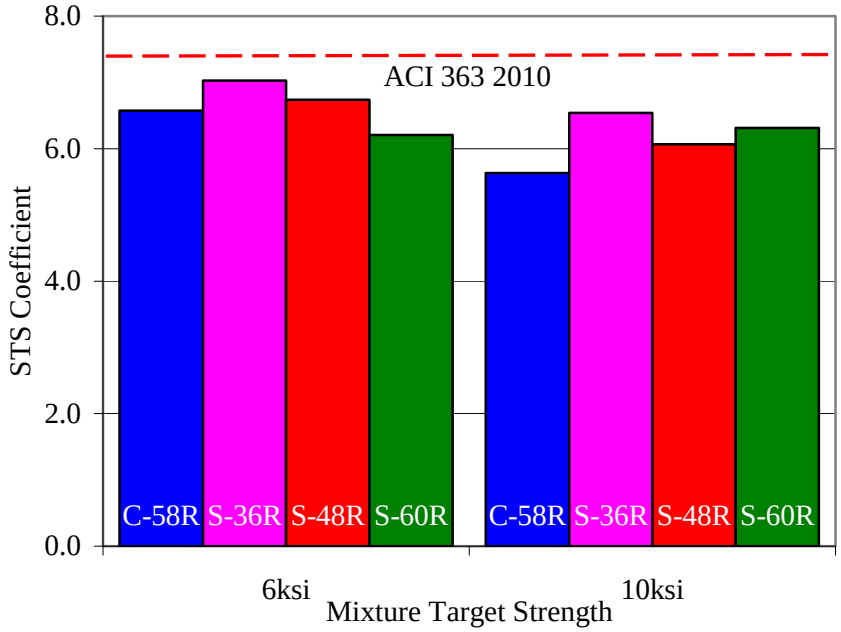

(b) River gravel mixtures

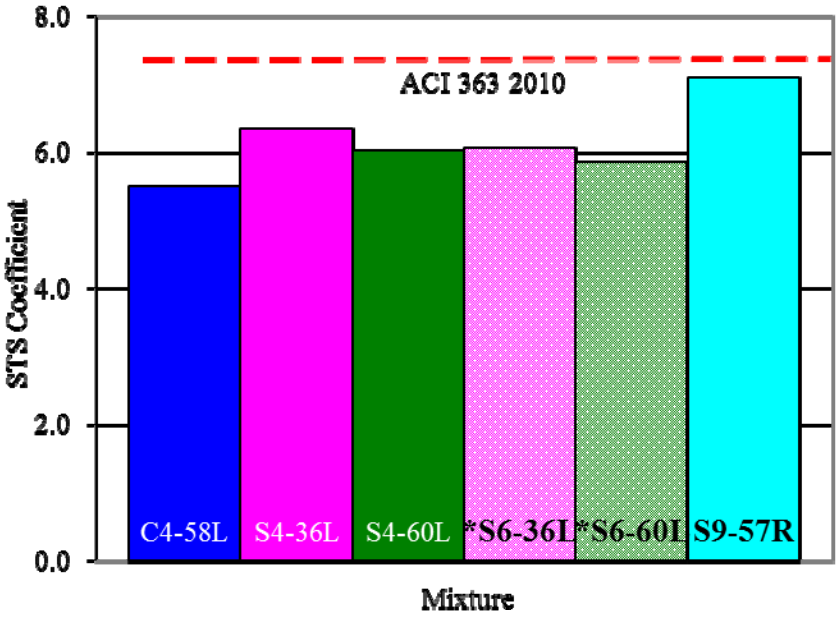

(c) Additional Mixtures; 4 ksi limestone, 6 ksi re-batch, and 9 ksi pea gravel

Conversion: 1 ksi = 6.89 MPa

Figure 5.8 – Normalized "Ultimate" STS

Figures 5.5 and **5.6** both show that the higher strength mixtures as well as the river gravel mixtures tend to have higher values of MOE and STS compared to the lower strength limestone mixtures. The coefficient for MOE of normal density concrete (90 – 160 lb/ft^3 [1440 – 2560 kg/m^3]) is permitted to be taken as 57000 (ACI 318 2011). The MOE coefficient for normal density high strength concrete is variable as it consists of a coefficient plus a constant as is shown in **Eq. 5.1** (ACI 363 2010). It should be noted that this empirical model was developed as a lower bound predictor for HSC.

$$E_c = 40000\sqrt{f'_c} + 10^6 \quad \text{(psi)} \qquad \left[E_c = 3320\sqrt{f'_c} + 6900\right] \quad \text{(MPa)} \qquad (5.1)$$

The ACI coefficients for MOE are indicated in **Figure 5.7**. Both the normalweight and normal density high strength MOE coefficient predictors were shown since the target strengths were exceeded for all concrete batch proportions as indicated in **Table 5.2** and **Table 5.3** above; the result is that some mixtures may be better predicted by high strength models, and this is explored. The limestone mixtures were slightly less stiff than predicted by the normalweight concrete approximation, but more closely matched the high strength model. The river gravel mixtures were reasonably estimated by either ACI approximation when normalized for compressive strength, but again even more accurately by the high strength model (ACI 318 2011; ACI 363 2010). The lower MOE coefficient of the limestone mixtures could be due to the weak or soft nature of Missouri limestone aggregates.

ACI 318 does not address STS for anything other than lightweight concrete; therefore, the ACI 363 source is quoted. As all target strengths were exceeded as

mentioned previously, the ACI 363 approximation is likely valid. The ACI coefficient for STS is given by committee 363 as 7.4 and it can be seen in **Figure 5.8** that all mixtures had significantly lower coefficients for all strengths, but especially the 6 ksi (41.4 MPa) target strength limestone series. For each test series, the CC of that series exhibited lower STS than the SCC; this could be due to improved consolidation and homogeneity of SCC during placement. The very low coefficient for STS of the limestone, but only slightly low for the river gravel, could indicate weak transition zones between the aggregate and paste, or more likely, it could be indicative of again having weak Missouri limestone aggregates such that a fracture develops and propagates through the aggregate rather than taking the longer path around the aggregate in the interfacial transition zone (Mindess 2003). The argument for weak limestone aggregates is supported by the recorded STS fracture plane; limestone specimens had much more coarse aggregate fracturing in the failure plane, usually 90-100%, while river gravel specimens consistently had only 65-75%.

From the hardened concrete properties tests there is a clear understanding of concrete compressive strength, f'_c, modulus of elasticity, E_c (MOE), and splitting tensile strength, f_{sp} (STS), of the concrete batch proportions used. The strength development was "high-early" and was consistently higher than targeted or predicted "ultimate" strengths, while maintaining low variability between mixtures that hold the w/c ratio and aggregate type constant. The MOE for each concrete was known; the limestone mixtures were slightly lower than what would be predicted by ACI; this was thought to be due to the soft nature of the Missouri limestone used. The STS for all mixtures were lower than what would be predicted by ACI, especially the 6 ksi (41.4 MPa) target strength

limestone mixtures. The low STS of the limestone mixtures could be caused by poor bond between the mortar and aggregate or, more likely, again because of the weak nature of Missouri limestone aggregates (ACI 318 2011, ACI 363 2010).

6. PUSH-OFF TEST

6.1 INTRODUCTION

The push-off test is a non-standard, but widely recognized, test used in the testing of shear in concrete. Early researchers include Mattock (1969; 1972), Reinhardt (1981), and Walraven (1981; 1994). Later studies in shear using reinforced panels have refined, but also confirmed, the validity of the models derived from using push-off specimens (Vechio and Lai 2004). The push-off test has the advantage of being relatively small, inexpensive, easy to perform, and not needing any highly specialized pieces of testing equipment; studies using shear panels require the use of a dedicated and expensive test apparatus. The ease with which one can test push-off specimens allows for many variables to be tested, even in relatively small studies. As was done in similar investigations, the specific materials and variables tested were employed to evaluate aggregate interlock shear behavior and evaluate trends. This study investigated varying levels of concrete compressive strength, coarse aggregate type, and coarse aggregate to fine aggregate volume ratios, and cast companion push-off specimens for small prestressed precast beams. The full push-off test matrix is located in **Section 4** and listed in **Table 4.1**. After completion of the push-off test, the tested specimens were retained and images of their cross-sections were made to investigate segregation as well as correlating C.A. volume fraction with shear resistance.

This section will detail the push-off test setup and procedure and the subsequent digital imaging performed. There were several difficulties experienced while performing the push-off tests; these difficulties will be shown, and the actions taken to remedy them

will be explained. The specimen size, geometry, and reinforcement will be detailed. Next, the test results will be presented and an analysis will follow. Lastly, conclusions will be made and summarized.

6.2 TEST SETUP AND PROCEDURE

Because the push-off test is non-standard, a detailed description of the test setup and procedure used throughout this study is necessary. Any departures from other researchers, whether done purposefully, or as an oversight, may be important to the resultant findings. The goal of this section would be for future researchers to be able to replicate the tests performed throughout this investigation and to confirm the findings.

6.2.1 Test Setup The shear test used in this study consists of two distinct steps; the first step is to "precrack" the specimen, the second is the actual "push-off" test where the bulk of shear behavior information is gathered. See **Figure 6.1** for an elevation view of both the precrack and push-off test. The precrack test is necessary, as it develops the shear crack initial condition. Researchers have also found that precracking is necessary to achieve an actual pure shear interface, otherwise shear along the interface with high concentrated tensile stresses at the ends of the notched insets develop just prior to cracking (Barragan 2006). Barragan developed a finite element model (FEM) representing an uncracked specimen loaded as in a push-off test, the high tension regions can be seen in **Figure 6.2** below, these tensile stresses are alleviated if precracking is performed.

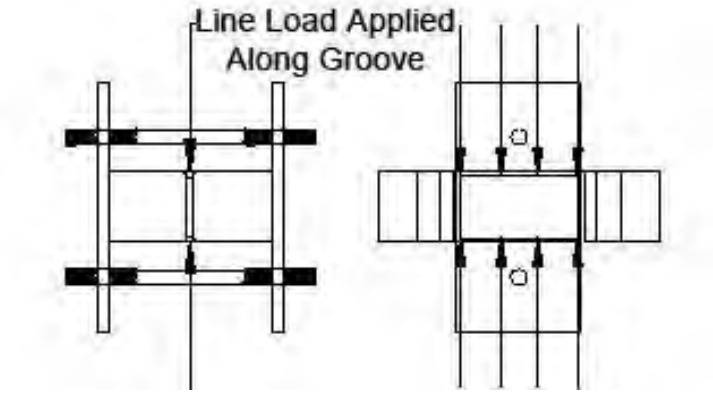

(a) Precrack Test

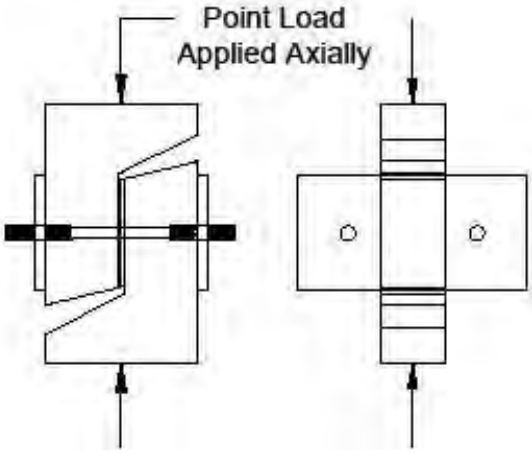

(b) Push-off Test

Figure 6.1 – Aggregate Interlock Test Orientations

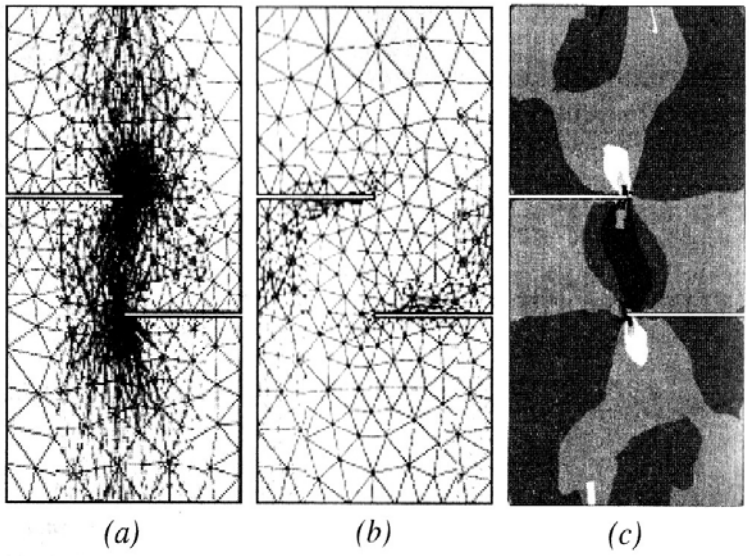

-Finite element mesh used and distributions of: (a) compressive; (b) tensile; and (c) shear stresses (darker areas indicate higher magnitudes of stress).

Figure 6.2 – Precracking Shown to Alleviate Tensile Regions by Barragan

The externally reinforced test specimen was used as described by Walraven and Reinhardt (1981). Some researchers have used this test setup with internal reinforcement to restrain the two sides, some have used external reinforcement for restraint; this investigation chose to use external reinforcement because of the variables important to the study. The variables of interest in this project were all constituents of the concrete contributing to the mechanism of aggregate interlock; whereas, internally reinforced push-off tests also introduce variables of reinforcement ratio and the mechanism of dowel action contributing to shear.

Data collected from the shear testing includes: the precrack load (P), crack opening (ω), crack slipping (δ), normal stresses (σ), and shear stresses (τ). The crack opening was measured and averaged by two separate point – symmetrically positioned

linear voltage displacement transducers (LVDTs) placed perpendicular to the crack, on opposite ends of the specimen, and on opposite faces as shown in **Figure 6.3**. Crack slippage was also measured with an LVDT as in **Figure 6.3**. The slip LVDT was placed parallel to the crack, across the notch to measure relative displacement of the two sides of the specimen. The load applied by the Tinius Olsen load machine was divided by the interfacial area and results in the applied shear stress. The normal stress was measured using two strain gages applied to each of the two external restraining bars positioned as in **Figure 6.4**. The strain in the bars was taken as the average of the two strain gages applied to each bar. The strain was converted to stress, and then force, with the known Young's modulus and cross-sectional area of the steel bars. The force acting within the restraining bars is thought to act uniformly over the shearing interface of known area and is the resulting normal stress of interest.

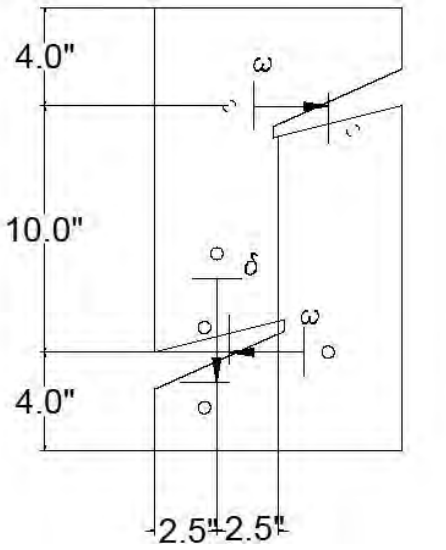

Conversion: 1 inch = 25.4 mm

Figure 6.3 – LVDT Placement for Measuring Crack Opening and Slip

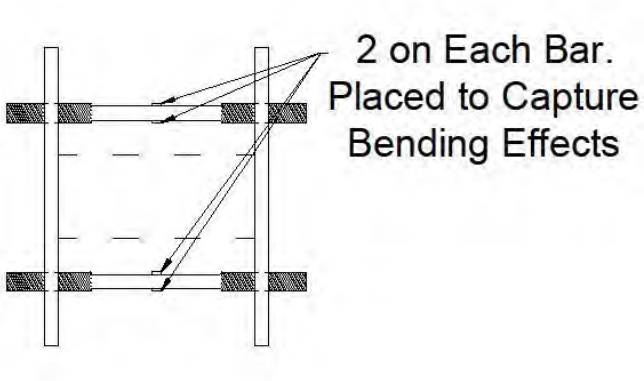

Figure 6.4 – Strain Gage Location on External Reinforcement

The size and geometry of the specimens used in this study were unique. The adjusted size was in response to some earlier experienced issues with testing and will be discussed in **Section 6.3** in detail. The resultant dimensions are shown in **Figure 6.22**.

The load blocks used for the precrack and push-off tests also warrant discussion. The load blocks are shown in **Figure 6.5**. The precrack load block consists of a piece of 2 x 2 x 1/4 inch (51 x 51 x 6.4 mm) steel angle welded to a 7.5 x 3 x 3/4 inch (191 x 76 x 19 mm) steel plate with a notch cut out from the center. The angle portion of the block fits into the groove that is cast into the side of the precracked specimen so that a line load is applied along this groove. The notch in the plate exists to allow clearance for the external reinforcing bar that confines the push-off specimens. The push-off blocks are simple 8 x 2 x 1/2 inch (203 x 51 x 13 mm) steel plates. A neoprene pad of durometer 60 hardness was placed between the flat plate and the specimen to mitigate the effects of specimen surface roughness. The push-off blocks were placed on top and bottom of the push-off specimen axially, so that bending moments were not induced.

(a) Precrack Load Blocks

(b) Push-off load blocks and pads

Figure 6.5 – Aggregate Interlock Specimen Load Blocks

6.2.2 Test Procedure This section is meant to delineate the sequence of the precise actions taken in order to perform the aggregate interlock testing which consists of both the precrack and push-off tests so that future researchers may replicate and confirm

the findings. The procedure described assumes that a specimen has already been cast and cured as will be described in **Section 6.3**.

In preparing the specimens, any imperfections on the edges or groove were chiseled and/or sanded away; this permitted full contact of the plates confining the specimens and adequate seating of the precrack load blocks within the cast groove. For positioning of the specimen within the test apparatus, the shear interface surface was projected and drawn on the apparatus as in **Figure 6.6** below. The specimen was slid into place within the apparatus, held to the right height by positioning blocks and metal shims, and then the apparatus was moved until the projected surface on the apparatus aligned with the test surface as determined by use of a carpenter's square. The bolts on the apparatus were tightened until snug and the positioning blocks were removed. A specimen properly positioned within the apparatus with key positions indicated is shown in **Figure 6.7** below.

(a) Projected on Both Surfaces (b) Accurately Drawn

Figure 6.6 – Projected Surface on Apparatus for Positioning

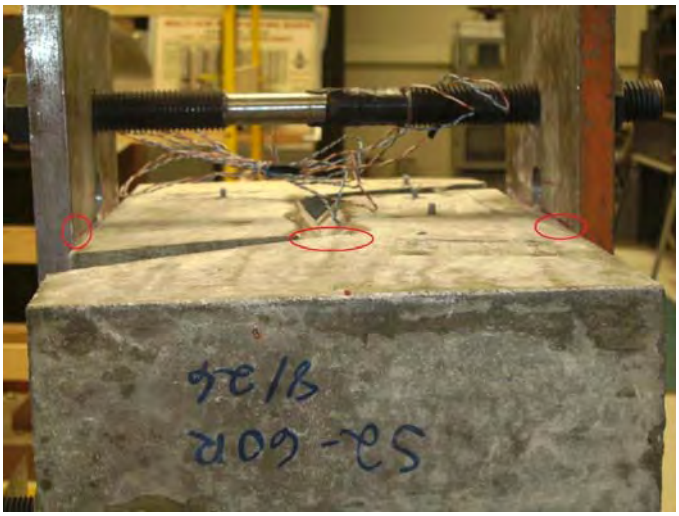

Figure 6.7 – A Properly Positioned Specimen

Instrumentation is the next sequence of steps. As will be described later in **Section 6.3**, anchor bolts were cast into the proper position for attaching the necessary LVDTs for measuring crack opening and slip. The LVDT mounts and associated reaction mounts were attached by hand tightening a nut using a wrench over the cast in place anchor bolt; taking care that the mounts were positioned parallel and perpendicular to the crack for the crack opening and crack slip LVDTs respectively. The parallel and perpendicularity of the mounts was again determined through the use of a carpenter's square. Next, the LVDTs themselves were attached and secured by using a double bolt around the mounts. See **Figure 6.8** for properly anchored LVDTs. The strain gages, already attached to the apparatus through common practices, protected from damage by a gummy overlay, and wiring held secure by electrical tape were then attached to the data acquisition system (DAS). **Figure 6.9** shows the strain gages attached to the DAS; each gage was attached by two wires, a positive and a negative. Before each precrack test, the

nuts on the apparatus were tightened such that the strain readouts from the DAS for each bar were averaged to about 110-165 microstrain, resulting in approximately 100 - 150 psi (0.69 – 1.03 MPa) on the shear interface for steel bars of about 3/4 inch (19 mm) diameter and a shear interface of about 3.75 x 7.50 inches (95 x 191 mm). Fortunately, the DAS was capable of zeroing strain readings, so periodically the gages were attached to the DAS with no normal strain applied and re-zeroed; however, the gages maintained their datum consistently and this was done as more of a check than to correct any drifting benchmark.

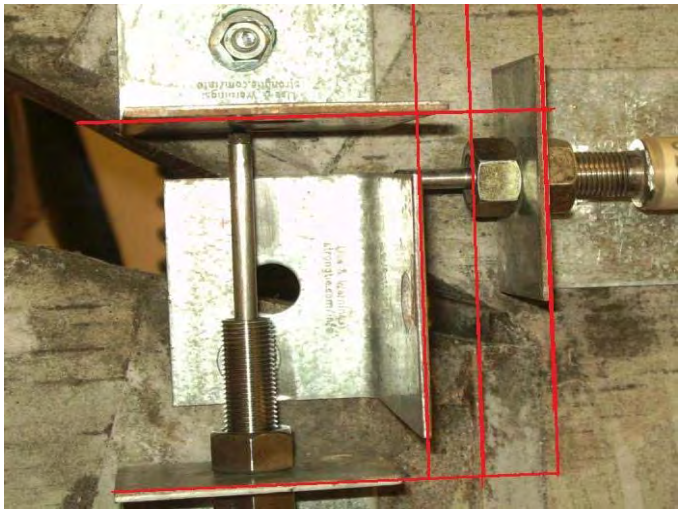

Figure 6.8 – Properly Anchored LVDTs, Parallel and Perpendicular to Groove

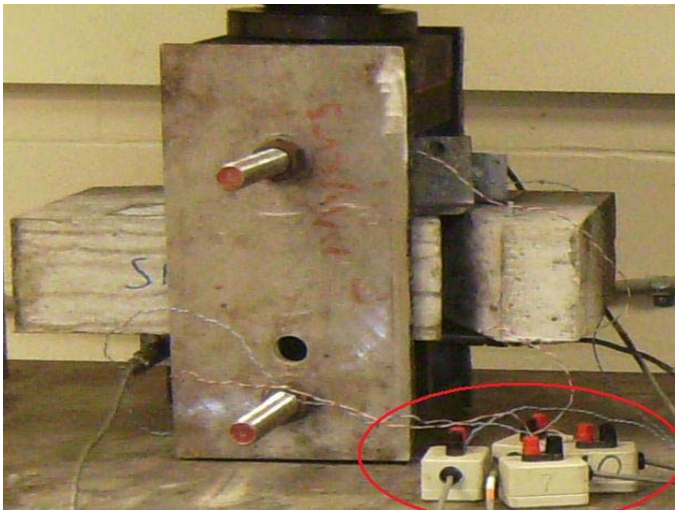

Figure 6.9 – Strain Gages Attached to Data Acquisition System (DAS)

Next, the apparatus and specimen were positioned upon the Tinius Olsen loading machine for the precrack test. **Figure 6.9** above actually shows the final position of the precrack test. The specimen was lifted to the height of the Tinius Olsen bottom table by a hand operated fork lift, dragged from the fork lift onto the table, and placed in the horizontal position. Metal shims were placed under the plates that comprise the apparatus so that the specimen was raised to provide adequate clearance for the load block to be placed on the bottom groove of the specimen. The metal shims were removed and the grooved specimen was allowed to settle onto the bottom load block as shown in **Figure 6.10(a)**. The top load block was then placed on the top groove of the specimen and allowed to settle into place as shown in **Figure 6.10(b)**; additional blocks were added as on the bottom to provide adequate spacing between the load applying crosshead of the Tinius Olsen machine and the apparatus. **Figure 6.10(c)** shows the precrack specimen completely positioned and ready for loading; **Figure 6.10(c)** also highlights the gap

between the bottom platen of the Tinius Olsen machine and the test apparatus so that the load is channeled through the load blocks and onto the grooved specimen as intended.

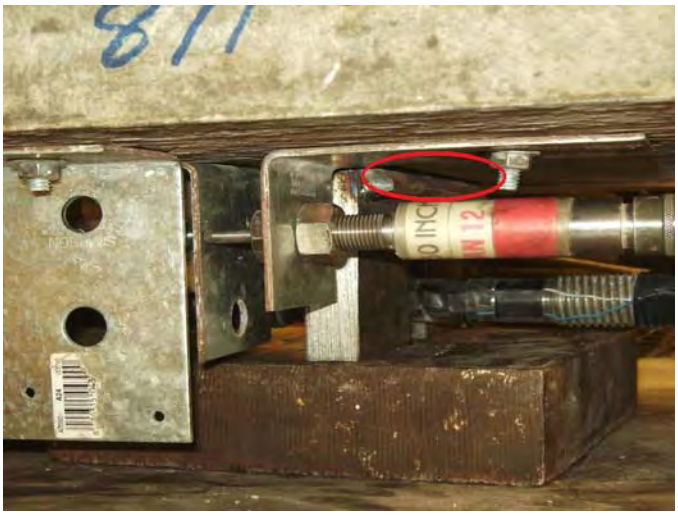

(a) Bottom Load Block Seated into Specimen Groove

(b) Top Load Block Seated into Specimen Groove

(c) Precrack Specimen Ready for Loading, Space Provided Between Apparatus and Load

Figure 6.10 – Precrack Specimen Positioning

A preload was applied by a displacement-controlled application at the rate of 0.05 in/sec (1.3 mm/sec) until 100 lb (445 N) of force was applied to the specimen; this helps to settle the load blocks into the specimen and against the Tinius Olsen machine. After the preload was reached, the load was applied by a load-controlled application at the rate of 100 lb/sec (445 N/sec) until the specimen ruptured. The ruptured specimen often had a crack opening in the order of 0.02 – 0.04 inch (0.5 – 1.0 mm) If the ruptured specimen opened less than 0.02 in (0.5 mm), loading was allowed to continue at the rate of 100 lb/sec (445 N/sec) until this minimum was achieved. Upon rupture or attaining the minimum crack opening, loading was stopped, the load platen was returned to the test starting position, and the data acquisition was stopped. The precracking load would be either the load that caused rupture, or the load necessary to attain the minimum crack

opening of 0.02 in (0.5 mm), whichever was greater. The information gathered from this test was the precracking load and the crack opening at the end of the test.

After the precrack test was complete and the Tinius Olsen cross head was raised, the specimen was placed in the vertical position. The push-off loading blocks with their associated neoprene pads were then placed axially concentric with the now cracked shear interface. **Figure 6.11(a) – Figure 6.11(c)** below shows the upright positioning of the push-off specimen along with the neoprene pad and block placement. It should be mentioned that the same attachment to the Tinius Olsen load machine was used for both the precrack and push-off test; the attachment is a spherically seating bearing block of the same type allowed in testing compressive strength cylinders. The spherically seating bearing block allows for some rotation and will help mitigate the generation of moment during the tests. **Figure 6.11(c)** shows the neoprene and bearing block placement as well as the spherically seating bearing block attachment to the Tinius Olsen machine.

(a) Vertical Orientation with Bearing Blocks Axially Located

(b) Bottom Bearing Block with Neoprene Between Specimen

(c) Top Bearing Block with Neoprene and Spherically Seating Attachment Block

Figure 6.11 – Push-off Test Positioning

The loading used for the push-off test was the same as the loading used for the precrack test; a 100 lb (445 N) preload achieved at 0.05 in/sec (1.3 mm/sec) and a 100 lb/sec (445 N/sec) load rate thereafter. The loading was then manually halted when the slip LVDT measured a total slip of approximately 0.25 inches (6.4 mm). The load

platen was returned to home, the position before the loading commenced, and the specimen was removed. After the apparatus was loosened from around the specimen, one half was discarded and the other half was retained for dimensional confirmation measurements and for the cross-sectional imaging investigation. The information gathered from the push-off test is much more complex than that gathered from the precrack test and will be discussed in full with the analysis of the results in **Sections 6.4** and **6.5** to follow.

Section 6.2.3 ImageJ Analysis Procedure The cross-sectional imaging was aided by several factors. Current work at the Missouri University of Science and Technology campus was undertaken in which very precise and sophisticated imaging was necessary. The researcher constructed a photo booth which addressed all of his various needs specifically, and which more than addressed the needs of this project. **Figure 6.12** below shows the photo booth used in this investigation; it does not look very impressive, but has several features worth mentioning. The four chip cans each hold an LED light bulb, the aluminum interiors act as reflectors with the lids behaving as diffusers. The use of four light sources helps to eliminate shadows on the rough surface being photographed. The LED bulbs were connected to a direct current source so that the photo would not be hindered by the off portion of an alternating current. Secondly, the software used in this investigation, ImageJ, was available for download from the National Institutes of Health website (NIH 2004). The software was developed for the medical field and is much more sophisticated than necessary for this investigation. ImageJ also has numerous users and many contribute to online tutorials and walkthroughs.

Figure 6.12 – Photo Booth Used For Cross-Sectional Imaging

Photographs of the cross-sections of the push-off specimens were taken using the photo booth described and shown above. The digital pictures were cropped down to the size of the push-off specimen cross-section using Microsoft® Office Picture Manager, then imported into ImageJ. The picture was split into the three separate red, green, and blue channels which comprise the original color image. A threshold was then applied to the red and blue channels (the green channel added more "noise" than useful information and was thus deleted) to tell ImageJ which pixels should be included in the analysis based on intensity; these are the coarse aggregate particles of interest to this study. The threshold was set to constant levels between all images. The red and blue channels were then converted to binary images; this separated the pixels of interest (coarse aggregate) from the pixels not of interest (paste matrix). The red and blue channels were then added back together using the image calculator available within ImageJ. A few particles were measured to determine an appropriate particle size to include in the analysis; this eliminated isolated pixels or small clumps of pixels from being counted as coarse

aggregate. The analysis was then performed by ImageJ to determine the number of aggregates counted, the average size, the area fraction, and where the center of mass of the particle was located within the image. A sample cross-section can be found in **Figure 6.13** in which the original cross-section is shown along with the subsequent processes carried out using ImageJ. Large pictures are shown for added visual clarity.

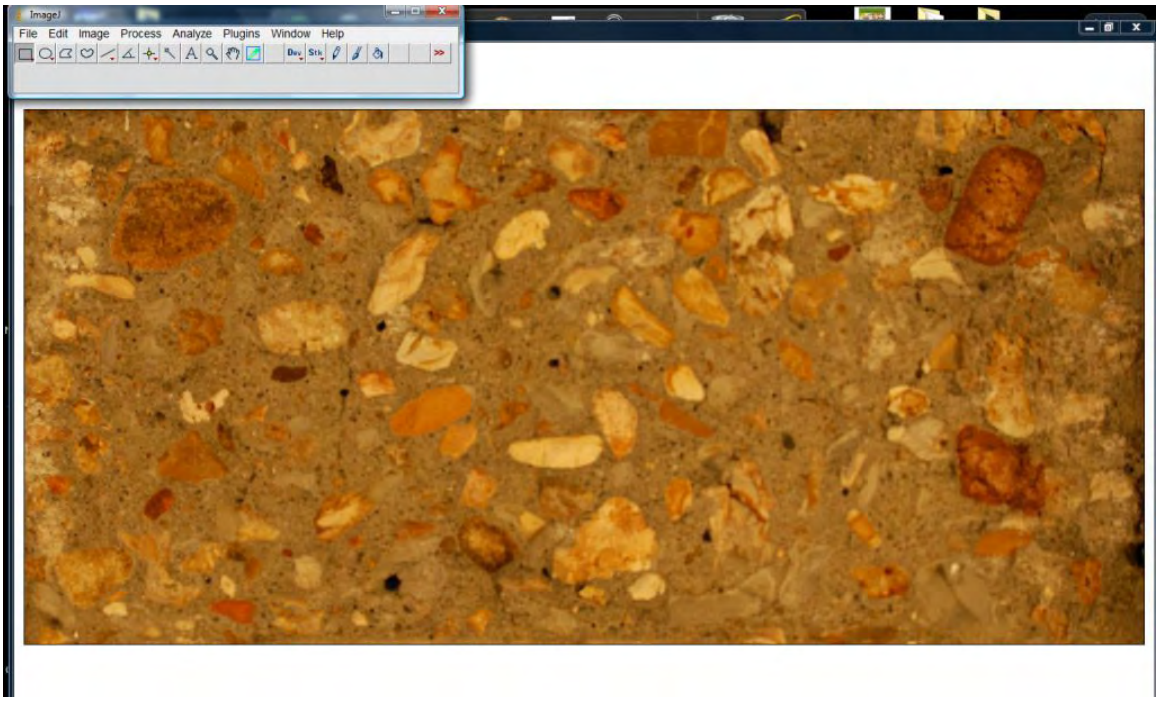

(a) Sample cross-section

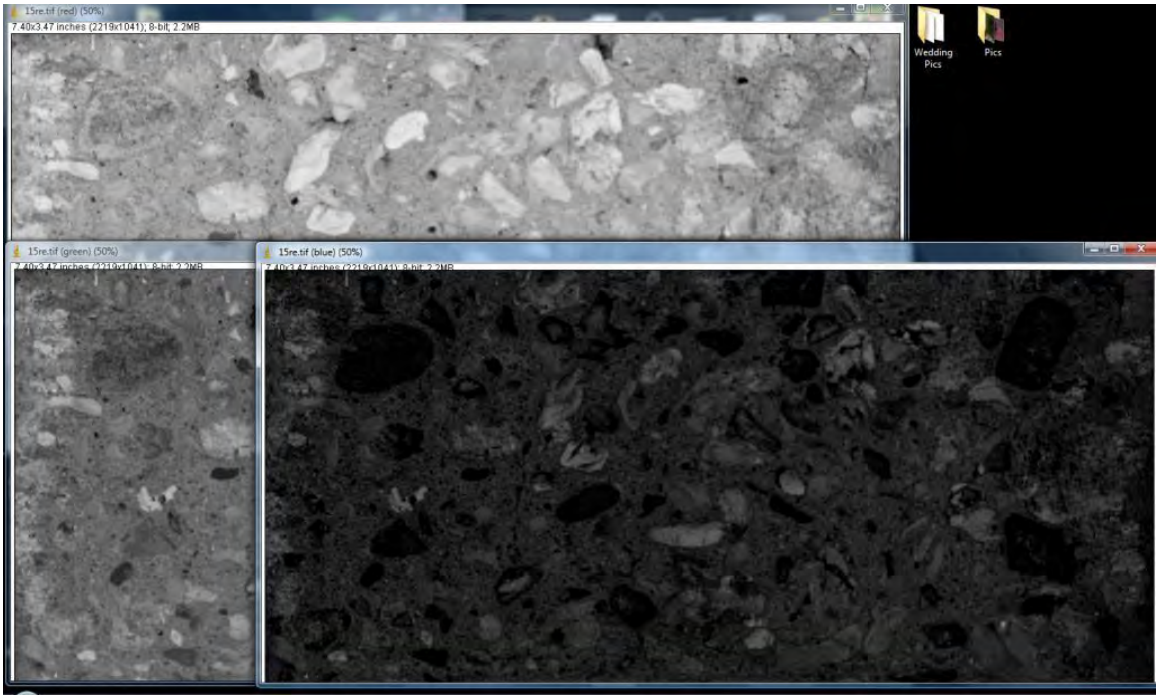

(b) The color image is split into the constituent red, green, and blue channels

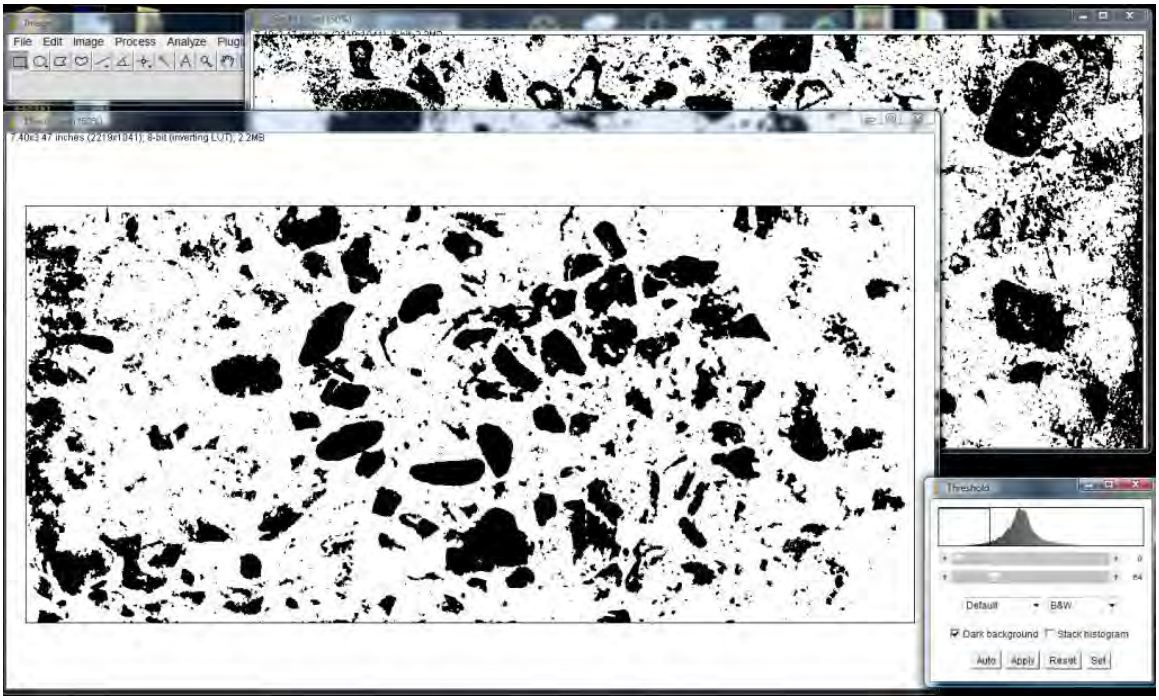

(c) Setting the threshold isolates pixels of interest

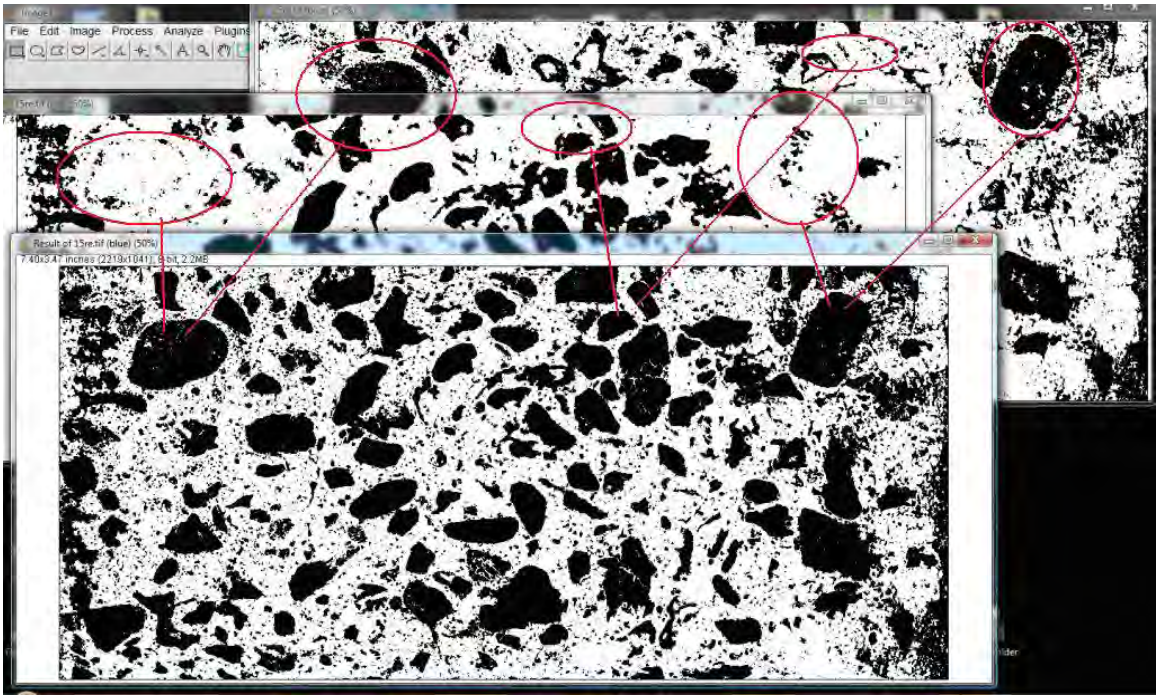

(d) The red and blue channels are added, consolidating all detected particles of interest

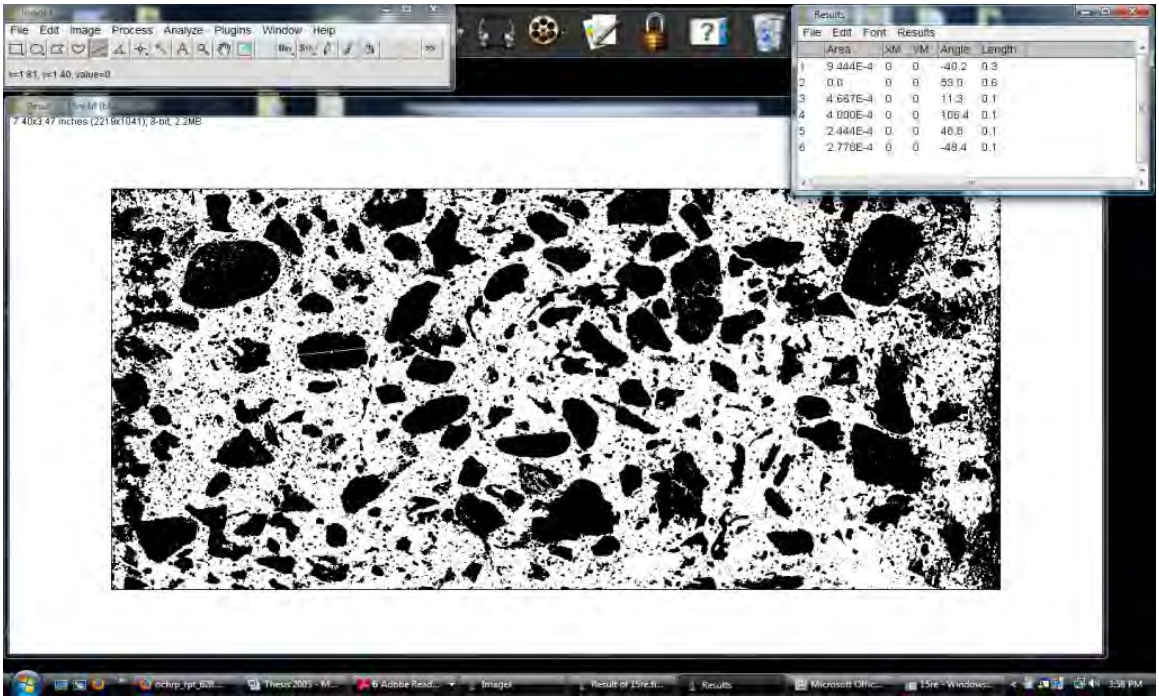

(e) The particles are measured to count only aggregate and not the surrounding “noise”

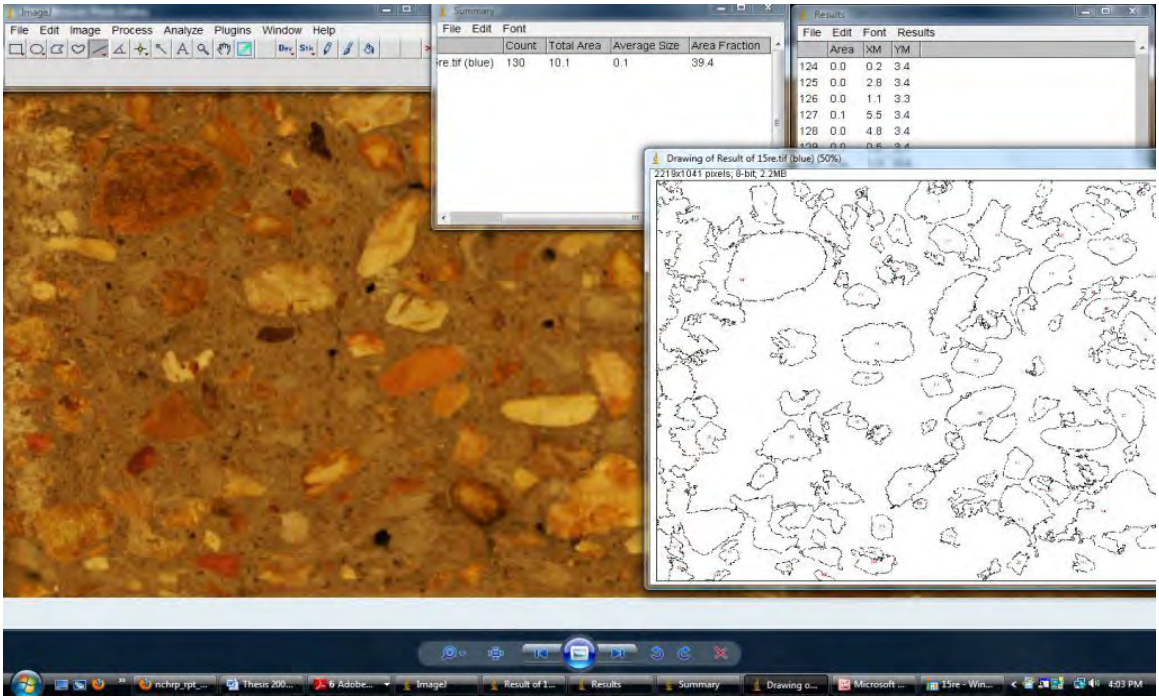

(f) Results are summarized and an outline drawing of the counted particles is produced

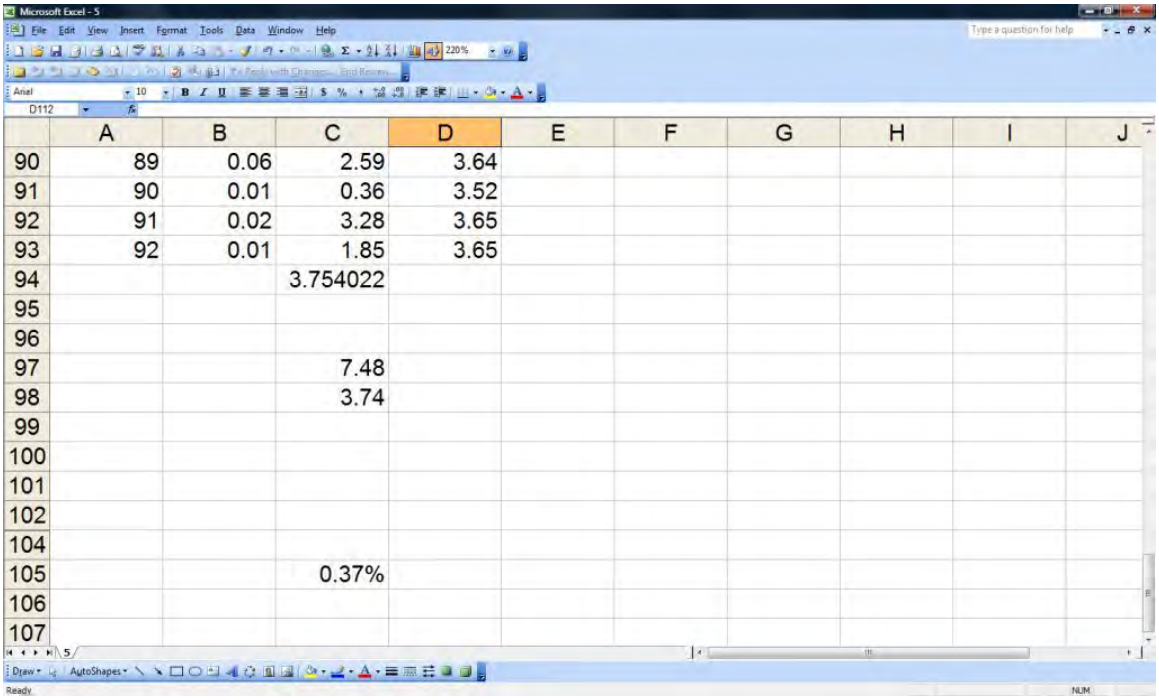

(g) The center of mass is determined and segregation is quantified

Figure 6.13 – ImageJ Sample Analysis

As a check on the analysis, the area fraction can be compared to the absolute volume of the coarse aggregate in the batch proportions for the mixture under investigation. Segregation can be detected by determining the location of the center of mass for all aggregates counted. Finally, an outline drawing of the particles counted in the analysis was also produced by ImageJ. The results of the forensic imagine investigation will be presented in **Section 6.4.3** below.

The non-standard precrack and push-off tests have been explained in detail. The exact setup used for this study has been explained. Along with the setup, the precise actions executed during the test procedure for this investigation have been made clear such that a reader could replicate this work. The imaging technique and software used were also shown. Next, the actions taken to fabricate the specimens will be discussed along with the reasoning for the exact specimen and apparatus geometry and detailing used.

6.3 SPECIMEN DESIGN AND FABRICATION

The use of the push-off test was new to the Missouri University of Science and Technology at the start of this project, and there was therefore no firsthand experience from which to draw any insights into how to fabricate or test the specimens; all of the knowledge was gained from other researcher's published works. Some issues arise when attempting to replicate other's work because even the most thorough author likely has typos, omissions, or may downplay certain issues; on top of these shortcomings, the information is then left to be interpreted by the reader and may be done so erroneously. The point to all of this is that throughout this study, there were several instances where

previous research provided the framework within which to work; however, the details were changed so that the desired outcome could be achieved or enhanced. Several times, the initial design proved inadequate, or the initial procedure was cumbersome or unacceptable. This section attempts to thoroughly discuss the specimen fabrication and design, and the iterations that took place from the beginning of the project to the end.

6.3.1 Initial Design and Fabrication Initially, the previous works of Mattock (1969;1972), Walraven and Reinhardt (1981), Albajar (2008), and Kim et al. (2008) were surveyed for dimensions, reinforcement, and external reinforcing apparatus details. The dimensions and exact geometry varied from project to project. The work of Kim et al. (2008) was chosen as the effort most closely resembling the scope of this project; the material used, SCC, the information gathered, and the goal of his study most resembled that of this investigation. With the intention of being able to draw parallels, use similar findings, or simply fill in additional data points, the specimen details were initially based on the work from Kim et al. (2008). So, specimens were cast to conform to the dimensions as shown in **Figure 6.14**. The specimens were cast horizontally, on their sides. The specimens were cast with a groove cast not only along the shear interface, but also through one of the end corbel as shown in **Figure 6.15.** The top of the specimens would then be finished by hand with a groove finished into the surface along the shear interface and the end corbel opposite the end corbel with the groove cast into the bottom surface. The continuation of the groove was to facilitate tight clearance tolerances for the precrack load blocks between the specimens and the test apparatus. Also, the portions of formwork protruding into the interior of the member in **Figure 6.15** formed what are being referred to as notches. The notch forms consisted of thin sheet metal cut and

deformed into shape with expansive foam providing a rigid backing; upon form removal, the foam would be slid out of place, the sheet metal was then easily removed, and the remainder of the formwork was stripped away. **Figure 6.16** shows that up to four specimens could be easily cast at a time on the forms created.

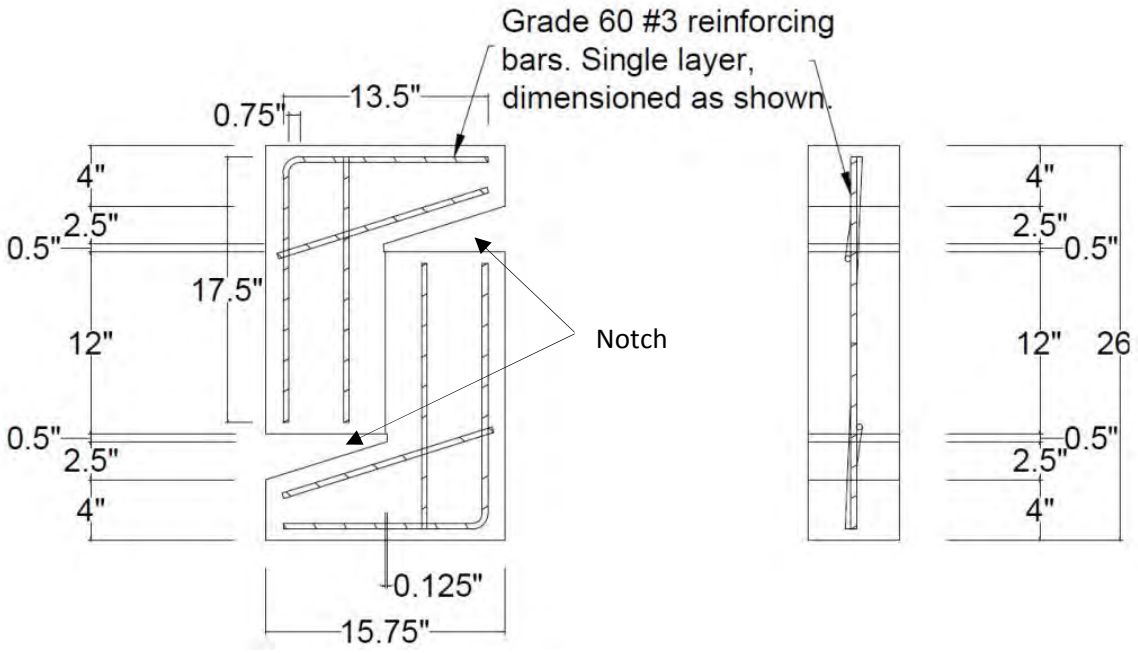

Conversion: 1 inch = 25.4 mm

Figure 6.14 – Initial Specimen Dimensions and Reinforcement

Figure 6.15 – Plan of Initial Specimen Form, Showing Cast Groove and Reinforcement Layout

Figure 6.16 – Complete Initial Formwork, Up To Four Specimen Cast at a Time

The casting of specimens was going fine and no major issues were readily identified. Later, when the first trial batches were tested for precrack and push-off data many issues become apparent and ways to remedy them were subsequently utilized.

6.3.2 Problems Encountered, Proposed Remedies The issues that arose while testing will all be discussed in the order encountered. The problems essentially consisted of surface finishing, surface mounting, large specimen size, and premature failures during testing. The actions taken to fix the issues will then be described. The final specimen design will then be discussed in the next section.

Casting of the specimens seemed to be going well, although there were some evident issues. Hand finishing the top surface with a smooth groove proved difficult. Minor errors in finishing the grooves could be corrected by using an electric grinder or sandpaper, but this proved somewhat inconsistent as well as very time consuming.

It was also realized from early trial batches that cast in place anchor bolts would be ideal for attaching the mounts necessary to hold the LVDTs in place during testing as described in **Section 6.2.2** above, and the initial formwork provided no such luxury. The other method of attaching the LVDT mounts was by drilling a pilot hole into the concrete surface using a concrete drill bit on a hammer drill, inserting a small plastic anchor (that was usually too large to fit easily into the hole), and finally securing the LVDT mount with a washer and screw placed into the anchor. This process was time consuming and the anchors, shown in **Figure 6.17**, were difficult to achieve anchorage, sometimes pulled out easily, and would become loose if handled much at all. Additionally, the use of a hammer drill invokes questions regarding damage to the surrounding concrete of the untested specimen.

(a) Concrete Drill Bit and Plastic Anchor

(b) Screw, Washers, Mount, and Anchor Layout

(c) Mount Installed, Anchor Expands

Figure 6.17 – Unsuccessful Drilled Anchor System

Notice in **Figure 6.15** that the underside of the notch, the side of the notch facing the shear interface, extended perpendicularly from the shear interface. Also, note the placement of the mounts per **Figure 6.3.** Because the LVDTs were placed around the shear interface, and because the mounts were so narrow, it was difficult to position the mounts such that they provided acceptable clearance for the precrack load block, but also allowed measurement of crack opening.

The size of the specimens also was a bit of an issue. The bulky specimens were too large and heavy to be moved and positioned by one researcher. The size also created tight clearance tolerances for the precrack load blocks to fit between the specimen and the test apparatus. The tight clearance for the load blocks also created the potential to damage the fragile strain gages and their wires attached to the test apparatus.

Next, when all of the anchors were finally successfully placed, the LVDTs and strain gages were attached to the DAS, and the trial specimens were ready to be tested, additional problems were encountered. Premature failure occurred away from the intended shear interface. **Figure 6.18(a) – Figure 6.18(c)** shows the three undesirable modes of failure experienced with the first round of trial batches. It was unfortunate that such difficulties were experienced; yet, the underlying issue to each mode of failure was thought to be understood, and subsequent testing of the changed specimens confirmed this belief. The failure modes shown in **Figure 6.18(a)** and **Figure 6.18(b)** were thought to be the result if insufficient reinforcement and/or insufficient reinforcement anchorage or development length; therefore, these failures could be avoided by increasing the amount of reinforcement and by providing anchorage of the reinforcement. The failure shown in **Figure 6.18(c)** was believed to be caused by the unlevel surface of the end corbel as it contacted the spherically seated load block of the Tinius Olsen machine. The uneven loading caused high compressive stresses on one side of the specimen and

essentially caused failure by crushing on the highly stressed face. Luckily, this mode of failure could also be avoided by improving forming techniques, grinding the ends to level, or by casting some form of a cap on the specimen.

(a) Cracking and Downward Movement of End Corbel

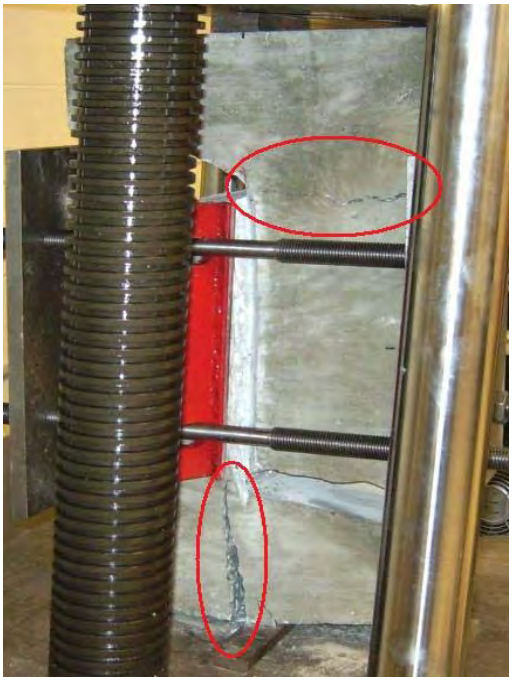

(b) Cracking and Rotation of End Corbel

(c) Spalling of Surface on One Side, Followed by Crack Development

Figure 6.18 – Undesirable Modes of Failure Experienced During Trial Testing

The difficulties experienced with finishing the specimens, anchoring LVDT mounts, the specimen size, and premature failures have all been discussed. Next, the actions taken to fix the problems are discussed.

Because the list of concerns with the specimen was so long, it was decided that the best thing to do would be to completely redesign the specimens. It was decided to cast the specimens in a vertical fashion so that problems with finishing a grooved surface could be avoided; this fix simultaneously enabled level finishing of the end corbel which would eliminate premature failures during testing of the type shown in **Figure 6.18(c)**. An image of the new form is illustrated in **Figure 6.19**.

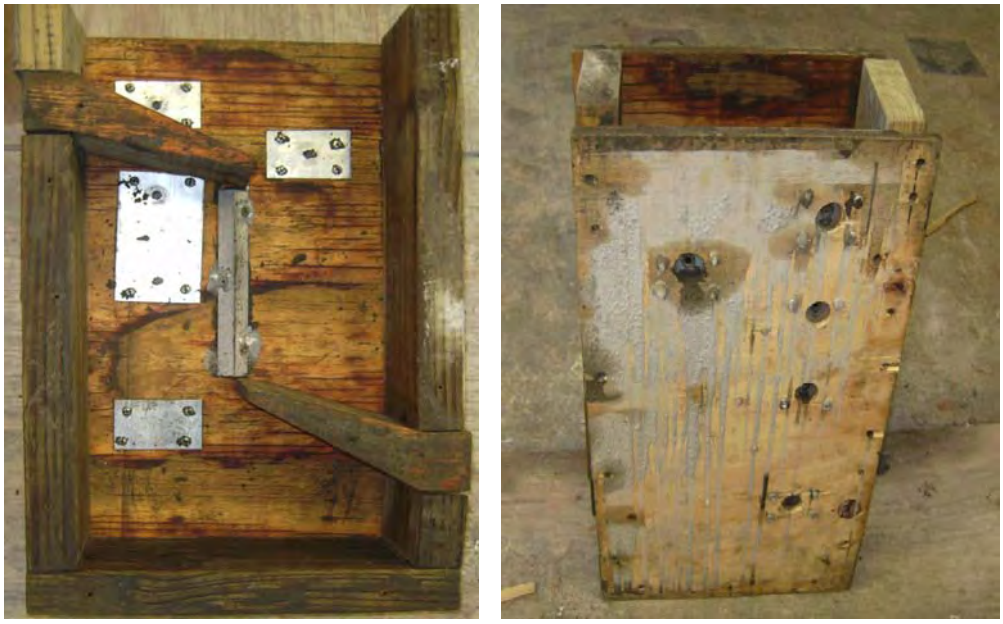

(a) Groove, Notch, and Anchor Forms (b) Cast Upright

Figure 6.19 – Newly Designed Formwork

Casting the specimens vertically also corrected an issue which had not been perceived previously; the fidelity between the push-off specimens and beams cast as infrastructure elements. The segregation potential for SCC mixtures is relatively high if batch proportioning and moisture condition measurements of the constituent materials are not properly performed. A beam cast from SCC would be cast in the vertical direction. In a segregating mixture, a disproportionate amount of coarse aggregate would sink below the tension reinforcement, may not contribute as well to aggregate interlock, and would not be included in the area usually used to calculate shear stress, b_w*d_v, where b_w is the width of web and d_v is the shear depth of the member. The vertical casting of the new push-off specimens would allow segregating mixtures to behave as they would for real beams; a disproportionate amount of coarse aggregate could sink below the shear interface and end up in the bottom end corbel. The reduced aggregate in the shear

interface may impact aggregate interlock; the new test specimens would capture this potential.

Since both faces upon which LVDTs were to be mounted were now cast within the new forms, it was possible to include cast in place anchor bolts. **Figure 6.20** shows where a portion of the plywood forms were drilled away, a sheet metal overlay attached, and a hole drilled into the sheet metal so that an anchor bolt could be positioned using a double bolt tightening system. The resulting anchor is shown in **Figure 6.21**. The cast in place anchor bolts not only provided more secure mounting, but also ensured point symmetric positioning of the crack opening LVDTs and consistent mount positioning from test to test.

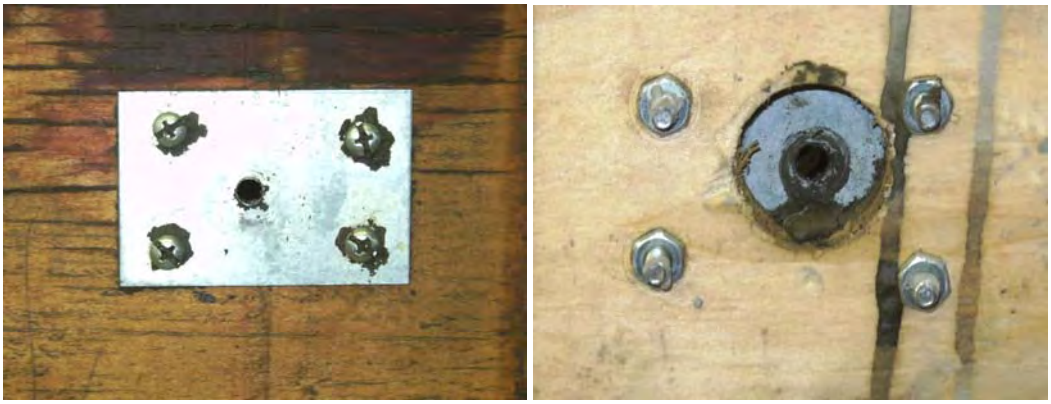

(a) Inside Forms, Metal Sheet Attached with a Hole Drilled (b) Outside Forms

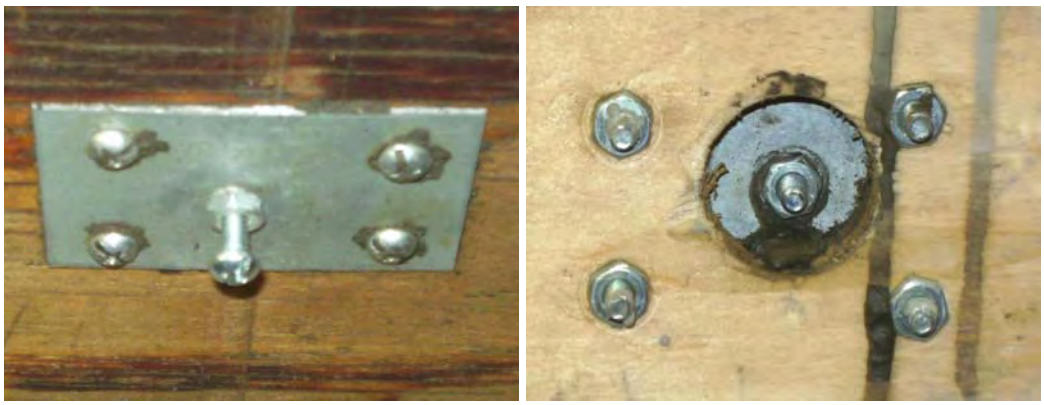

(c) Inside Forms, Anchor Attached (d) Outside Forms

Figure 6.20 – Anchor Bolt Formwork

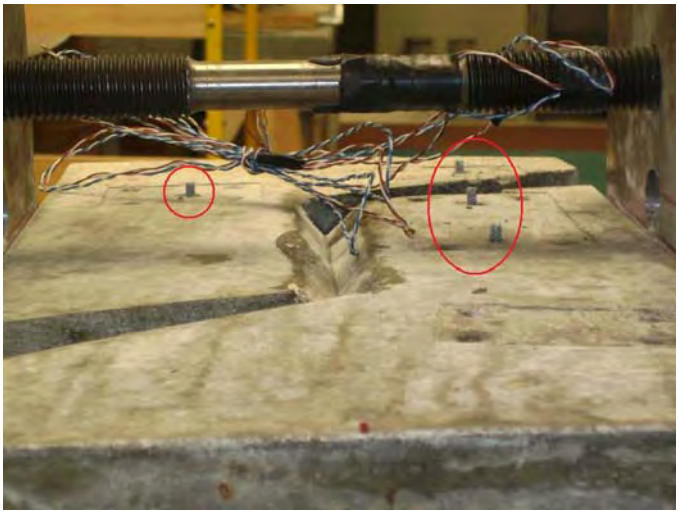

Figure 6.21 – Resultant Cast in Place Anchors

It was mentioned above that it was difficult to measure crack opening around the shear interface when the notch protruded perpendicularly from the interface. As can be seen in **Figure 6.19** above, the notches were made to protrude away from the shear interface at an angle; this provided more clear cover for the anchor bolts selected to be put at this position.

Next, it was decided to reduce the size of the specimens. Shrinking the specimens enabled the testing to be performed by one researcher and made the testing much faster. Problems with clearance between the specimen and test apparatus were completely alleviated. The strain gages and wires were damaged less with more tests and the whole test procedure was more resilient. Some readers may raise alarms when changing size. The size effect of shear is a well-documented fact; however, this test results in a comparative assessment of the concrete tested within this study. Because the analysis always consists of comparing one test result from this study to another test result, there is ultimately no concern for size effects. It should also be mentioned that the size of the

originally designed specimen, and the size of other researcher's push-off tests, may not be very realistically sized when compared to prestessed girders anyway; yet accurate models for shear behavior were determined. So, since this study is essentially comparing conventional concrete aggregate interlock potential to that of varying types of SCC, and because a slightly larger specimen has no more fidelity to beams used in infrastructure, but has proved useful for modeling, it was deemed acceptable to change the size of the test specimens. The new specimen dimensions will be detailed below in **Section 6.3.3**.

Lastly, the reinforcement was increased and the reinforcement was anchored. Reinforcement was doubled over the trial specimens by adding a second bar of the same size. The short corbels did not provide adequate development length, so anchorage was deemed necessary. Improvements in reinforcement detailing eliminated the concern of premature failures of the type shown above in **Figure 6.18(a)** and **Figure 6.18(b)**. The new reinforcement detailing is shown in **Section 6.3.3**.

6.3.3 Final Design and Fabrication With all of the previously discussed issues being corrected it is necessary to discuss the resultant test specimens and method of forming them.

The new formwork was shown in **Figure 6.19** above. The exact dimensions of the specimens being created with the new formwork are shown below in **Figure 6.22**. Points are marked and the spacing dimensioned where the cast in place anchor bolts where to be placed. All of the dimensions were selected based on the 3.75 x 7.50 inch (95 x 191 mm) shear interface; all other dimensions were roughly proportioned from the original specimen design so that the various aspect ratios remained similar. The new reinforcement layout is also detailed. Fortunately, the two layers of reinforcement could

be tied together with a lateral piece of reinforcement; this lateral reinforcement acted to consistently space the two layers of rebar as well as acted as an anchor when the rebar was hooked around it.

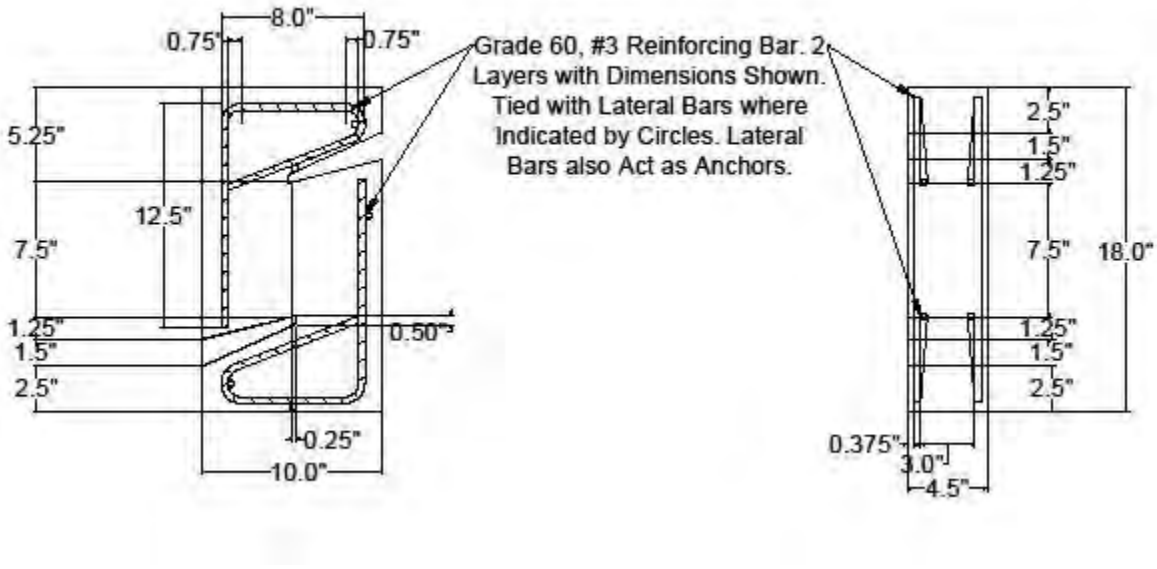

Conversion: 1 inch = 25.4 mm

Figure 6.22 – Final Specimen Dimensions and Reinforcement

The method of casting the specimens is not as straight forward as for the originally horizontally placed specimens and requires some discussion. The placement technique of the conventional concrete varied from the placement of SCC. Each concrete mixture was placed in three layers; yet, the conventional mixtures were internally vibrated, while the SCC mixtures were not consolidated.

The conventional concrete mixtures were consolidated using vibration because of the inability to properly rod the material. Internal vibration conformed to section 7.4 of ASTM C 192: Standard Practice for Making and Curing Test Specimens in the Laboratory (ASTM C 192 2007). The bottom end corbel was filled and consolidated,

followed by the shear interface, the top rebar cage was inserted, and finally concrete was placed in the top end corbel and consolidated. The top surface was then hand finished with care being taken to ensure a level finish, to avoid the undesirable premature failure during testing shown in **Figure 6.18(c)**.

For the SCC mixtures, care was taken not to induce any additional consolidation during placement. **Figure 6.23(a) – Figure 6.23(c)** illustrates the placement technique used for the SCC mixtures. Basically, the bottom end corbel was filled and tilted to allow escape of all entrapped air. The middle, shear interface, section was then filled and tilted the opposite direction to permit entrapped air to escape. The top rebar cage was inserted and SCC was placed into the top end corbel. The top surface was allowed to self-level and was not finished.

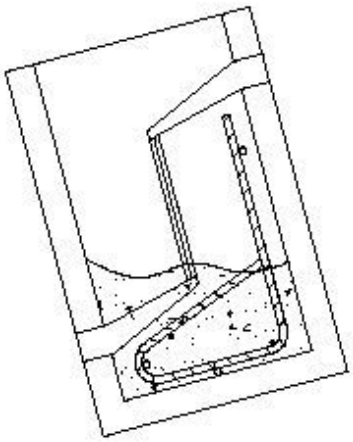

(a) Placement in Bottom End Corbel Tilted to Release Entrapped Air

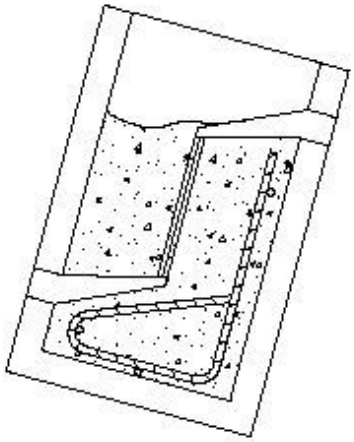

(b) Placement in Middle Section Tilted to Release Entrapped Air

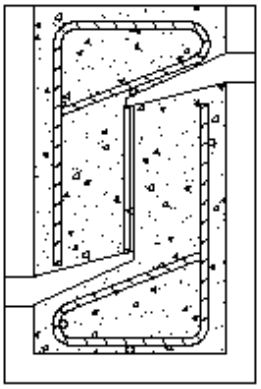

(c) Top Reinforcement and SCC Placement

Figure 6.23 – SCC Placement Technique into New Formwork

With this, the specimens have been completely described in their final state. The specimens dimensioned as in **Figure 6.22** and fabricated as in **Figure 6.23** were then ready for testing. The results of the tests performed as described in **Section 6.2** will be presented next, followed by a thorough analysis. The results will be assessed for their import to how SCC behaves in aggregate interlock relative to CC and what this may mean for overall shear behavior of SCC.

6.4 TEST RESULTS AND ANALYSIS

The results for the precrack and push-off tests will be shown, discussed, and analyzed. Details of how the data were reduced will be shown for transparency and for the sake of future researchers. The findings and their impact to this and future investigations will be shown. The post-test cross-sectional investigation will also be discussed with the results presented.

6.4.1 Precrack Results and Analysis This section presents the results from the precrack tests that precede the push-off shear tests. The section focuses on showing the results, correlating the precrack results to material and test variables, and also on how the results can be used for future researchers.

First, **Tables 6.1(a-f)** show the averaged results for the maximum load and crack opening achieved when precracking the specimens and show the mechanical test results with the associated concrete mixtures. Notice the low coefficient of variation for the compressive strength tests, which is common. Also, note that the crack opening and precrack load variation is of a similar magnitude as the splitting tensile test results.

Table 6.1 – Mechanical and Pre-Crack Properties

Conversion: 1000 psi = 6.89 MPa

(a) 6 ksi (41.4 MPa) target strength limestone

		*S6-36L	S6-48L	*S6-60L	C6-58L
Compressive Strength, f'c	Avg. (psi)	10,770	8140	9400	7600
	Std. Dev. (psi)	224	159	310	233
	COV (%)	2.1	2.0	3.3	3.1
Splitting Tensile Strength, T	Avg. (psi)	580	460	570	370
	Std. Dev. (psi)	43	112	58	57
	COV (%)	7.4	24.4	10.2	15.4
Precrack Load, P	Avg. (lb)	23,990	26,590	29,190	25,930
	Std. Dev. (lb)	1210	3510	100	3710
	COV (%)	5.0	13.2	0.3	14.3
Crack Opening, w	Avg. (in)	0.028	0.018	0.047	0.019
	Std. Dev. (in)	0.011	0.003	0.007	0.007
	COV (%)	39.3	16.7	14.9	36.8

*Indicates the re-batch for earlier poor shear test results discussed above and in section 5

(b) 10 ksi (68.9 MPa) target strength limestone

		S10-36L	S10-48L	S10-60L	C10-58L
Compressive Strength, f'_c	Avg. (psi)	12,580	13,740	13,880	11,210
	Std. Dev. (psi)	936	382	572	180
	COV (%)	7.4	2.8	4.1	1.6
Splitting Tensile Strength, T	Avg. (psi)	580	760	800	540
	Std. Dev. (psi)	144	71	28	62
	COV (%)	24.8	9.3	3.6	11.5
Precrack Load, P	Avg. (lb)	33,430	28,490	34,560	30,970
	Std. Dev. (lb)	6320	3490	11,260	8270
	COV (%)	18.9	12.2	32.6	26.7
Crack Opening, w	Avg. (in)	0.031	0.036	0.022	0.024
	Std. Dev. (in)	0.008	0.009	0.005	0.003
	COV (%)	25.8	25.0	22.7	12.5

(c) 4 and 9 ksi (27.6 and 62.0 MPa) target strength additional mixtures

		S4-36L	S4-60L	C4-58L	S9-57R
Compressive Strength, f'_c	Avg. (psi)	5850	5490	6130	9190
	Std. Dev. (psi)	328	171	177	116
	COV (%)	5.6	3.1	2.9	1.3
Splitting Tensile Strength, T	Avg. (psi)	440	380	390	680
	Std. Dev. (psi)	40	22	13	71
	COV (%)	9.1	5.8	3.3	10.4
Precrack Load, P	Avg. (lb)	20,940	17,030	31,110	26,590
	Std. Dev. (lb)	1430	2300	2260	6500
	COV (%)	6.8	13.5	7.3	24.4
Crack Opening, w	Avg. (in)	0.021	0.021	0.019	0.016
	Std. Dev. (in)	0.001	0.003	0.001	0.005
	COV (%)	4.8	14.3	5.3	31.3

(d) 6 ksi (41.4 MPa) target strength river gravel

		S6-36R	S6-48R	S6-60R	C6-58R
Compressive Strength, f'_c	Avg. (psi)	10,640	10,530	8710	10,750
	Std. Dev. (psi)	453	650	508	300
	COV (%)	4.3	6.2	5.8	2.8
Splitting Tensile Strength, T	Avg. (psi)	720	690	580	680
	Std. Dev. (psi)	69	142	40	105
	COV (%)	9.6	20.5	6.9	15.5
Precrack Load, P	Avg. (lb)	30,640	33,280	31,200	30,150
	Std. Dev. (lb)	2930	3780	7160	8090
	COV (%)	9.6	11.4	22.9	26.8
Crack Opening, w	Avg. (in)	0.025	0.022	0.021	0.024
	Std. Dev. (in)	0.006	0.003	0	0.006
	COV (%)	24.0	13.6	0.0	25.0

(e) 10 ksi (68.9 MPa) target strength river gravel

		S10-36R	S10-48R	S10-60R	C10-58R
Compressive Strength, f'_c	Avg. (psi)	14,510	14,420	13,920	9450
	Std. Dev. (psi)	476	386	530	74
	COV (%)	3.3	2.7	3.8	0.8
Splitting Tensile Strength, T	Avg. (psi)	790	730	740	550
	Std. Dev. (psi)	124	68	34	68
	COV (%)	15.7	9.4	4.6	12.4
Precrack Load, P	Avg. (lb)	35,200	38,240	31,320	29,920
	Std. Dev. (lb)	5470	1160	5270	5800
	COV (%)	15.5	3.0	16.8	19.4
Crack Opening, w	Avg. (in)	0.027	0.032	0.021	0.033
	Std. Dev. (in)	0.004	0.008	0.001	0.014
	COV (%)	14.8	25.0	4.8	42.4

(f) Beam companion specimen

		S6-48L	C6-58L	S10-48L	C10-58L
Compressive Strength, f'_c	Avg. (psi)	7270	7560	9610	8880
	Std. Dev. (psi)	---	---	---	---
	COV (%)	---	---	---	---
Splitting Tensile Strength, T	Avg. (psi)	---	---	---	---
	Std. Dev. (psi)	---	---	---	---
	COV (%)	---	---	---	---
Precrack Load, P	Avg. (lb)	24,980	22,910	29,170	27,170
	Std. Dev. (lb)	---	---	---	---
	COV (%)	---	---	---	---
Crack Opening, w	Avg. (in)	0.033	0.025	0.020	0.020
	Std. Dev. (in)	---	---	---	---
	COV (%)	---	---	---	---

From these test results, several correlations can be shown. As is expected for concrete loaded and failed in all manners of orientation or mode, there is a positive proportionality between the ultimate precrack load achieved and the square root of concrete compressive strength (f'c) as shown in **Figure 6.24**. Notice that the intercept is not set to the origin. A positive y-intercept would imply that a concrete with no strength would still exhibit a precracking load, and this is obviously illogical; yet, a possible explanation exists. By dividing the y-intercept of 3500 lb (15600 N) by the target cross-sectional area of the crack of 3.5 x 7 in. (89 x 178 mm) it is found that the stress resisting cracking with no concrete contribution is about 140 psi (0.96 MPa) which is close to the initial prestressing applied by the confining test apparatus. The average initial prestress was calculated and can be seen in **Figure 6.26** to be close to 140 psi (0.96 MPa).

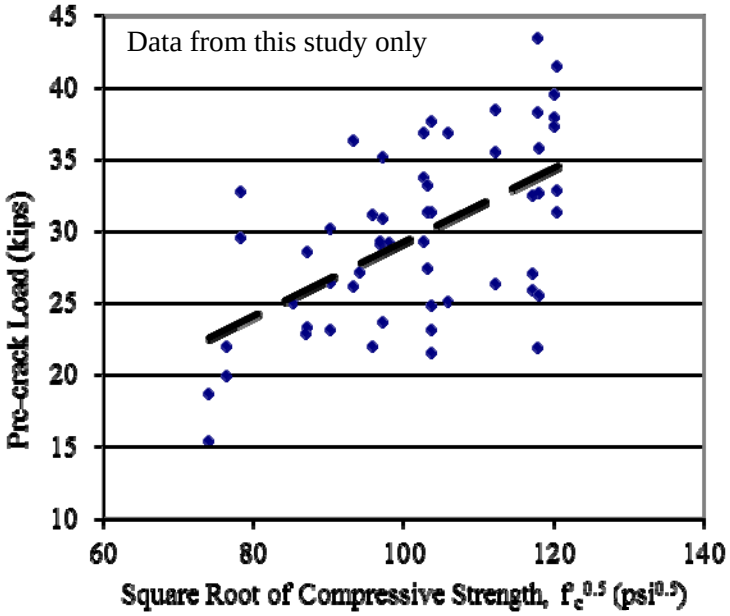

Conversion: 1000 psi = 6.89 MPa
1 lb (force) = 4.45 N

Figure 6.24 – Increasing Precrack Load with Increased Compressive Strength

Figure 6.25 also demonstrates a positive relationship between the ultimate precrack load and the STS of the concrete. Because the precrack specimens are failing due to a similar mechanism as in a STS test, net tension, it makes sense that as a batch proportion improves in STS, it also experiences an increased ultimate precracking load.

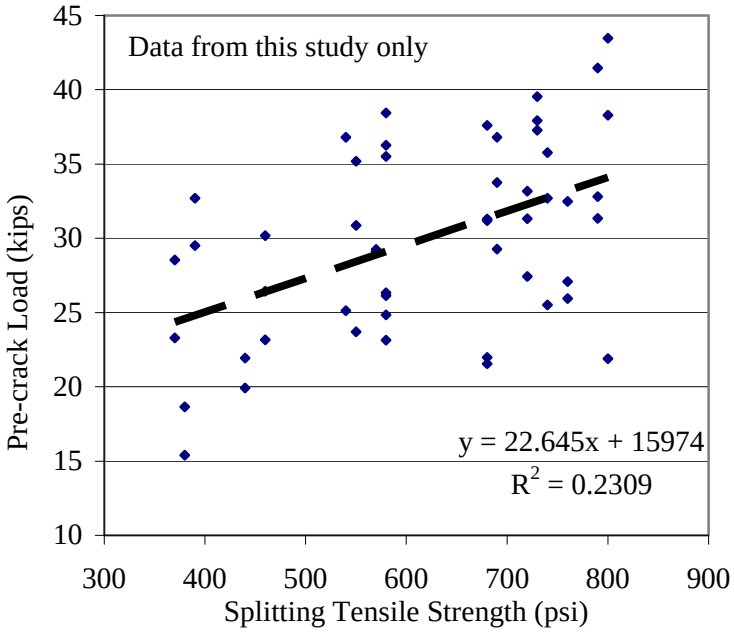

Conversion: 1000 psi = 6.89 MPa
1 lb (force) = 4.45 N

Figure 6.25 – Increasing Precrack Load with Increased STS

The correlations between maximum precrack load and square root of concrete compressive strength and STS appear relatively weak at a coefficient of determination (R^2) of only about 0.33 and 0.23 respectively. The low correlation is typical of all relationships developed from the precrack testing as will be seen. There are numerous and valid reasons for weak relationships in this test. There is an inherent and complex interaction due to the differences associated with the variations in the constituent materials and percentages alone in the test orientation. The material strength inconsistency can be seen in the similarly oriented STS test discussed earlier and which is widely recognized as a reliable test, but with wide variability. Within the precrack and push-off test there is also the added complexity of test variability due to slight changes in

the initial condition from the external restraining frame. These changes in the initial condition will also be reviewed for their impact on the test results.

The initial normal stress applied by the externally restraining frame appears to be important in determining both the ultimate precrack load as well as the maximum crack opening, which sets the initial condition for the push-off test to follow. The initial normal stress was controllable to a certain amount of precision by tightening the nuts threaded onto the restraining frame; although, some variability in initial normal stress was inevitable. No previous researchers had advised a target initial normal stress and variation of this stress was examined for test result impact. **Figure 6.26** shows that as the initial normal stress increases, so does the ultimate precrack load; the added confinement acts as a compressive force on the cracking plane that must be overcome before net tension and eventual cracking can occur. Additional insight can also be obtained from this simple plot. Similar to **Figure 6.24** above, there is a positive y-intercept. By eliminating the confinement effect, the average concrete resistance to cracking can be determined. Dividing the y-intercept of **Figure 6.26** by the area yields about 780 psi (5.4 MPa). The average compressive strength was determined to be 10540 psi (72.6 MPa). Normalizing 780 psi (5.4 MPa) by the square root of the average compressive strength yields 7.6, a typical value for the concrete resistance to tensile rupture.

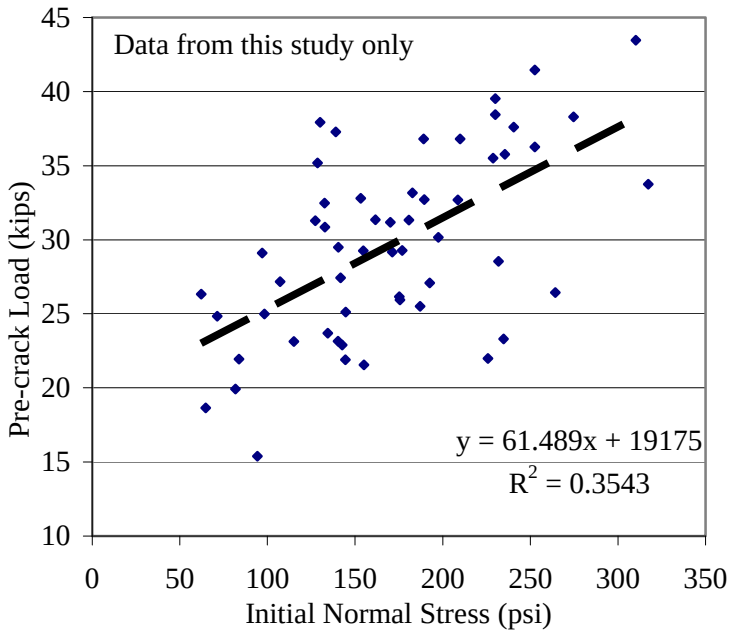

Conversion: 1000 psi = 6.89 MPa
1 lb(force) = 4.45 N

Figure 6.26 – Increasing Precrack Load with Increased Initial Normal Stress

Increased initial normal stress also acts to decrease the maximum crack width developed from the test as shown in **Figure 6.27**. The specimen engages a stiffer frame when cracking under increased confinement and is thus unable to expand to as large of an opening as when not confined. The level of confinement can be controlled in order to control crack opening.

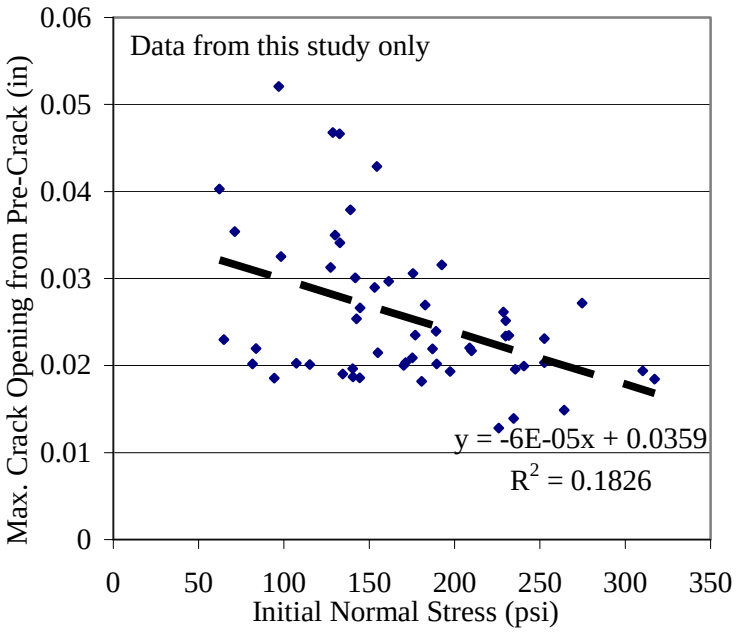

Conversion: 1000 psi = 6.89 MPa
1 inch = 25.4 mm

Figure 6.27 – Decreasing Crack Opening with Increased Initial Normal Stress

So, as discussed earlier, because some of the increase in precrack load can be attributed to increased initial normal stress, as well as increased compressive strength, the coefficients of determination seem falsely low for the direct comparison of only two variables at a time. It is sufficient at this time to assume the relationships shown are valid, and that a multivariable equation could be derived to fully characterize the precracking behavior.

For the use of possible future researchers, another useful relationship is shown. **Figure 6.28** shows that as the initial normal stress increases, the ratio of the normal stress after the crack develops to the initial normal stress actually decreases.

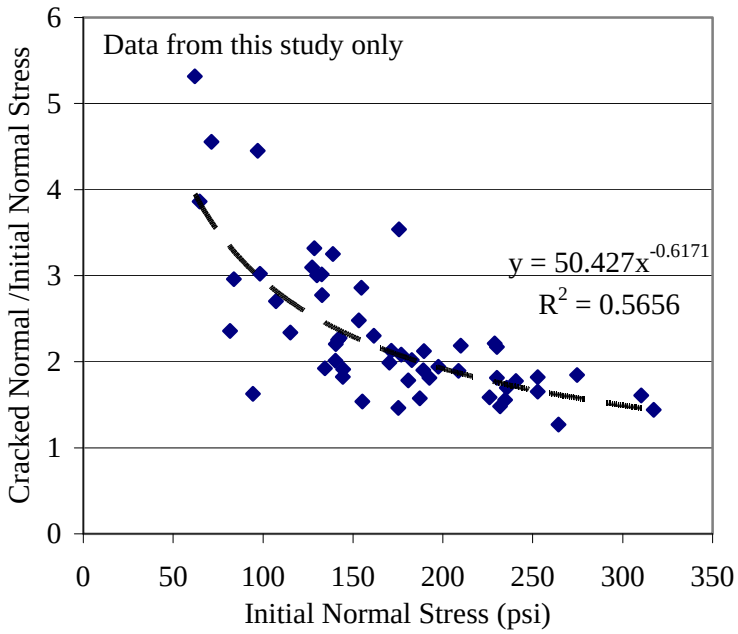

Conversion: 1000 psi = 6.89 MPa

Figure 6.28 – Decreasing Stress Ratio with Increased Initial Normal Stress

The reason researchers could benefit from the relationship shown in **Figure 6.28** is that it shows that increasing the initial normal stress decreases the sudden increase in normal stress caused by cracking of the specimen, and appears to decrease variability of this stress rise. Pairing the results from **Figure 6.27** and **Figure 6.28**, one can conclude that a researcher could achieve smaller crack openings with more consistency by increasing initial confinement; because crack opening sets the initial condition for the push-off test that follows, it is important to control this variable as much as possible.

The precrack test results have been shown for each batch proportion. The precrack results were then correlated to concrete compressive strength, splitting tensile strength, and initial confining normal stress from the test frame, with all showing positive proportionality. The crack opening from the test was then shown to decrease with

increased initial confinement. The specimen was shown to crack more gradually if increased initial confinement was used. The last two relationships can be important for future researchers because together they show that increasing initial normal stress of the test frame decreases crack opening widths and that these smaller crack widths develop more gradually with a greater degree of control. This is important, as other researchers have discussed these tests using small crack widths, some arbitrarily specify smaller than 0.02 inches (0.5 mm), but gave no advice as to what confinement would result in that size of crack width (Kim 2008; Walraven and Reinhardt 1981). One could consistently achieve crack widths smaller than 0.02 in (0.5 mm) using the mixtures and restraining system of this research tightened to an initial normal stress of approximately 300 psi (2.07 MPa) or greater as shown by **Figure 6.27**; this research attained larger crack openings, approximately 0.03 in (0.76 mm) on average. It would be advisable to use increased confinement, and continue the precracking test load until the desired crack opening is achieved, this would produce very consistent crack openings to be used for the initial condition of the push-off test.

6.4.2 Push-Off Results and Analysis After the precracking test established the initial crack condition of the shear specimens, the push-off test was performed. The push-off test setup and procedure has been described; although, some discussion of how the raw data collected were formatted and reduced to a consistent and useful form is justified because no previous researchers addressed exactly how their data were analyzed. The data formatting procedure will be detailed. The push-off test results and an analysis of the results will be shown.

As discussed previously, the data collected during push-off testing consisted of the shear loading applied by the testing machine, the normal stress developed in the external test frame bars due to crack dilation and deformation, and the crack slip and opening as measured by LVDTs attached parallel and perpendicular to the cracked plane respectively. All of this data was being collected over each of the roughly five minute push-off tests. The data collection frequency was two points per second; this frequency balanced the collection of too much data with gathering enough data to show high resolution of the results and could have been increased to generate more points during rapid deformation.

The shear load applied by the machine was zeroed before the initialization of load and therefore the applied and effective shear loads are considered equivalent. The strain gages attached to the test frame bars, from which the normal stress was computed, were set to zero strain on the DAS when no stress was applied; therefore, any time the test frame was attached to the specimens (even at the beginning of testing) there was some normal stress, and this was considered the effective normal stress. The crack opening and slip were not considered zero at the beginning of push-off testing. When shear load was applied to the specimen, the crack would actually slip very little (about 0.005 – 0.010 inches [0.127 – 0.254 mm]), and close slightly before dilating; the minimum crack width, or the point at which the crack began to re-open was considered the zero point for crack opening and crack slip. The “zero” crack opening is demonstrated in **Figure 6.29** as the shear stress, and consequently the normal stress, is increased during loading. This “initial” crack condition is important for the remainder of the crack analysis because it normalizes the crack condition between specimens. As shown in the previous section, the

pre-cracks may have been larger for some specimens than for others and the push-off crack closing magnitude would vary in proportion to the pre-crack opening; this can lead to inconsistencies in determining the slip to opening relationship.

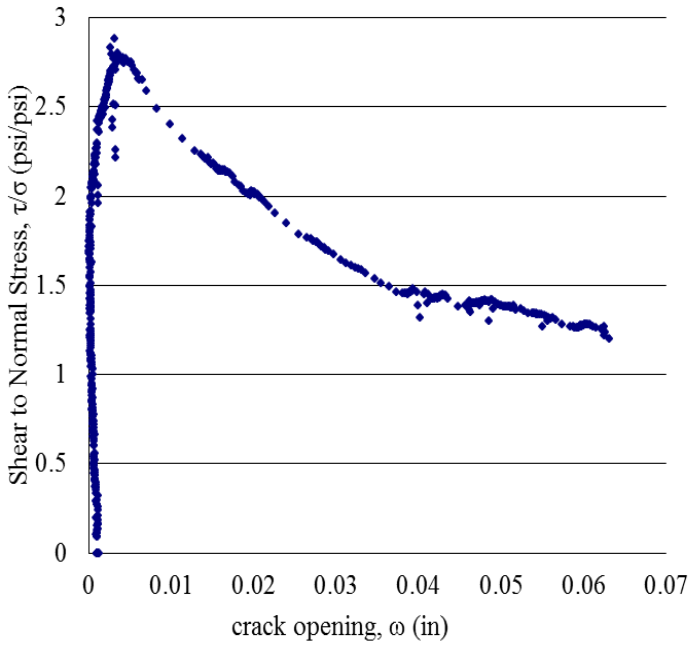

Figure 6.29 – Determining "Zero" Crack Opening

Another relationship being demonstrated by **Figure 6.29** is that shear stress is developed at a different rate than normal stress with respect to crack opening (and therefore also crack slip). **Figure 6.30** and **Figure 6.31** demonstrate the difference in shear and normal stress development as the specimen deforms. Notice that there is an initial normal stress, but not an initial shear stress because of the way the test is performed. Notice also that the applied load is in shear and thus the shear stresses develop at a higher rate than the indirectly induced normal stresses caused by crack

dilation and specimen deformation. The normal stresses do not begin to increase until an adequate amount of shear stress is applied to cause crack dilation and deformation, the maximum shear stress to normal stress ratio will indicate the capability of that particular concrete batch proportion to resist shear stress. The shear to normal stress ratio is also dependent upon crack opening as shown in **Figure 6.29**; this was theorized by Walraven (1981) and demonstrated by Walraven and Reinhardt (1981) due to aggregate contact areas. The shear to normal stress ratio will be discussed further below when the test results for each mixture are shown and analyzed.

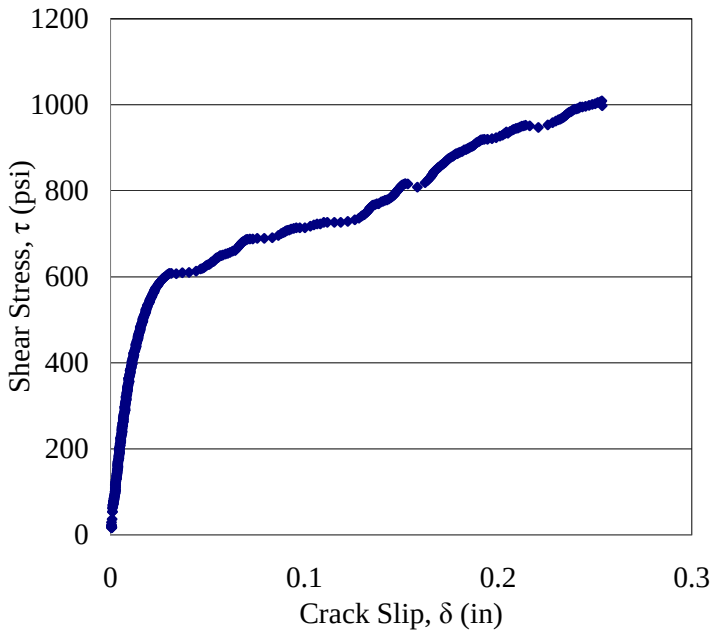

Figure 6.30 – Shear Stress Development over Crack Slip Range

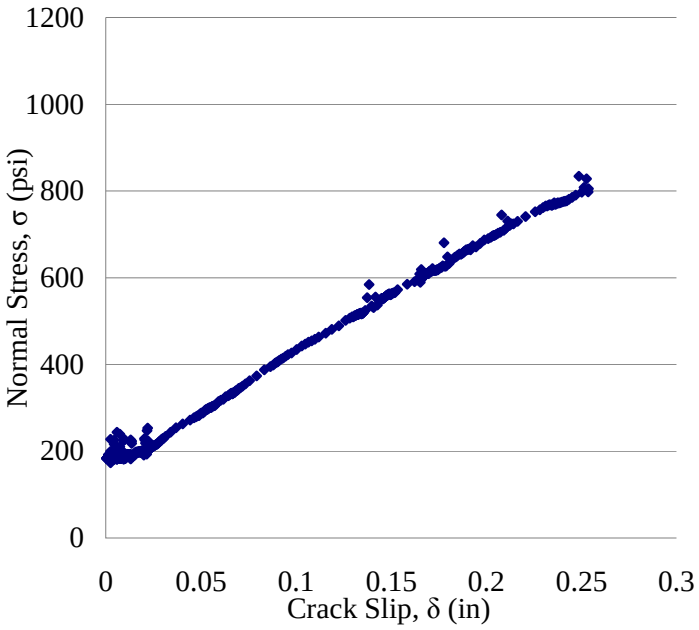

Figure 6.31 – Normal Stress Development over Crack Slip Range

As mentioned, the ratio of shear to normal stress indicates a mixture's ability to resist shear, this resistance changes with crack opening; however, a plot such as **Figure 6.29** does not include information about the crack slip. Recent researchers have proposed and used a method of normalizing the shear to normal stress ratio up to a given slip known as the slip limit, δ' (Barragan 2006; Kim 2008). The normalized value is known as an E-value and is used to describe the mixture's ability to resist shear in aggregate interlock. The E-value at a given slip limit is found from determining the area under the curves of **Figures 6.30 – 6.31** and dividing the prior by the latter. The equation for E-value would then be given by **Equations 6.1 – 6.3** below. The E-value over the whole range of slip limits for the example data set shown is demonstrated in **Figure 6.32** below.

$$E(\delta') = \frac{V_{Eq}(\delta')}{N_{Eq}(\delta')} \tag{6.1}$$

Where the equivalent shear and normal stresses (V_{Eq} and N_{Eq} respectively) are given by:

$$V_{Eq}(\delta') = \frac{\int_0^{\delta'} \tau(\delta) d\delta}{\delta'} \tag{6.2}$$

$$N_{Eq}(\delta') = \frac{\int_0^{\delta'} \sigma(\delta) d\delta}{\delta'} \tag{6.3}$$

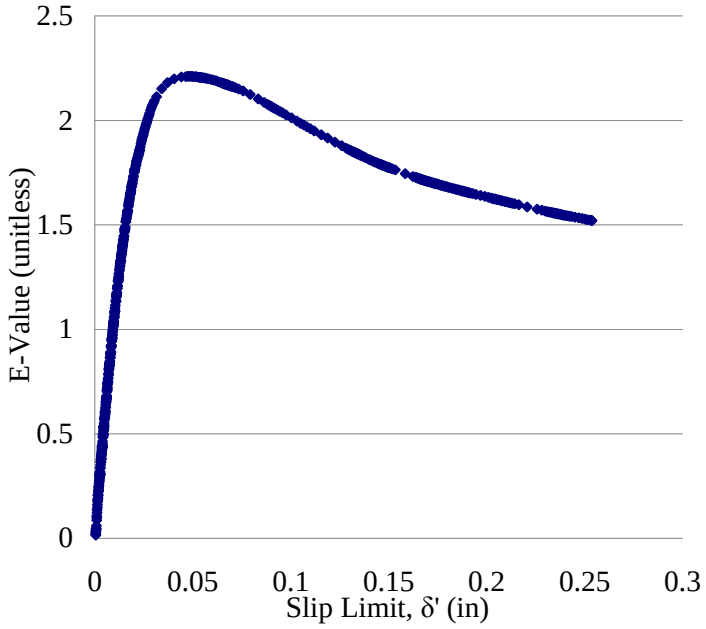

Figure 6.32 – E-value over Full Range of Slip Limits

The E-value at a given slip limit is then essentially an averaged shear to normal stress ratio over the entire slip range rather than an instantaneous shear to normal stress at that given slip.

This E-value could be a useful and powerful tool for comparative analysis; still, this should be investigated further. Other researchers have relied heavily on the E-value to perform comparative assessments, but there may be variables, such as the initial normal stress, that may require control to avoid impacting results (Kim 2008). For instance, if **Figure 6.31** had an increased initial normal stress, this researcher suspects it would require greater slips for the curve in **Figure 6.30** to overcome that normal stress, and the peak of **Figure 6.32** would thus be translated to the right. The E-value peak would likely be more rounded and of smaller magnitude. In order for researchers to rely so heavily on the E-value, they should have investigated sensitivity to test variability, and explained that all variables were controlled and to what level; though, this was not done. Because this researcher did not control the initial normal stress at the beginning of push-off test, nor know to what level or extent previous researchers controlled this or similar variables, such a thorough E-value analysis will not be performed. The E-value has been computed, the results will be shown, and trends can be identified; yet, a detailed analysis is unjustified and not shown.

The shear to normal stress ratio (τ/σ) across crack opening relationship as demonstrated in **Figure 6.29** was replicated for all tested concrete batch proportions. The point shown for each of the plots in **Figure 6.33** represent the average of at least two test results. For some mixtures tested, the crack did not open the full viewable range of 0.045 inches (1.14 mm). There may be a relatively large stress ratio change or termination of

plotted points when one or more tests terminated without reaching large crack openings for a given batch proportion.

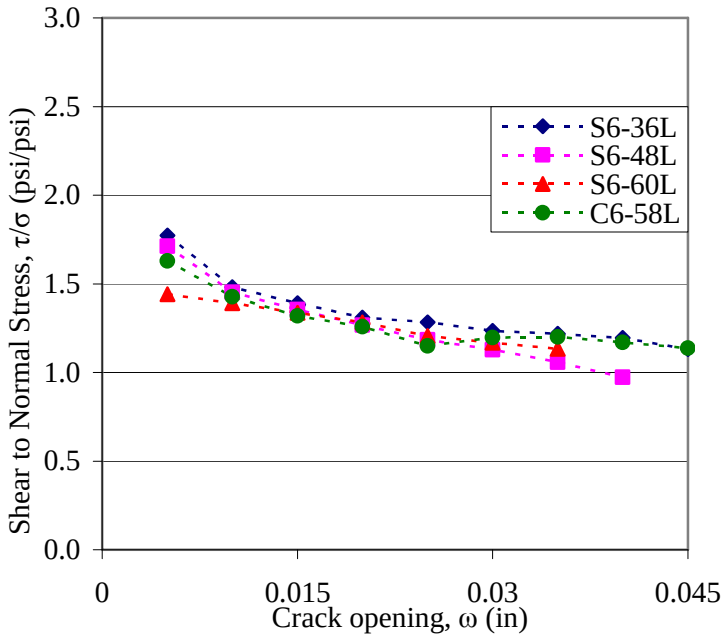

(a) 6 ksi (41.4 MPa) target strength limestone mixtures

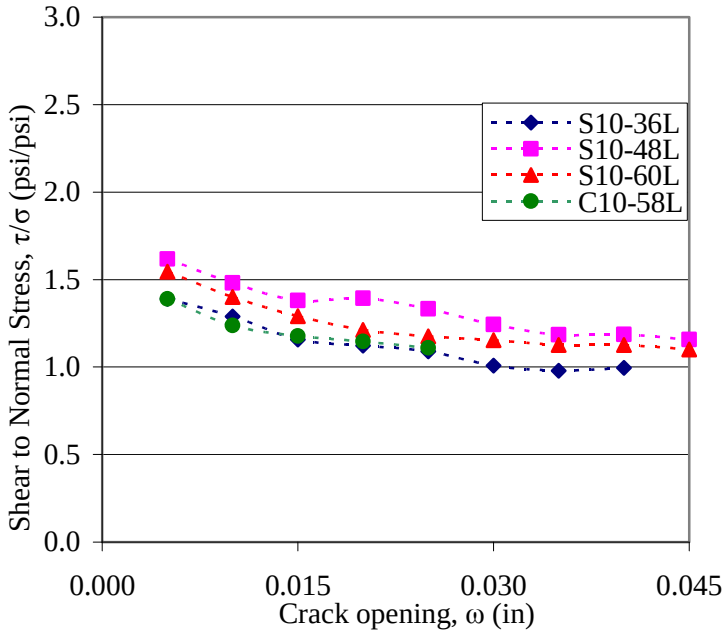

(b) 10 ksi (68.9 MPa) target strength limestone mixtures

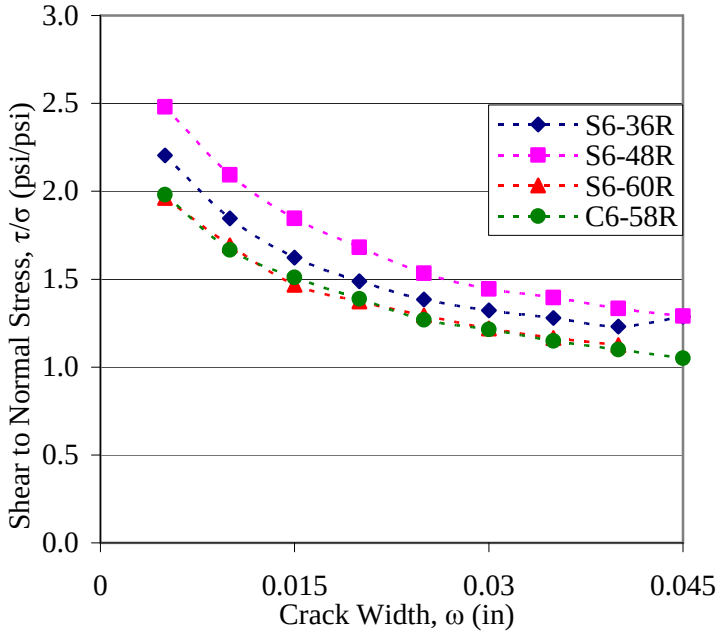

(c) 6 ksi (41.4 MPa) target strength river gravel mixtures

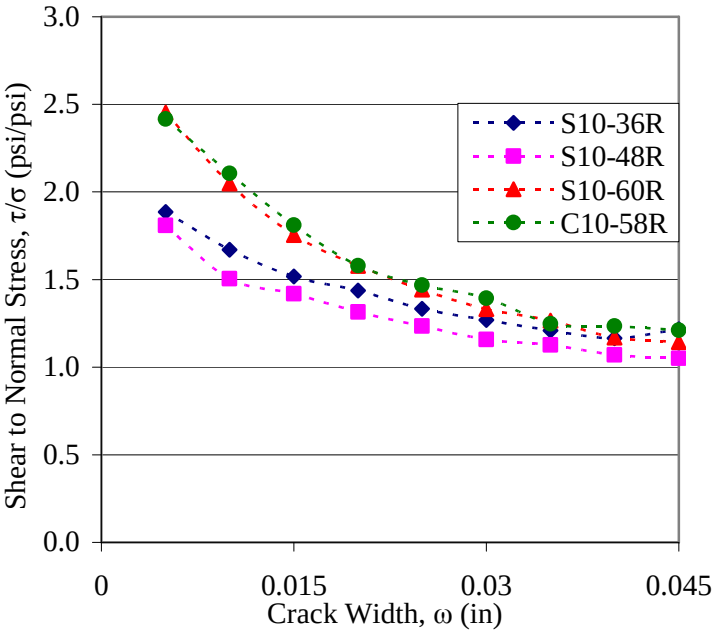

(d) 10 ksi (68.9 MPa) target strength river gravel mixtures

Conversion: 1 inch = 25.4 mm

Figure 6.33 – Shear to Normal Stress Ratio vs. Crack Opening

From the four basic strength and aggregate batch proportion groups represented in **Figure 6.33** trends were identified. Between plots (a) to (b) and to a lesser extent between (c) to (d) there seems to be a reduction of shear stress capacity when increasing compressive strength. This appears to be marginal for the batch proportions shown; however, recall that the 6 ksi (41.4 MPa) target strengths were much higher than anticipated, so the strength variation from the "low" to "high" strength mixtures may be slight. **Figure 6.34** shows the additional mixtures tested along with the average limestone batch proportions; because the 4 ksi (27.6 MPa) target strength mixtures actually maintained lower strengths, they really did exhibit a much improved shear to normal stress ratio at small crack widths indicating greater relative shear resistance.

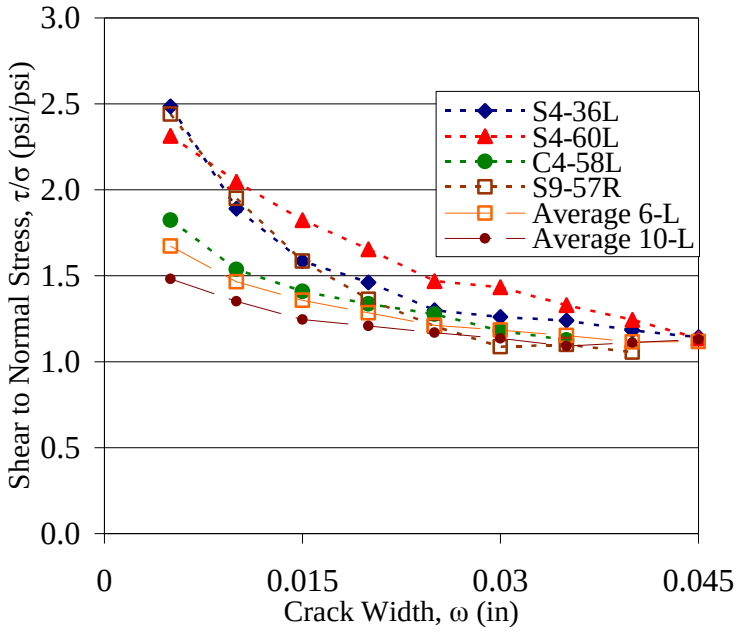

Conversion: 1 inch = 25.4 mm

Figure 6.34 – Reduced Compressive Strength Improves Relative Shear Resistance

The plots in **Figure 6.33** also show two more trends. When comparing plots (a) and (b) to (c) and (d) there is an obvious improvement in the shear capacity of the river gravel over the limestone mixtures. The improved shear strength of the river gravel mixtures is due to the fact that the aggregate are harder and therefore fractures less along the cracked plane than the limestone. The river gravel mixtures demonstrate the improved shear resistance through openings of about 0.03 in (0.8 mm), with diminishing effects thereafter. Lastly, the final trend identified is that there seems to be no distinction of the shear capacity for CC and SCC mixtures of the same strength and aggregate type investigated within this study. Each of the plots in **Figure 6.33** show tightly bunched data points between all mixtures of the same strength and aggregate type; additionally, the aggregate fraction that appears to resist shear most efficiently for one mixture does not necessarily demonstrate that efficiency for all strength levels or aggregate types. **Figure 6.35** below shows how the shear beam companion specimens cast at Coreslab Structures Inc. compare to the average of all mixtures of the same target strength level tested. Note that there was only one shear beam companion specimen of each batch proportion. From the plot, the average 6 ksi (41.4 MPa) target strength mixtures tested performed very similar to both the 6 ksi (41.4 MPa) CC and SCC companion specimens cast at Coreslab Structures Inc. The 10 ksi (68.9 MPa) CC companion specimen performed better than average; whereas, the SCC companion specimen performed worse than average. The apparently poor performance of the SCC cast at Coreslab Structures, Inc. should not be scrutinized too harshly considering it was produced from a single test specimen.

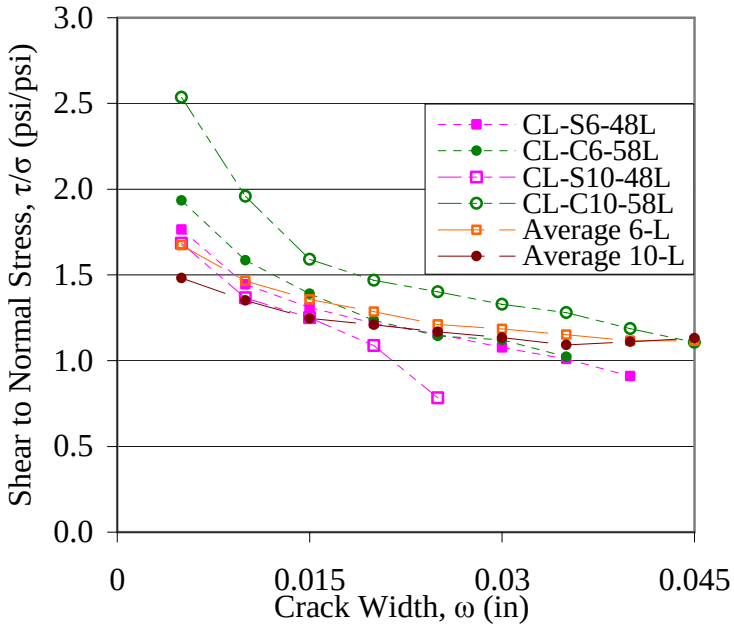

Conversion: 1 inch = 25.4 mm

Figure 6.35 – Performance of Specimens Cast at Coreslab Structures, Inc.

These same relationships can be identified in plots of the E-values over various values of slip limits, δ'. The four basic batch proportion groups can be reviewed in **Figure 6.36**. Recognize that the same trends identified are still present, but over a range of slip limits, not crack width openings. The strength of the mixture seems to have a small impact, the aggregate type appears to have the largest implication, and the C.A. percentage seems to have little influence on the ability of the mixture to resist shear.

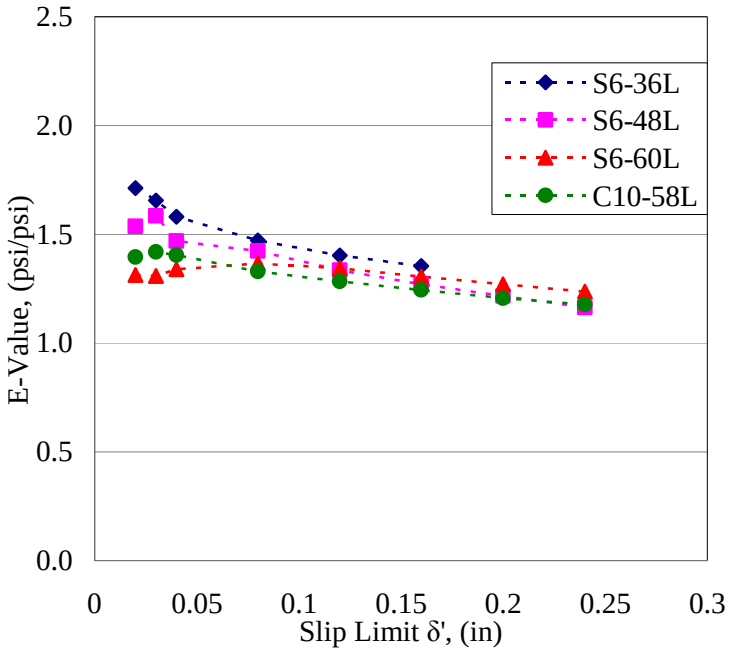

(a) 6 ksi (41.4 MPa) target strength limestone mixtures

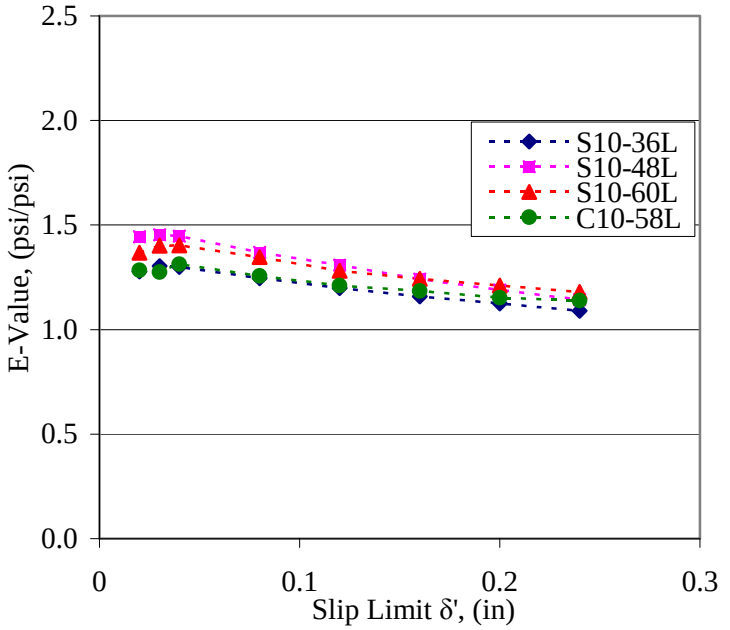

(b) 10 ksi (68.9 MPa) target strength limestone mixtures

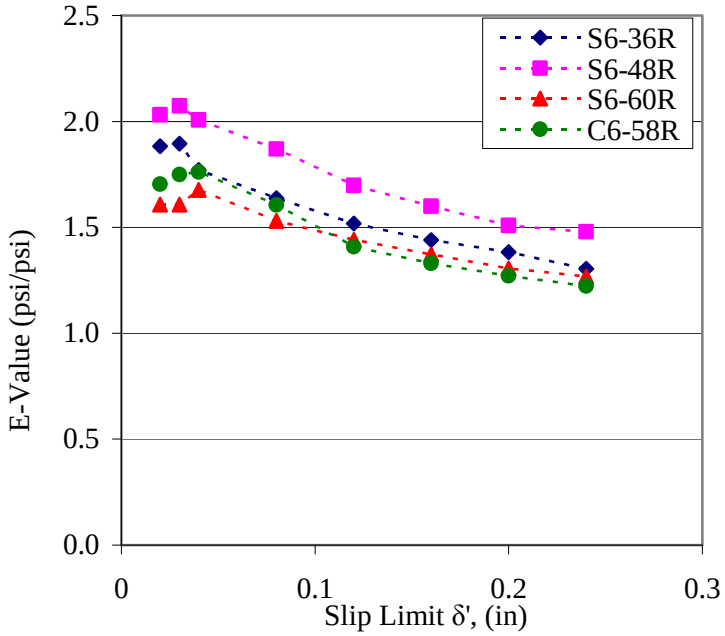

(c) 6 ksi (41.4 MPa) target strength river gravel mixtures

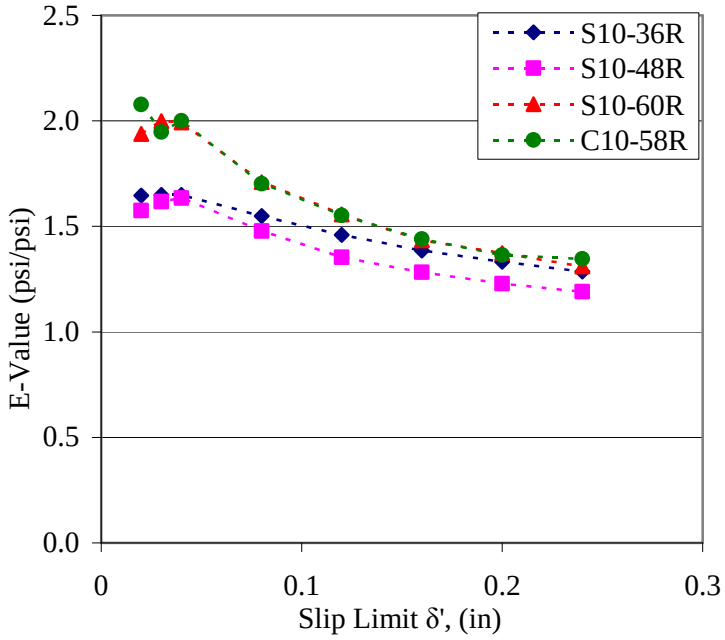

(d) 10 ksi (68.9 MPa) target strength river gravel mixtures

Conversion: 1 inch = 25.4 mm

Figure 6.36 – E-value across Slip Limit Range

Next, the push-off tests can be used to examine the slip to width relationship. Returning to the theory explained by Walraven, as a crack opens during shear, it also slips. If the roughness of the cracked interface is reduced, there is less resistance to slip for the same amount of crack opening. Thus, if two separate concrete batch proportions are compared and one exhibits increased slip at the same crack opening, it can be concluded that it has a decreased roughness profile. The decreased roughness might be caused by less aggregate, smaller aggregate, more fractures within the aggregate along the crack, or a more finely graded aggregate (Walraven 1981). Because the crack slip to width relationship can convey so much information about the mechanism of aggregate interlock, the test results will be shown and discussed. **Figure 6.37** shows the crack slip to width relationships for the four basic mixtures tested.

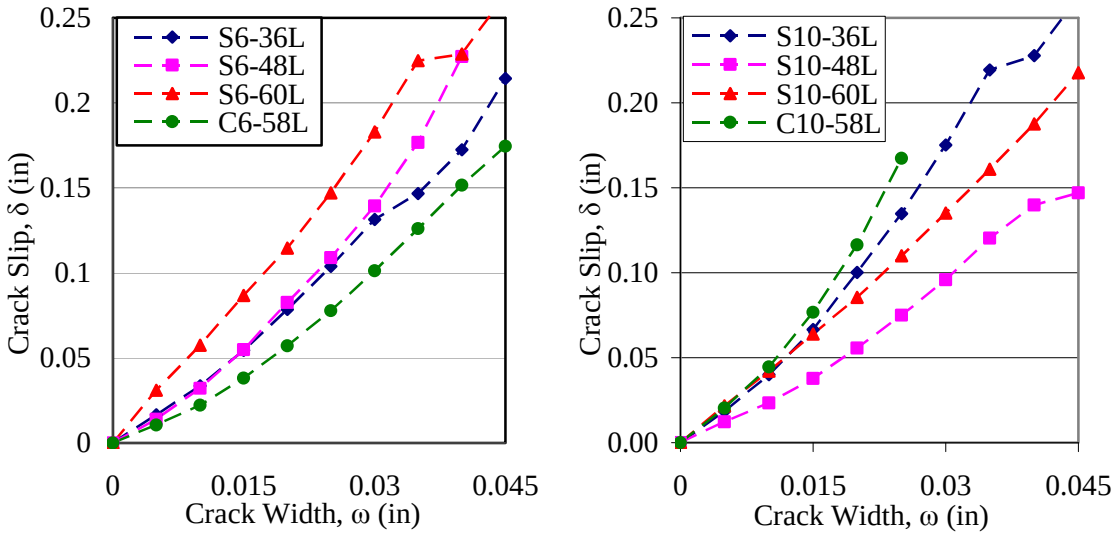

(a) 6 ksi (41.4 MPa) limestone

(b) 10 ksi (68.9 MPa) limestone

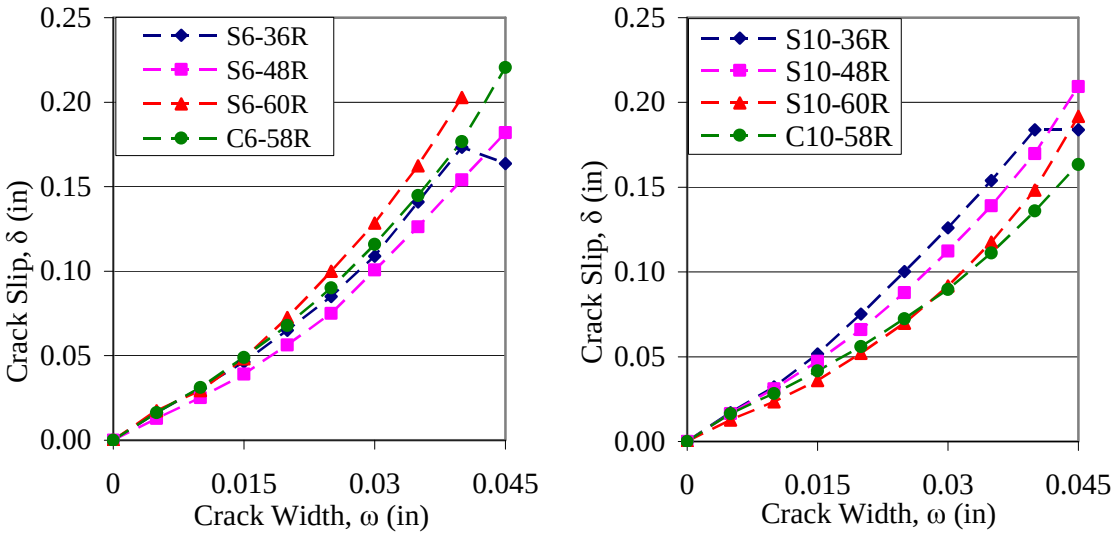

(c) 6 ksi (41.4 MPa) river gravel (d) 10 ksi (68.9 MPa) river gravel

Conversion: 1 inch = 25.4 mm

Figure 6.37 – Crack Slip to Opening Relationship

From the results shown in **Figure 6.37**, the largest factor governing the slip to width relationship appears to be aggregate type; the crack slip at a crack opening of 0.045 inches (1.14 mm) of limestone mixtures is about 0.25 inches (6.4 mm) as compared to the reduced 0.20 inches (5.1 mm) of the river gravel batch proportions. When comparing all plots, there doesn't seem to be a significant difference between SCC or CC mixtures or between batch proportions of varying C.A. percentage. When comparing the plots of (a) to (b) or (c) to (d) there is little difference between the curves due to strength. **Figure 6.38** shows the averaged results for each strength level of the limestone mixtures and compares them against the averaged limestone results determined by Kim et al. and the river gravel curve developed by Yoshikawa (Kim et al. 2008; Yoshikawa 1989).

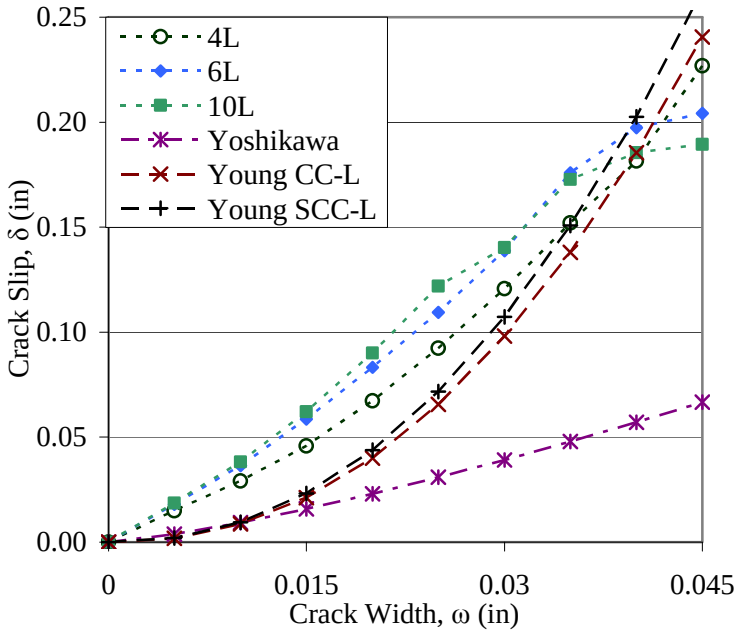

Conversion: 1 inch = 25.4 mm

Figure 6.38 – Limestone Mixtures Tested Compared to Previous Researchers

See that the 4 ksi (27.6 MPa) target strength mixture had improved slip resistance at given widths over the higher strength limestone mixtures tested. One can see that the limestone used in this study may have been weaker than that used by Kim et al. because it has more slip at given widths for all strengths tested. See also that all limestone mixtures performed poorly compared to the river gravel mixture tested by Yoshikawa; this is explained by the fact that limestone is generally weaker than river gravel and would therefore have more fractures along the cracked plane and an overall reduced roughness. **Figure 6.39** shows the averaged results for each strength level of the river gravel mixtures and compares them against the averaged river gravel results determined by Kim et al. (2008) and by Yoshikawa (1989).

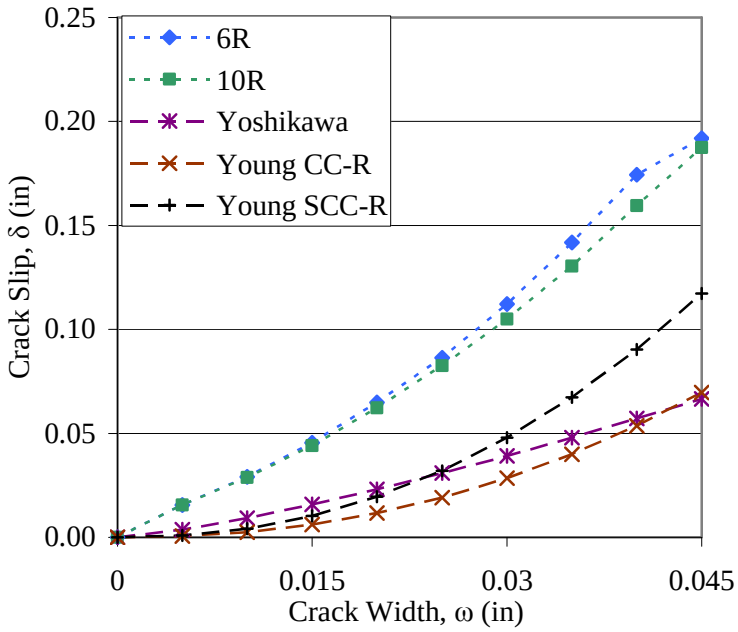

Conversion: 1 inch = 25.4 mm

Figure 6.39 – River Gravel Mixtures Tested Compared to Previous Researchers

The 6 and 10 ksi (41.4 and 68.9 MPa) target strength river gravel mixtures tested in this project exhibited very similar crack slip to opening behavior. The performance when compared to the river gravel mixtures tested by Kim et al. and Yoshikawa is not as good. The river gravel mixtures tested had a decreased roughness profile and increased rate of progressive aggregate fracture when compared to the other researchers. The inferior performance of the mixtures tested could result from possibly weaker river gravel than what was used by the other researchers, increased concrete compressive strengths which increases aggregate fractures along cracked planes, or both working together. It is still readily evident that the river gravel mixtures performed better than the limestone mixtures of this study.

The push-off test data analysis methodology has been described and thoroughly detailed. It was shown through use of an example specimen how the datum or “zero” point was set for the crack opening and slip from the raw data. Representative shear stress to crack slip and normal stress to crack slip plots were shown. The E-value, used extensively by other researchers was determined for the sample results. The means of determining the E-value by graphical and calculable methods was described. The shear to normal stress ratio was examined over a range of crack openings for all concrete batch proportions tested in this study.

The results demonstrate that concrete type (CC or SCC) and C.A. % makes little difference to the aggregate interlock capability of the concrete batch proportions tested. The strength of the concrete has a noticeable effect, but most dramatically when examining the 4 ksi (27.6 MPa) limestone mixtures in relation to the other higher strength limestone mixtures. Reduced compressive concrete strength improves the relative shear resistance. The strength effect seen in this study is reasonably minimal because the 6 ksi (41.4 MPa) target strength mixtures actually achieved much higher strengths of about 8 - 10 ksi (55.1 – 68.9 MPa). Other researchers have found that the aggregate interlock mechanism of shear resistance diminishes with increased concrete compressive strength, the effect is essentially ignored at strengths above 10 ksi (68.9 MPa) (Bentz et al. 2006; Kim 2008; Walraven and Stroband 1994). This was the whole reason a 4 ksi (27.6 MPa) mixture was developed and tested, so that strength effects could be investigated. Next, the effect of aggregate type appeared to be the most dramatic. The weak nature of Missouri limestone and the improved strength of river gravel led to improved shear resistance of all river gravel mixtures over all limestone concrete batch proportions.

The E-value was discussed in detail. The extensive use of the E-value by other researchers as an analytical tool was called into question. The E-value can be used as a comparative tool and perhaps an analytical one if all variables are controlled and conveyed sufficiently. This researcher examined the E-values and made similar conclusions as from the shear to normal stress over crack opening investigation. No additional analysis was performed as it was considered unjustifiable.

Next, the crack slip to opening relationships were shown and discussed. It was shown that as a mixture exhibited less slip at a given crack width, it demonstrated improved shear resistance. Improved shear resistance results from greater crack profile roughness and reduced propagation of aggregate fracture. An initially rough cracked plane will have less slip than an initially smooth cracked plane. A mixture containing easily fractured aggregate will have increased rates of slip as compared to a mixture containing hard aggregate that resist shear at all crack widths.

The results of the push-off test confirm theoretical relationships between strength and shear capacity, and aggregate strength or fracture along cracks and shear capacity. The effect of concrete type between SCC and CC and the effect of C.A. percentage was not seen. The variation between specimens of a given batch proportion was large enough that the results from other batch proportions of the same strength and aggregate type could not be differentiated. For some combinations of concrete compressive strength and aggregate type, a given SCC would appear to perform the best, but at other strengths and aggregate types another SCC or the CC would appear the most efficient. From the results, no conclusion can be made about the superiority of SCC or CC. Based upon the material

constituents and batch proportions investigated, there does not appear to be significant variations worthy to suggest the SCC mixes studied would yield reduced shear capacity.

After the push-off tests, the cross-sections of the failed specimens were photographed and investigated for segregation and actual C.A. percentage along the cracked plane. The following section discusses the results from the post-testing forensic sectional investigation.

6.4.3 Cross-Sectional Imaging Results and Analysis The NIH software ImageJ was used to analyze the post-failure cross-sections of the precrack and push-off tests. The goal was to examine the cross sections for the actual segregation and actual C.A. percentage as the specimens were cast and across the cracked plane. The process by which the cross-sections were analyzed has already been described in **Section 6.2.2**. The results will now be presented with conclusions drawn.

Because the imaging software was used by isolating the different color intensities present in each cross-section, and because some of the mineralogy present in the limestone aggregate was difficult to accurately distinguish from the surrounding paste matrix, the investigation focuses only on the river gravel specimens. The information chosen to be gathered from the analysis consists of the size and location of particles of interest; in this case the particles represent aggregate. The size threshold was set to gather only information about C.A. or, more precisely, particles with an area in excess of 0.008 in^2 (5.16 mm^2) or a diameter of about 0.10 in (0.25 mm). The area fraction was determined for the C.A. over the entire cross-section. The X and Y coordinate location of each aggregate within the cross section was also determined. The C.A. area fraction could then be determined and compared to the designed C.A. percentage to see if there were

any large discrepancies as to what was actually cast. The coordinate location of each aggregate could be used to determine segregation in both the vertical direction, the segregation due to gravity and placement method, and in the horizontal direction, segregation due to placement method.

The determination of segregation was based on ASTM C 1610 – 2010: Standard Test Method for Static Segregation of Self-Consolidating Concrete Using Column Technique. The equation from ASTM C 1610 – 10 is shown as equation 6.4, the equation used to determine segregation of the hardened specimens is shown as equation 6.5.

$$S = 2\left[\frac{\left(CA_B - CA_T\right)}{\left(CA_B + CA_T\right)}\right] * 100 \tag{6.4}$$

Where S is segregation percentage, CA_B and CA_T are the washed and oven dried C.A. masses of the bottom and top sections of the segregation column.

$$S = 2\left[\frac{A_p}{A_T} X_i - \frac{X}{2}\right] * 100 \tag{6.5}$$

Where S is the segregation percentage, X_i and X are the center of the i^{th} particle and the total length respectively, and A_P and A_T are the area of the i^{th} particle and the total area of all particles respectively. The equation used is computing the mass weighted centroid and comparing it to where the centroid should be expected, half of the length. This was then replicated in the Y-direction.

Table 6.2 summarized the findings from the segregation analysis. The segregation was investigated in both the vertical and horizontal direction. The horizontal position could be considered the segregation just by placement method and the fact that concrete is non-homogeneous and will inevitably exhibit some spatial variation of the constituent materials. Segregation in the vertical direction could be considered the real segregation that is due to the combination of placement method and gravity, just as would be experienced by any concrete placement.

Table 6.2 – ImageJ Segregation Results

Mix	Vertical Segregation, %	Horizontal Segregation, %
S10-36R	14.07	15.99
	6.88	1.70
	20.60	4.29
S10-48R	5.54	0.83
	13.98	1.72
	9.21	1.93
S10-60R	5.51	9.92
	12.84	4.59
	3.19	5.27
C10-58R	2.55	14.87
	4.01	25.33
	5.02	4.97
S6-36R	6.16	8.30
	19.46	18.59
	3.20	6.15
S6-48R	7.68	4.36
	25.67	6.26
	11.34	11.58
S6-60R	10.67	2.32
	10.99	5.20
C6-58R	8.01	2.73
	21.45	3.67
	11.70	1.48
CIP	5.61	9.09
	7.17	5.29
Average	10.51	6.49
CC Average	8.79	8.84

From the results, the segregation of all mixtures is reasonable. The placement segregation (horizontal direction) of the SCC was less than that of the CC, which may be reasonable because less effort is actually used to manually place the SCC. More segregation was seen by the SCC in the vertical direction when compared to the average CC segregation. Although there was more segregation for the SCC batch proportions, it was still reasonably low at an average of only 10.51 percent. SCC is considered robust if it can demonstrate a column segregation of 10 percent, so the average SCC mixture tested was very close to this target.

Next, the actual C.A. percentage present was compared to the C.A. calculated based on batch proportions. Throughout this report, the mixtures have been characterized by their C.A. percentage of total aggregate volume; however, this number no longer applies when examining the C.A. percentage of total hardened concrete volume. The latter, C.A. of total volume percentage is calculated from the batch proportions used. It should be noted that neither the volume of air nor the volume of water should be considered in the total hardened volume presented here either. Because the cross-section of a specimen is being viewed, whatever water or air voids that were present at the time of casting are now being looked through, to whatever paste or aggregate happens to be exist behind it on that specific cracked plane. So, the equation for determining C.A. volume fraction of total hardened volume for comparison to the ImageJ results is given as equation 6.6.

$$C.A._{TotalVolume} = \frac{C.A.}{C.A. + F.A. + Cem. + Ash} \tag{6.6}$$

The C.A. volume fraction of the hardened concrete is then the volume of C.A. divided by the total hardened volume given as the sum of C.A., F.A., cement, and fly ash. **Table 6.3** shows the calculated C.A. volume for each river gravel batch proportion tested, and the average C.A. volume determined by the ImageJ analysis.

Table 6.3 – Calculated and Actual C.A. Volume Fractions

Mix	Theoretical C.A. Volume, %	Calculated C.A. Volume, %	Percent Variation
S10-36R	26.06	24.44	6.21
S10-48R	34.74	35.30	1.60
S10-60R	43.43	58.71	35.18
C10-58R	41.98	40.37	3.85
S6-36R	29.44	29.03	1.41
S6-48R	39.25	38.90	0.88
S6-60R	49.06	47.87	2.43
C6-58R	47.43	44.12	6.99
CIP	45.29	36.79	18.77

The results of the ImageJ investigation and the calculated theoretical results are in close agreement meaning the ImageJ analysis was accurate in detecting C.A. particles of interest. The small variation also helps to make the findings discussed previously of **Table 6.2** valid. The S10-60R specimen may have needed additional calibration as there were many more aggregate particles counted than there should have been present; although, this could have actually been the case. Perhaps some segregation occurred prior to casting the push-off specimen and a disproportionate amount of C.A. was actually included in the test specimen.

Overall, the ImageJ results were good for the river gravel mixtures. The software was not able to distinguish some of the limestone aggregate from the surrounding paste

matrix; therefore, the forensic analysis of the limestone batch proportions was not performed. Segregation seemed to be minimal for all river gravel mixtures tested, including SCC mixtures. Because the theoretically calculated C.A. volume percentage matched closely to the results of the ImageJ analysis, the analysis appears to have been accurate and justified.

6.5 CONCLUSIONS

The smaller scale experimental shear test program proved valuable. The precrack and push-off tests were thoroughly described in setting up the test, and what steps were necessary to perform the tests. The specimen design was also discussed. There was a preliminary specimen formwork, dimension, and reinforcement that proved inadequate; the problems encountered, the failure mechanism, and the underlying reason were all discussed. The specimen design was re-written and proved much more reliable for testing. The results from the precrack and push-off tests were shown. The post-failure cross-sectional imaging analysis was described and the results presented. The results for all tests were analyzed.

The precrack test was investigated with greater detail than by previous researchers. Prior studies have conveyed no information about what impact the magnitude of the initial normal stress has on the precrack load or the crack opening. It was determined that for the mixtures tested for this project, the initial normal stress leads to increased precrack loads, but more importantly, it leads to reduced crack opening. Higher initial normal stress also appears to reduce the sudden rise in normal stress after crack development, meaning the opening of the crack is less explosive. These findings

are important for researchers seeking to maintain small crack openings (anything less than 0.02 inches [0.5 mm]). From the concrete batch proportions tested, an initial normal stress of about 350 psi (2.41 MPa) should consistently lead to precrack maximum crack widths of less than 0.02 in (0.5 mm). If the crack opening is less than desired, continued loading will gradually open the crack; this process also allows more control over the crack opening size, leading to superior results. Unfortunately these findings were a result of this research and could not be used throughout the testing. Additionally, there was a correlation between increased precracking load to both STS and the square root of concrete compressive strength; this should be expected since the failure mechanism is similar to that of the STS and because increased compressive strength should also improve tensile strength.

The push-off test results demonstrated valuable relationships. The methodology of analyzing the push-off data was described in greater detail than by previous researchers; this improves the repeatability of this research and allows for more transparent findings. The shear to normal stress ratio across crack width relationship was used to determine which concrete batch proportions demonstrated improved resistance to shear. The plots were grouped by target compressive strength and aggregate type. When examining each plot, it showed a CC mixture and three SCC mixtures of varying C.A. percentage; there seemed to be little impact of C.A. fraction or of concrete type. When comparing the plots, trends were identified. There seemed to be a slight effect due to concrete compressive strength; this was very slight and was investigated further by developing three additional low strength concrete batch proportions. The reason for the very slight difference between the 6 – 10 ksi (41.4 – 68.9 MPa) mixtures was likely because the target strengths

were exceeded by almost all mixture; the actual strengths achieved were in the range of about 9 – 12 ksi (62.0 – 82.7 MPa). Researchers have shown that high strength concrete has reduced shear resistance from aggregate interlock because a larger fraction of the aggregate actually fracture along with the paste matrix. The additional low strength (4 ksi [27.6 MPa] target) mixtures proved to a more noticeable degree that this trend was identified in this study. The largest effect on shear resistance appeared to be aggregate type. There was a clear distinction when comparing the limestone results to those produced by the river gravel mixtures. There was benchmarking to previous studies and some discussion about the E-value used by other researchers. The E-value can be a useful comparative tool, just as what was described by the shear to normal stress ratio; yet, this researcher believes it has been used too exhaustively by other researchers and the reasons for this questioning were outlined. The E-value was shown for the mixtures tested, and the conclusions drawn were the same as those just described. Lastly, the push-off test was used to investigate the crack slip to width relationship. The trends identified are given more substance when examined in this way. It is easily seen that mixtures that performed poorly at resisting shear stress exhibited increased slips and increased slip rates at a given crack opening. This is explained by knowing that a surface that is less rough, a smooth crack, will not be engaged by as much aggregate area at a certain crack opening as compared to a very rough crack with protruding aggregates.

The forensic cross-sectional imaging was then discussed. The segregation seen from the imaging software was small. It was interesting to note that SCC exhibited less segregation than CC in the horizontal direction; this is explained by knowing that SCC is allowed to flow into position whereas CC is manually consolidated, this action actually

disturbs the position of aggregate in the side to side direction. SCC did show more segregation in the vertical direction than CC, but the magnitude was still small, suggesting the mixtures tested were robust and resistant to segregation. The C.A. volumetric percentage of the hardened volume was calculated and compared to that counted by the imaging software. The calculated theoretical C.A. volumetric fraction was close to that determined from the analysis; this confirms that the imaging process was accurate and valid.

The smaller scale shear specimen tests have been performed. The results of the tests have been shown. An analysis of the results have been covered and concluded. The next step is to review the large shear specimen tests performed. For this research project, the large shear specimens are precast, prestressed concrete beams.

7. PRECAST, PRESTRESSED BEAM TESTS

7.1 INTRODUCTION

Precast, prestressed beams were fabricated and tested in shear for this investigation. The four baseline mixtures used throughout this project 6 ksi (41.4 MPa) target strength limestone CC and SCC, and 10 ksi (68.9 MPa) target strength limestone CC and SCC) were tested under four point loading. The beams were tested to evaluate the concrete shear strength prediction equations from ACI, AASHTO, and the MCFT. Crack propagation patterns and deflections during beam loading were also recorded.

This section will detail the beam test setup and procedure. There were issues experienced with the initial test setup; the problems encountered and the actions taken to correct them will be discussed. The beam reinforcement detailing and fabrication procedure will be shown. Next, the beam test results will be given. Lastly, the beam shear test results will be analyzed such that conclusions can be drawn about SCC and the conformity of the material behavior to that of CC at similar strength levels.

7.2 TEST SETUP AND PROCEDURE

Numerous researchers have performed beam tests for shear; however, each test setup and procedure may vary slightly from study to study. This section will discuss the details of the shear beam test setup such as the positioning, load and reaction point locations, and the LVDT positioning to capture deflection. The specific procedural actions taken throughout the shear beam testing will also be discussed.

7.2.1 Test Setup The shear beam test was developed such that two shear tests could be performed on each beam. Initially, a three point load test was developed that would put the test region into high shear, but leave the remainder of the beam in relatively low shear and moment so as to avoid damaging the beam where it would be subsequently loaded again for the second test. The initial test setup can be seen in **Figure 7.1** below.

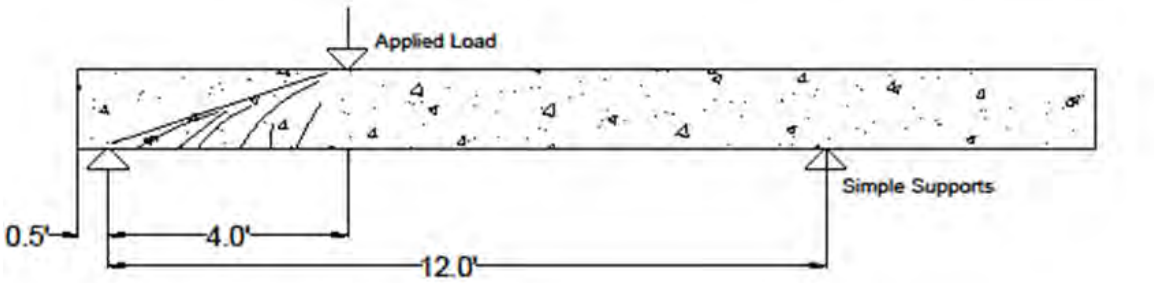

Figure 7.1 – Initial Three Point Shear Beam Test Setup

Upon testing of the first beam, it was determined that the three point loading was not effective with the test apparatus in use. **Figure 7.2** shows a picture of the load actuator being used for the testing; it can be seen that with several points of rotation, the load can (and did) become unstable and the apparatus can shift out of position, no longer applying load to the point desired. It should be noted that the beam tested under three point loading did carry enough load initially to develop flexural cracks and even some flexural-shear cracks, but did not fail prior to the apparatus rotating out of position; this disturbed test region was subsequently tested with the new test setup described below.

Figure 7.2 – Load Actuator used for Shear Beam Tests

It was determined after the trouble experienced on the first beam tested, to use a four point load test. The shear span on the test region was kept to 4 ft (1.22 m), so the same ultimate load could be expected. The other region of high shear in the first test on a given beam lies outside of the test region of the second test on that beam, so it was determined that each beam could still be used for two tests. There is an influence of the first test on the second, but this will be discussed further below. **Figure 7.3** and **7.4** detail the four point loading test used for all beam tests.

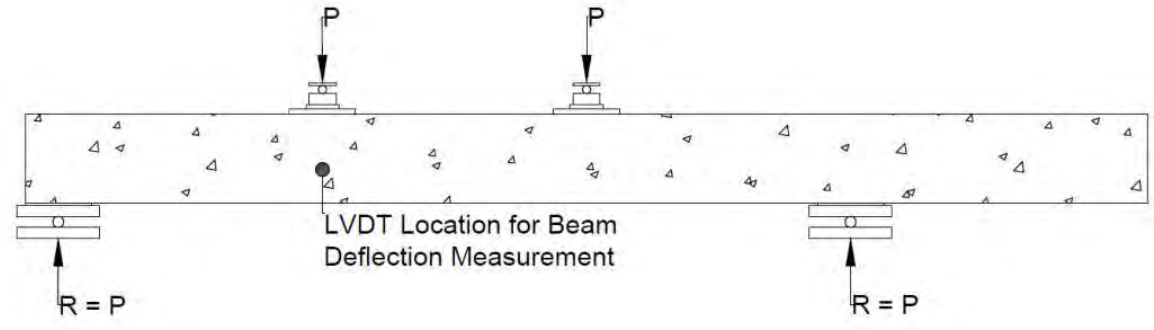

(a) First test on beam

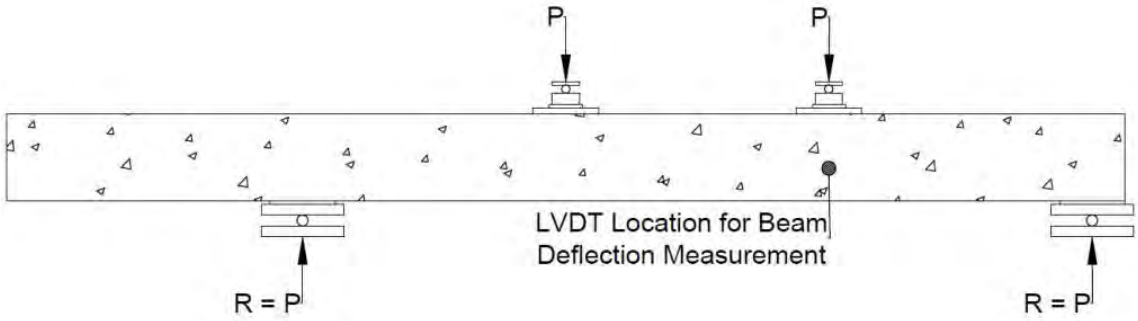

(b) Second test on same beam (moved left 4 ft [1.22 m])

Figure 7.3 – Four Point Shear Beam Test Setup

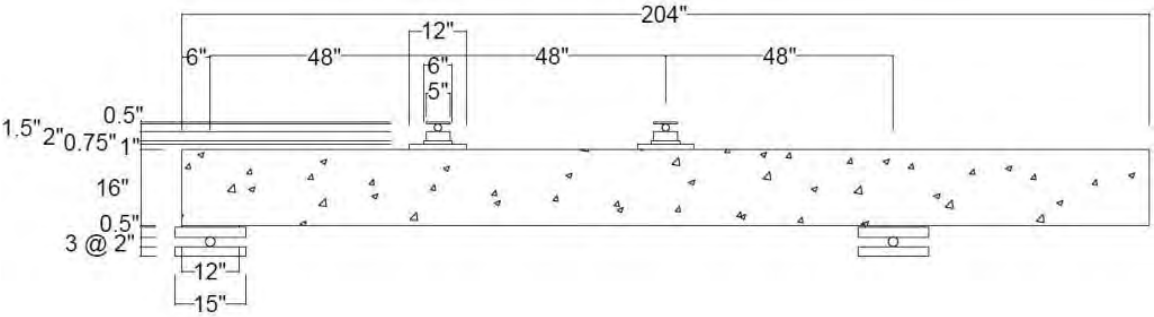

Conversion: 1 inch = 25.4 mm

Figure 7.4 – Beam Test Dimensions

An LVDT was attached at the first load point location using a concrete anchor placed well below the compression zone to measure beam deflections during testing; this is also shown in **Figure 7.3**. The LVDT was connected to a data acquisition system where the beam deflection was recorded. The load actuators were also connected to the DAS; actuator deflection and load information was recorded.

The test setup is simple in nature. There were issues with testing the desired three point loading with the test apparatus available; however, four point loading proved to be much more stable and still permitted two tests per beam.

7.2.2 Test Procedure The shear beams were tested at varying ages depending on test apparatus availability and when no scheduling conflicts arose; because the lab was busy, the test ages varied widely. Because of the large test age variance, there were also issues with the companion strength cylinders. The strength gain curves and resultant presumed test strength will be shown in **Section 7.4** below.

At the time of testing, each beam was moved into the position detailed above in **Figures 7.3** and **7.4** and the LVDT attached. At the location of the load points, a light dusting of #16 minus sieved sand was leveled below the load blocks so that uniform seating of the load could be accomplished. The load and reaction "points" were positioned into the center of the load and reaction blocks per the ACI 318 – 11 definition of shear span, a_v, "equal to distance from center of concentrated load to (b) center of support for simply supported members" (ACI 318 2011).

The load actuators were brought into contact with the top of the beam. Each actuator was adjusted such that 100 lb (445 N) of force was detected to seat the load, then the actuators' displacement datum were set to zero. The test commenced by displacement

control. Each manually initiated displacement step was 0.02 in (0.5 mm) and was reached in 1 minute. Between load steps, propagating cracks were marked to their current terminal lengths and the current load was indicated. At intervals, photographs were taken to help in recording the propagation of cracks. Throughout the test as previously stated, the beam displacement LVDT and actuator displacement and load data were recorded by the DAS. Loading continued in 0.02 in (0.5 mm) intervals until failure was accomplished.

After failure, the actuators were raised to remove the load, the DAS data was saved, and the failure was documented and photographed. The beam was then moved 4 ft (1.22 m) to the west in order to test the second test region on the same beam. After testing the second half of the beam, the beam was removed and discarded. This procedure was repeated for each of the four shear beams.

The first beam to be tested (S6-48L) actually failed in flexural crushing during the first four point test performed on that beam. Unfortunately, the crushing occurred near the load point at the midspan of the entire beam; this area would be under high moment in the second test performed on the beam. It was determined that the crushed area should be repaired. This repair was only performed on the S6-48L beam and was positioned away from the second test region such that two test results were still collected.

The procedure for repairing the beam consisted of several steps. The loose concrete cover from the crushed region was removed. The area was chiseled away to ensure that all of the disturbed concrete was removed. The repair area was ground square. It so happened that the repair area lie directly between two lateral ties, so the repair was approximately 12 inches (305 mm) in length and the full 8 inch (203 mm) width of the beam. The surface of the repair area was prepped with a “scrub coat” of Sikatop® 122

plus which achieves an ASTM-C882 modified 28 day bond strength of 2200 psi (15.2 MPa) when used in this fashion, see **Appendix A**. A repair grout was then placed into the repair area, compacted and worked into place, finished, and cured with burlap and plastic sheeting. The repair grout was actually a concrete mixture consisting of the same batch proportions of the beam being prepared (S6-48L), only the coarse aggregate was sieved to include only 0.50 inch (13 mm) minus particles. Twelve 4 x 8 inch (102 x 203 mm) cylinders were also cast and cured in the same fashion next to the repaired beam. The cylinders were used to track strength gain so that beam shear testing could commence when the patch achieved comparable strength to the remainder of the beam. **Figure 7.5** shows the steps taken to repair the previously damaged area of the S6-48L shear beam.

(a) Damaged area chiseled (b) Hammer drill used to chisel deep into the member

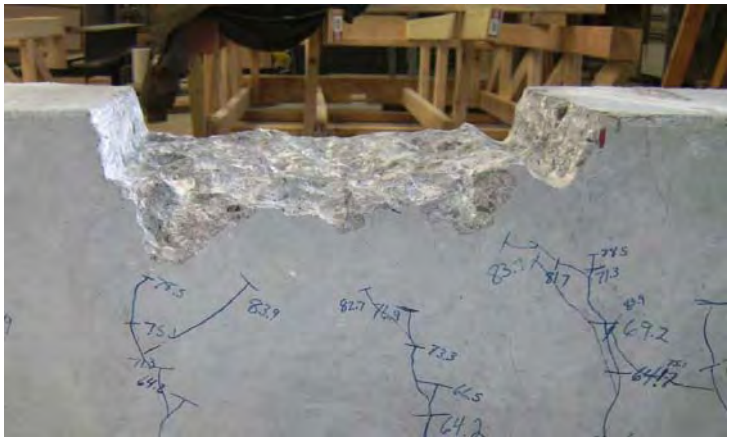

(c) Edges of damaged area were ground square

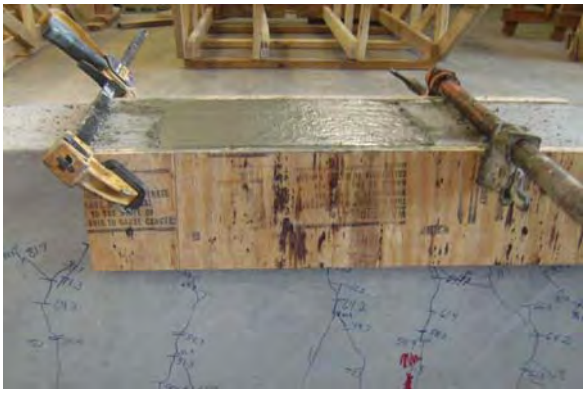

(d) “Scrub coat” and grout placed, finished

(e) Cured under burlap and plastic sheeting

Figure 7.5 – Shear Beam Repair Procedure

The procedure for testing the shear beams has been described. The precise actions taken throughout the tests were detailed. The unfortunate event of experiencing a crushing failure in the first test region on a beam was described; however, the repair process to enable testing of the second test region on the beam was detailed. Next, the beam reinforcing will be detailed along with the member fabrication process.

7.3 MEMBER DESIGN AND FABRICATION

First, the shear beam design methodology will be explained. The difficulty to design a beam to fail in shear, given the constraints imposed by the project funding will be discussed. The resulting member details will be presented. The member fabrication process, which took place at Coreslab Structures, Inc. in Marshall, MO will also be shown.

7.3.1 Member Design The first and most difficult constraint to overcome when designing the prestressed shear beams was that the cross-section was to be rectangular due to fabrication cost. Next, the beams had to be small enough that the prestressed concrete producer that fabricated the beams for the project could manufacture them for a reasonable cost to the project. The beams were designed against the simple calculations of ACI 318 2011. By using rectangular cross-section beams, the most typically experienced shear failure mode of prestressed beams or girders, what ACI denotes V_{cw}, is eliminated because the web stresses are not excessively high relative to the rest of the section (ACI 318 2011). The remaining shear failure mode is V_{ci}, the "nominal shear strength provided by concrete when diagonal cracking results from combined shear and moment" (ACI 318 2011). One can then imagine that it may be difficult to design a beam to fail in shear, when the beam is inherently experiencing simultaneous high moment and given the classically wide variability of shear capacity; that is exactly what was attempted.

In order to develop a reinforcement detail, a Microsoft Excel spreadsheet was developed such that numerous cross-sections with varying concrete dimensions and longitudinal reinforcing patterns could be checked rapidly. A sample spreadsheet beam

design aid can be viewed in **Appendix D** below. The input equations came from the ACI 318 2011 building code. The fiber stresses were computed in accordance with the "Basic Concept Method" as described by Nawy (Nawy 2010). The computed fiber stresses were checked against transfer stress limits of section 18.4.1 of ACI, top fibers in excess of the stress limit were reinforced with mild rebar (ACI 318 2011). The steel tendons were jacked to 70% of the specified tensile strength (f_{pu} = 270 ksi [1860 MPa]) to accomplish the fiber stresses desired. The stress in prestressing steel at nominal flexural strength, f_{ps}, was then computed by equation 18-3 of section 18.7.2 of ACI; this was important in computing the predicted nominal moment (ACI 318 2011). Using basic static equations, the shear that would be present at the predicted nominal moment was determined. Next, the basic shear equation 11-9 of section 11.3.2 ACI was used to predict nominal shear strength provided by concrete. Lastly, the predicted nominal shear strength was compared to the shear present at the predicted nominal moment; this ratio should be less than one to enable a shear mode of failure. It should be noted that a ratio less than one would predict a shear failure occurring before a flexural failure; however, each limit state prediction was made from equations developed empirically with their own ingrained variability, and a ratio below one does not ensure a shear failure. A lower ratio will more likely result in shear failure, so the goal of the analysis is to reduce the ratio while remaining within the constraints set by the code and by the cost of the project.

The resultant member design for the shear beams can be seen in **Figure 7.6** below and was used for all shear beams; the figure comes from the final shop drawings produced by Coreslab Structures, Inc. of Marshal, MO, the precast concrete producer aiding in fabricating the prestressed members for this research project. As shown in

Figure 7.6, the beams were actually cast on their side because it was easier for Coreslab Structures, Inc. to produce the formwork for this orientation.

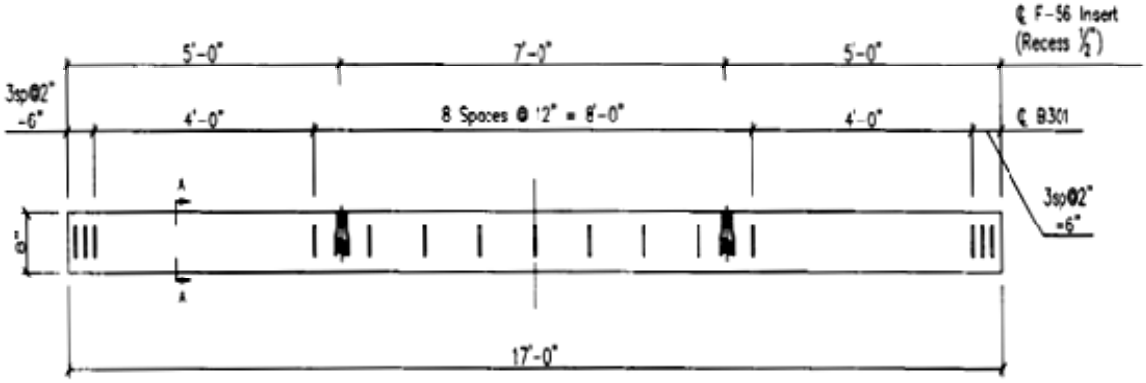

(a) Beam Elevation

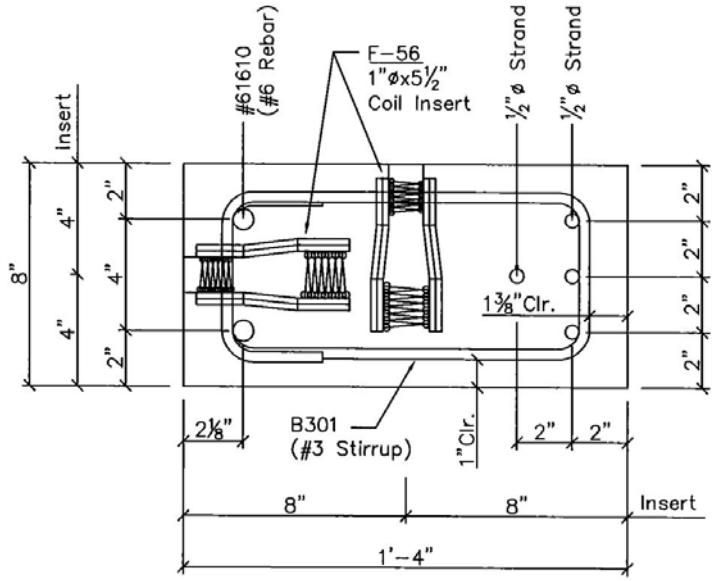

(b) Section A-A

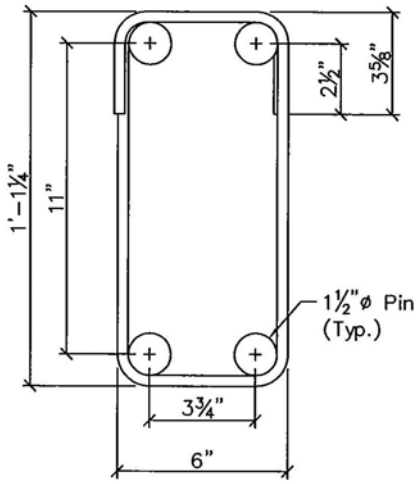

(c) Stirrup Detail

Conversion: 1 inch = 25.4 mm
1 foot = 305 mm

Figure 7.6 – Shear Beam Details

The final member design achieved a shear strength capacity to flexural strength capacity ratio of approximately 65-70% with the ACI equations used. The ratio achieved was presumed sufficient to produce shear failure of the test beams; the results are discussed below in **Section 7.4** where it will be seen that this presumption was not entirely accurate.

7.3.2 Member Fabrication The precast, prestressed shear beams were fabricated at Coreslab Structures, Inc. in Marshall, MO. The employees at Coreslab Structures, Inc. were very accommodating throughout the entirety of this research project. Coreslab Structures, Inc. participated in the SCC survey discussed in **Section 2**, lent one of their prestressing beds to this research project for four business days and a weekend, and helped fabricate the prestressed members investigated.

Fabricating the precast, prestressed shear beams was accomplished rapidly with the experienced crew at Coreslab. The mild reinforcing ties were placed around the prestressing steel tendons. The steel tendons were then placed in the desired configuration and prestressed to the initial jacking force specified. The formwork was placed and welded. The longitudinal mild reinforcing bars were placed within the lateral ties and suspended from rebar placed across the top of the formwork. The ties were spaced according to **Figure 7.6(a)** above, and tied to the prestressed tendons and the longitudinal mild reinforcement. All of these actions are represented in **Figure 7.7** and were accomplished by the Coreslab Structures, Inc. employees before the research team's arrival at 8:00am.

(a) "Dead end" steel tendons anchored into position

(b) Shear beam end

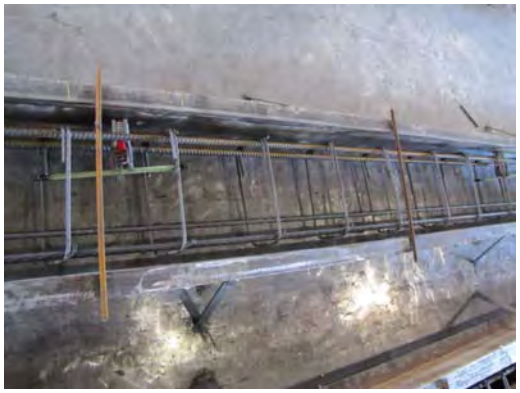

(c) Shear beam middle section

(d) Full prestressing bed with bond and shear beams in place

Figure 7.7 – Reinforcement and Formwork Positioned

Next, the concrete was batched at the on-site central batching plant. The batch proportions used for forming the beams were the four baseline mixtures described in **Table 3.6**. The concrete was then transported across the worksite in Coreslab's Tuckerbilt T630 off-road concrete hauler. A sample was taken from the Tuckerbilt® for fresh concrete properties testing by the research team. Meanwhile, the Coreslab Structures, Inc. crew placed, consolidated, and finished the bond and shear beams. **Figure 7.8** shows the crew placing the concrete.

Figure 7.8 – Coreslab Structures, Inc. Crew Places, Consolidates, and Finishes Concrete for Beams

The following morning, the Coreslab Structures crew stripped the forms. The research team had to then take several hours to instrument the precast bond beams. After instrumentation, the tendons were cut simultaneously. The beams were then stored outside, on site, until it was convenient for the Missouri S&T staff to haul them back to Rolla, MO for final testing. **Figure 7.9** shows the stripped forms and tendons being cut at the time of release.

(a) Forms are stripped

(b) Tendons are cut

Figure 7.9 – "Release" of Beams

At this stage, the beams had been designed for shear failure, the reinforcement detailed, the reinforcement placed and tied, the concrete cast, and the members returned to Rolla, MO for testing. The test setup and procedure have been detailed. The actual results of the precast, prestressed shear beams will be presented next.

7.4 TEST RESULTS AND ANALYSIS

The shear beam results must be presented and discussed. Data was collected for fresh concrete properties, mechanical properties, as well as shear properties for the concrete mixtures used to cast the shear beams.

The fresh concrete properties assessed were consistency, filling ability, passing ability, unit weight, and air content; these properties have been discussed in greater detail in **Section 4.3** above. The fresh concrete property test results are summarized in **Table 7.1** below. The consistency, filling ability, and passing ability were appreciably low for the 10 ksi (68.9 MPa) target strength mixtures; this could be the result of trial batches

being performed on a smaller mixer with presumably tighter quality control. The air content on the 10 ksi (68.9 MPa) target strength mixtures was much higher than the 3% target. The variation of the tested fresh properties from the targets did not impact the results of the shear tests; the high air content will hinder strength gain for the 10 ksi (68.9 MPa) target mixtures, but the effect of strength is conventionally normalize anyway.

Table 7.1 – Beam Fresh Concrete Properties

Date of Pour	Mixture	Slump/ Slump Flow (inches)	J-Ring (inches)	Unit Weight (lb/ft^3)	Air Content
7/21/2011	C6-58L	8.5	---	137.6	6.0%
	S6-48L	28	28	139.2	7.5%
7/25/2011	C10-58L	4.5	---	142.4	6.5%
	S10-48L	22	18	141.6	7.0%

Conversion: 1 inch = 25.4 mm
1 lb/ ft^3 = 16.02 kg/m^3

Compressive strength companion specimens were formed at the time of shear beam fabrication. The compressive strength test results are presented in **Table 7.2** below; the strength development curves for each concrete batch proportion used for beam fabrication are also shown in **Figure 7.10** below. The beams were cast at the same time as the precast, prestressed bond beams tested by another researcher on this project. The other researcher tested the bond beams previous to the shear beams, and broke all strength cylinders before the test date of the shear beams. There were several data points for strength gain, so a good strength development curve was created for each batch proportion; however, no actual strength cylinders remained at the time of shear beam testing.The shortage of test cylinders resulted from bad breaks necessitating additional

specimen testing at planned ages, as well as the addition of an unplanned 14 day break. Better coordination with the bond beam researcher would have been desirable.

Table 7.2 – Tested Beam Companion Compressive Strength Cylinders

		Test Age (days)				
		1	4	8	14	28
Compressive Strength (psi)	C6-58L	4810	5110	5620	5630	5730
	S6-48L	5660	5840	6690	6910	6950
	C10-58L	5670	7890	7950	8360	8480
	S10-48L	6330	8300	8600	9100	9250

Conversion: 1 lb/in^2 = 6.89 kPa

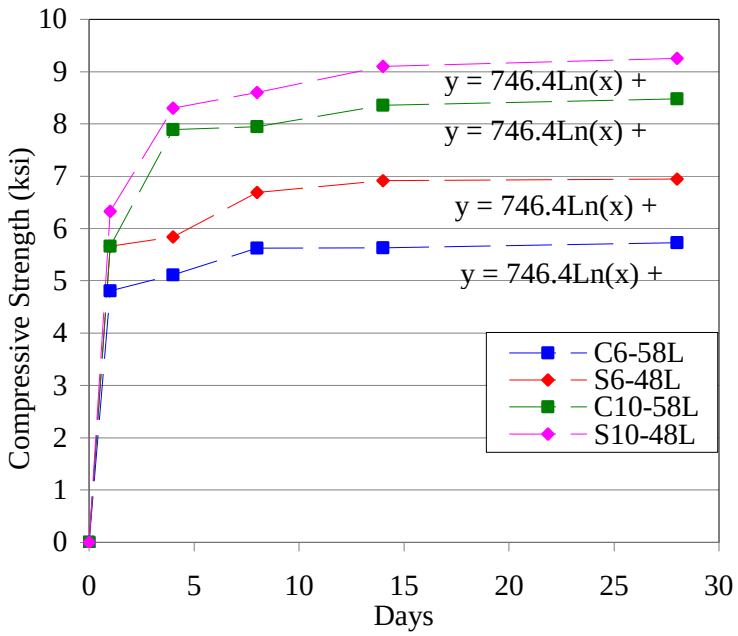

Conversion: 1000 psi = 1 ksi = 6.89 MPa

Figure 7.10 – Beam Strength Development Curves

The logarithmically fitted strength development curves of **Figure 7.10** were extrapolated to determine the compressive strength of each shear beam on the test date. The presumed compressive strength for each beam test is listed below in **Table 7.3**.

Table 7.3 – Extrapolated Beam Strength at Test Age

	Test Age Strength (psi)	
Mixture	South End	North End
C6-58L	7560	7570
S6-48L	7270	7490
C10-58L	8880	8880
S10-48L	9610	9620

Conversion: 1 lb/in^2 = 6.89 kPa

Next, the shear beam test results can be discussed. **Figure 7.11** below shows the load-deformation curves generated from each of the shear beam tests. Some differences and similarities between the CC and SCC curves are noticed immediately. First, at a given target strength level, the SCC beams tend to have higher ultimate loads paired with increased ultimate deflections over the CC beams. The increase deflections occur past the failure point of the comparison CC beams, similar member stiffness is experienced by all beams up to the point of companion CC beam failure; thus, the similar crack propagation behavior leads to similar member cracked moment of inertia and flexural resistance behavior. Similar behavioral trends such as SCC having increased deflections and increases in failure moment were identified by Kim et. al. (2008).

For all beams, the second shear test achieves a higher ultimate load and increased deflection; this is likely due to the effects of the overlapping previously tested region. The shape of the load-deflection curves indicates yielding of the prestressing tendons,

and would cause strain-hardening to develop in the tendons allowing for increase moment carrying capacity. The effects of cracking in the overlapping previously tested region would decrease the effective moment of inertia of the beam, decreasing stiffness, and increasing ductility when compared to an uncracked beam at low stress. The effect of cracking at high moments could increase the effective moment of inertia as compared to a "virgin" specimen due to previous strain hardening effects, or could decrease the stiffness due to increased cracks. Under each situation, the ductility of the secondary test will improve and maximum deflections will increase. The effect of increased ductility is believed to be the cause in the two separate failure modes and drastically different behavior in the two tests performed on the C10-58L beam. Although there is an obvious difference in the behavior of each "virgin" and secondary shear beam tests, both tests provide useful information and should be considered valid. As mentioned, the shape of the load-deflection curves indicates yielding of the prestressing tendons. Shear failures are typically brittle in nature with an elastic rise in load with sudden failure. For the test configuration and member geometry utilized, high moments and flexural stresses were imposed near the point of shear failure. These large bending moments likely lead to yielding of the reinforcement prior to failure. Information such as load-deflection shape, load at first cracking, failure mode, and failure load was collected from all shear beam tests.

The slight divergence in the slope of the S6-48L beam is thought to be resulting from the repair previously described. The repair was done on the top fibers of the beam near the point load for the first test of this beam. If the patch had higher stiffness than the virgin beam, this would result in a steeper initial slope-deflection as is seen in **Figure7.11 (b)** below.

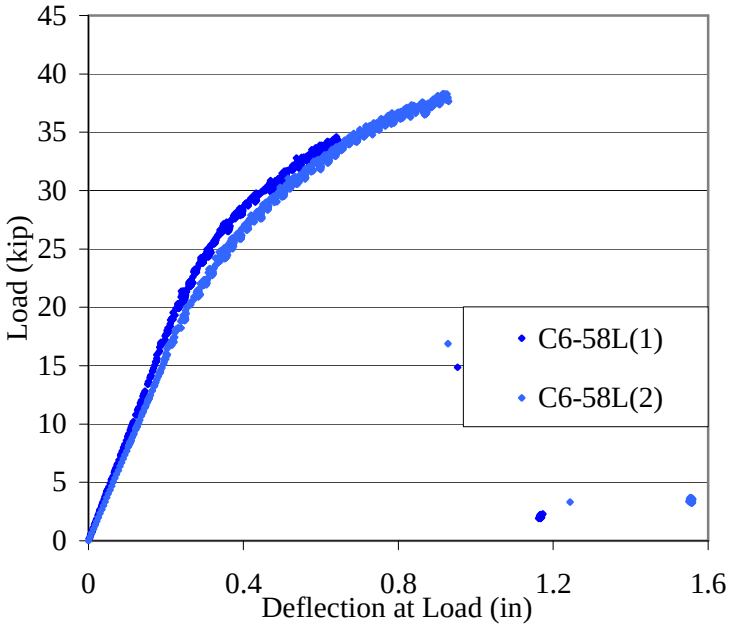

(a) 6 ksi (41.4 MPa) target strength CC beam

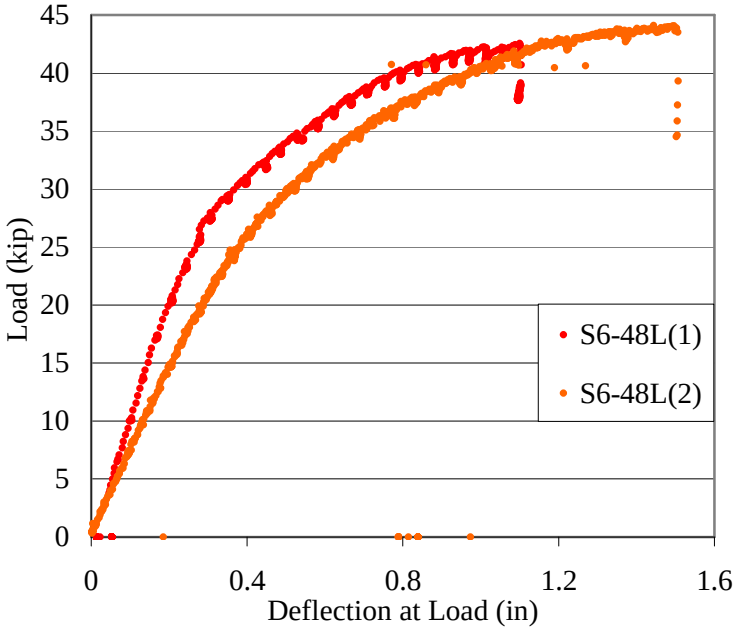

(b) 6 ksi (41.4 MPa) target strength SCC beam

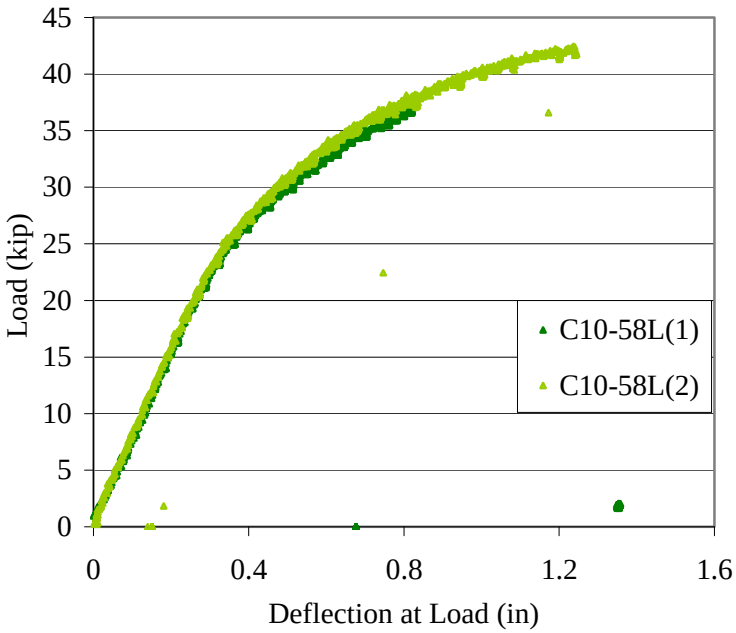

(c) 10 ksi (68.9 MPa) target strength CC beam

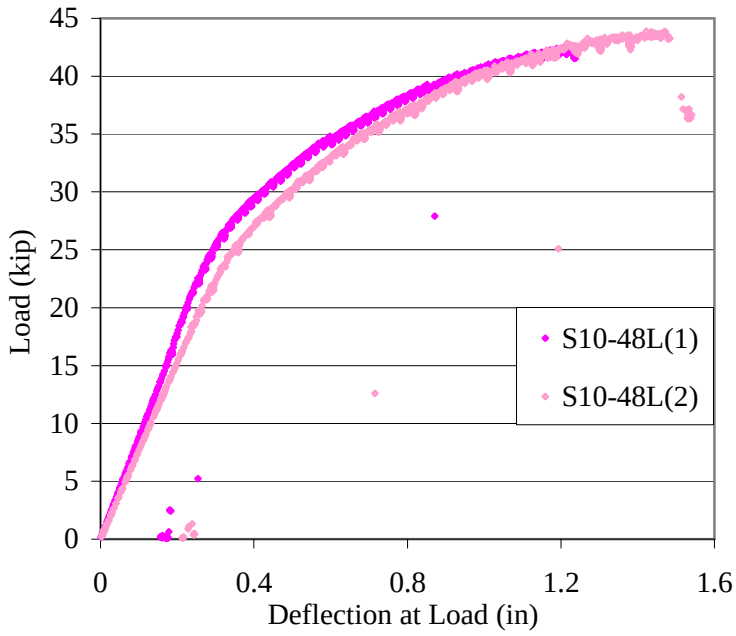

(d) 10 ksi (68.9 MPa) target strength SCC beam

Figure 7.11 – Beam Load-Deflection Response Curves

Although the load-deflection curves for CC and SCC mixtures have numerous differences, there is also some similarity between the curves. All of the beams tested resulted in load-deformation curves with distinct elastically and plastically behaving regions. **Figure 7.12** below compares the elastic region for all beams; it is clear that the CC and SCC mixtures tested have similar stiffness in the elastic range. The similar elastic range can be supported by the fact that the flexural stiffness is primarily driven by the concrete stiffness due to relative area of concrete to steel. From the testing of MOE shown in **Section 5**, specifically **Figure 5.7(a)**, the limestone SCC and CC batch proportions tested exhibited similar normalized MOE; therefore, similar flexural stiffness can be expected.

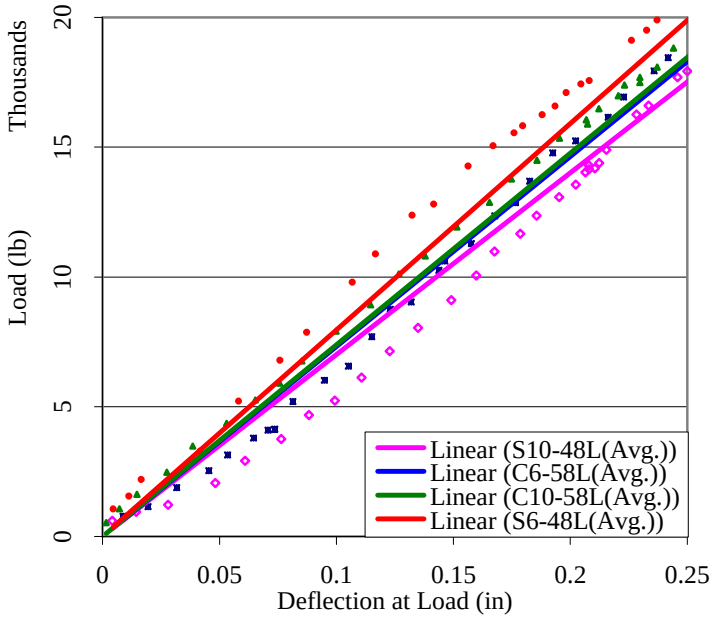

Figure 7.12 – Beam Elastic Range Load-Deflection Response

In order to more precisely examine how the SCC and CC compare in ultimate failure shear, each beam was normalized by the cross-sectional dimensions (constant for all beams) and the square root of the concrete compressive strength. The normalized graph is seen next in **Figure 7.13**. This re-iterates that the SCC did fail at higher shear stresses than the comparable CC batch proportions; yet, this trend diminished for the higher strength batch proportions.

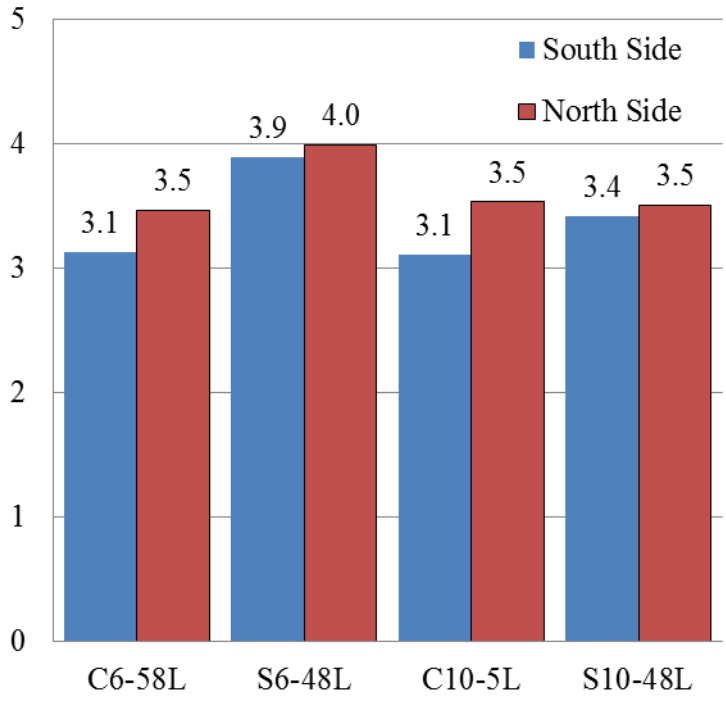

Figure 7.13 – Shear Stress Normalized by the Square Root of Compressive Strength

There was also a distinction between the CC and SCC mixtures with respect to how the specimens behaved and ultimately failed. The CC beams failed in shear while the SCC beams failed in concrete crushing of the top fiber. The CC beams would develop flexural cracking from which a flexural-shear crack would develop; yet, once the ultimate

load was achieved, an explosive shear failure would occur that did not align or interact with the flexural-shear crack. The SCC beams would develop flexural cracks, flexural shear cracks, and eventually concrete crushing would occur in the top fiber of the beam. The progression of cracks and the final failure have been documented and are shown graphically in **Figure 7.13** below.

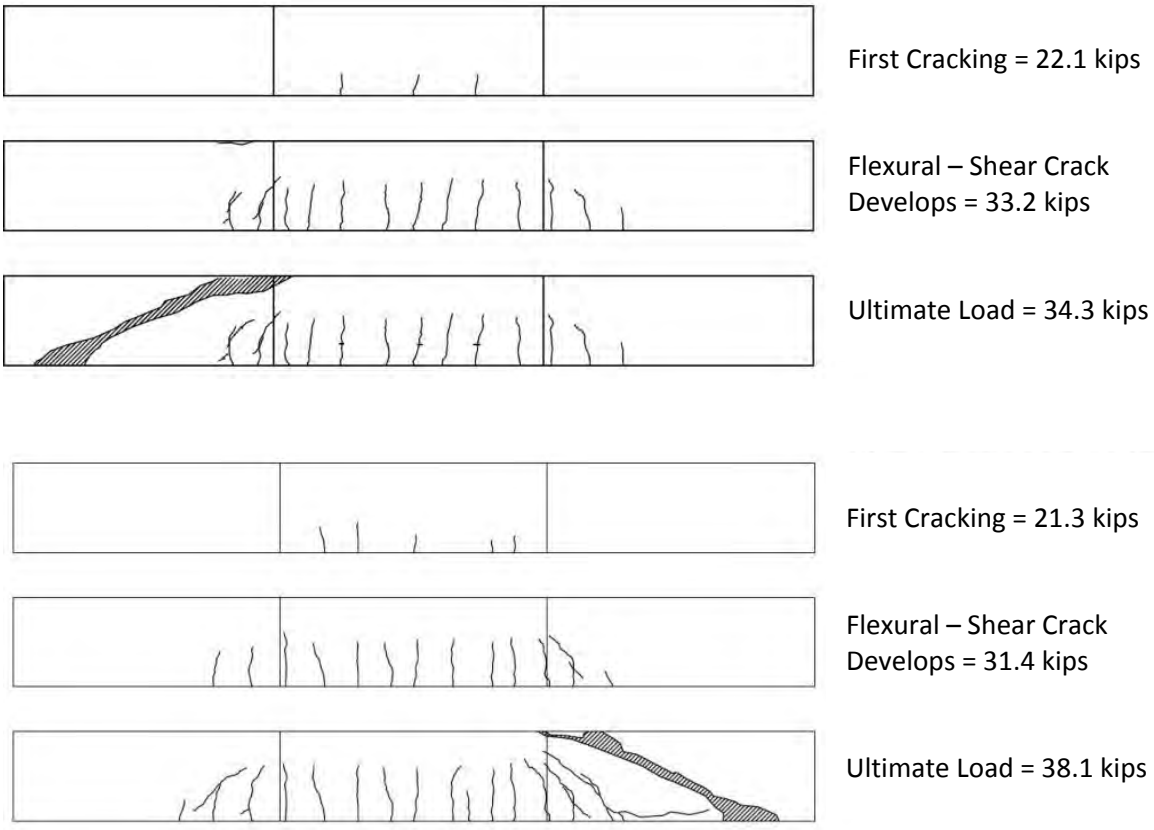

(a) C6-58L South / North Ends

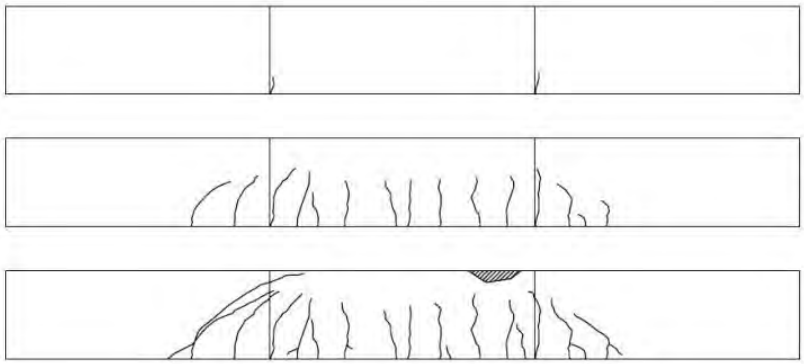

First Cracking = 23.4 kips

Flexural – Shear Crack
Develops = 34.6 kips

Ultimate Load = 42.0 kips

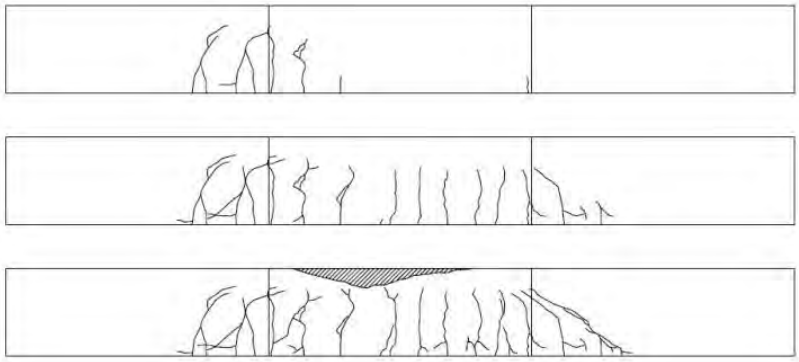

First Cracking = 24.4 kips

Flexural – Shear Crack
Develops = 37.7 kips

Ultimate Load = 43.7 kips

(b) S6-48L South / North Ends

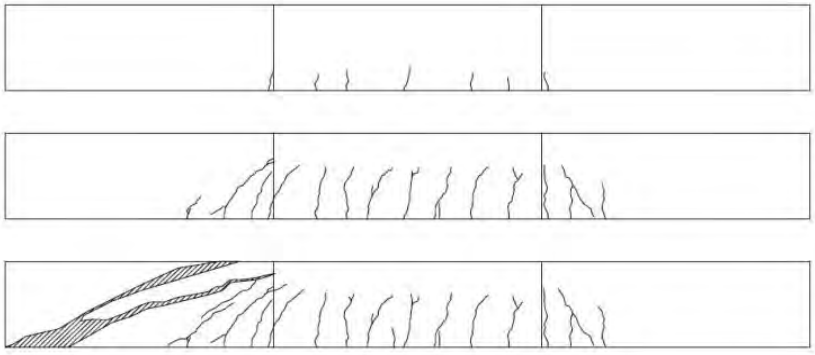

First Cracking = 21.5 kips

Flexural – Shear Crack
Develops = 34.9 kips

Ultimate Load = 37.0 kips

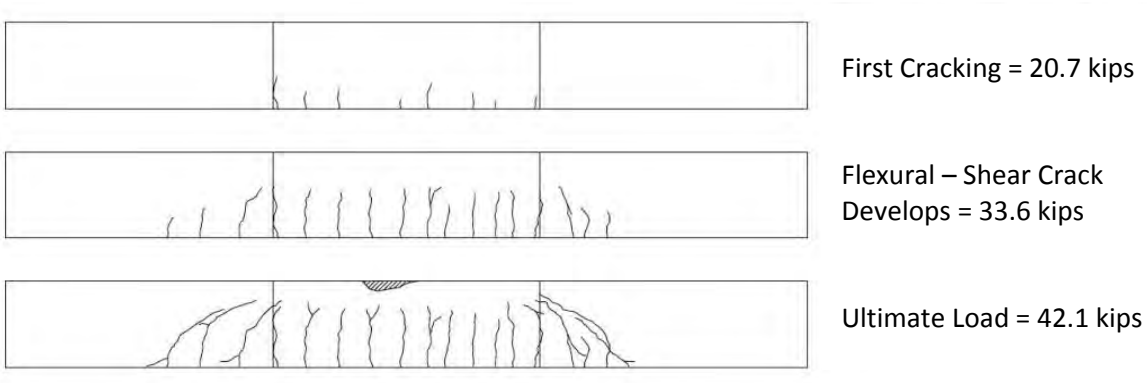

(c) C10-58L South / North Ends

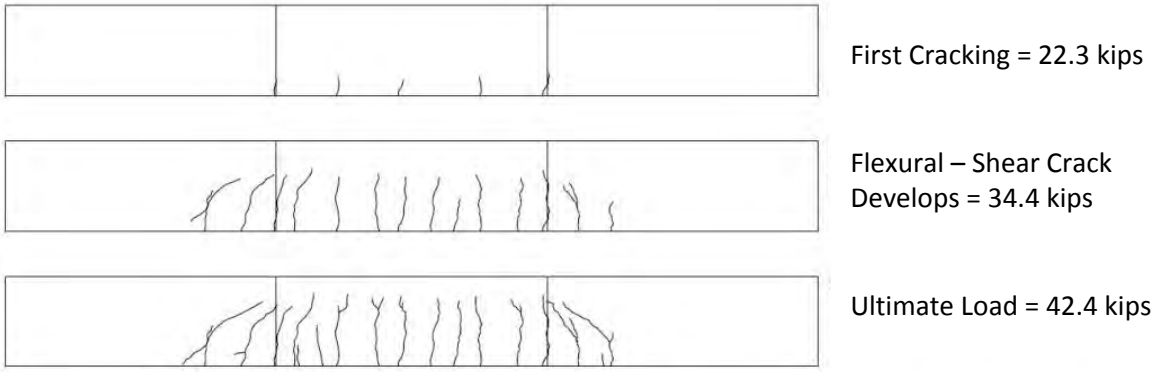

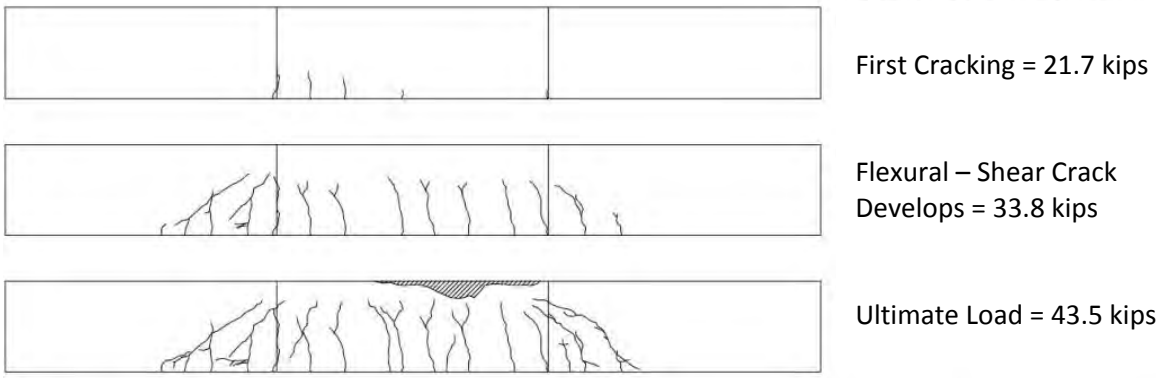

(d) S10-48L South / North Ends

Conversion: 1 kip = 6.89 MPa

Figure 7.14 – Crack Development Patterns with Applied Loads

The cracking, flexural-cracking, and failure loads and failure mode for each shear beam test has been shown. **Table 7.4** summarizes the findings against the predicted response of the various beams according to ACI, AASHTO, and the MCFT through use of Response 2000 created by Bentz and Collins while at the University of Toronto.

Table 7.4 – Predicted Shear Beam Behavior

	Predicted Failure (kips)			Average Actual (measured, self weight, and preload; kips)
	ACI	AASHTO	MCFT	
C6-58L	25.80	25.33	35.90	36.69
S6-48L	25.77	25.15	35.80	43.34
C10-58L	26.58	26.44	36.20	40.04
S10-48L	26.99	27.01	36.60	43.44

Conversion: 1 kip = 4.45 kN

Table 7.4 provides the predicted and actual shear that exists at d_v, the effective shear depth, or 12 inches (305 mm) from the edge of the support. It is seen from **Table 7.4** that the actual failure shears are substantially higher than the predicted failure shears. The underestimation of the models is good, it means they are conservative estimates. It is seen that the predicted failure load by ACI and AASHTO are very similar and are more conservative than the MCFT. This observation makes sense because the ACI and AASHTO predictive models are design models and are therefore lower bound solutions. The MCFT is a limit state model that is derived mechanistically, and then fitted to empirical failure data. Notice that none of the models predicted the trend of significantly increased shear resistance by the SCC; the models do not consider the SCC and CC differently since they have the same material constituents.

It has already been shown that the SCC beams failed at higher loads and therefore it is peculiar why they did not fail explosively in shear as the CC beams had. Because the SCC beams exhibited increased deflections, the shear test regions were evidently allowed to rotate more freely, relieving the shearing stresses enough that shear failure was not actually achieved. The question is then what allowed increased deflection of the SCC beams with respect to the CC beams.

This researcher proposes some possible mechanisms to consider when rectifying the improved performance of the SCC beams with respect to the companion CC beams. These are hypotheses, and unfortunately limited measurements were taken to confirm or deny these suppositions. First, the SCC beams at each strength level achieved higher strengths at the time of release. Improved strength at release will result in less camber, and more importantly, less elastic shortening of the steel tendon; this in turn provides increased clamping forces through the life of the beam. The improved clamping force in the SCC beams may be the reason that higher initial cracking loads were exhibited relative to the CC beams which can be seen in **Figure 7.13**. Decreased elastic shortening of the steel at release may also lead to reduced damage to the relatively “green” concrete beams; more strain energy from the steel tendon is released into a low strength beam, which will also be more susceptible to damage and micro-cracking. Next, improved clamping forces in the uncracked shear test region of the SCC beams relative to the CC beams may be the reason the CC beams failed in shear whereas the SCC beams failed in concrete crushing.

The effectively clamped SCC shear region, not subject to moments high enough to cause flexural cracking, could effectively rotate between the simple support and the test load

point. The companion CC beams, which were not as effectively clamped within the shear region, failed explosively in shear when the tensile strains reached concrete capacity. This same effect may be the reason why the C10-58L beam exhibited two separate behaviors. The virgin test side failed in shear; however, the secondary test was conducted on a cracked member that was more ductile and the shear test region was allowed to more freely rotate between the support and load point. Although the beams were not thoroughly instrumented to numerically support these mechanistic hypotheses, there is supporting evidence of their validity when examining cracking behavior, cracking loads, failure loads, and failure modes.

7.5 FINDINGS AND CONCLUSIONS

Precast, prestressed beams were fabricated and tested in shear for this investigation. The four baseline mixtures used throughout this project 6 ksi (41.4 MPa) target strength limestone CC and SCC, and 10 ksi (68.9 MPa) target strength limestone CC and SCC) were tested in four point loading. The beams were tested to evaluate the concrete shear strength prediction equations by ACI, AASHTO, and the MCFT. Crack propagation patterns and deflections during beam loading were also recorded.

The beam test setup and procedure were detailed. The problems experienced with the S6-48L beam were described and the method of repairing the damaged area was explained. The beams were fabricated at Coreslab Structures, Inc. in Marshall, MO.

The shear test results were shown. It was seen that the second test region of each beam experienced increased shear load and deflection over the first test region; this was explained by the reduced effective moment of inertia of a larger length of beam as well as

the strain hardening effect in the prestressing strand. These effects lead to increased ductility. It was also seen that all beams exhibited similar elastic stiffness prior to the first flexural crack development. The elastic stiffness is driven by the large area of concrete relative to steel, it was seen that the CC and SCC limestone batch proportions tested and described in **Section 5** exhibited similar stiffnesses. Also in **Section 5**, it was shown that SCC may exhibit improved tensile strength over CC, this may also help to explain improved resistance to initial cracking of the SCC. It was also shown that the SCC beams experienced increased deflections and failure loads over the CC beams. The improved deflection and load carrying capacity of the SCC is hypothesized to be explained by differences in prestress losses at time of release, and subsequently through concrete compressive strength development. The hypothetically decreased prestress losses of the SCC were believed to improve initial cracking resistance, mitigated damage of the concrete at release, and lead to improved failure behavior and loads. Finally, the failure modes differed from the SCC to CC. The SCC experienced flexure cracking, flexural-shear cracking, and finally concrete crushing; however, the CC experienced flexure cracking, flexural-shear cracking, then explosive shear failure which occurred at a location away from the developing flexural-shear crack. There was also improved shear resistance when comparing the higher strength CC or SCC to the lower strength CC or SCC respectively, as would be expected. The trend of increased release strength for improved shear resistance holds true when comparing the higher to lower strength batch proportions also.

The tests performed on the limestone batch proportions of this research project indicate improved performance of SCC when compared to CC. Improved SCC shear

resistance was unexpected. The expectation of SCC to have decreased shear capacity comes primarily from the effect of decreased C.A. fraction. The results from this investigation have shown that reduced C.A. fraction is not enough to conclude reduced shear capacity. The C.A. fraction may have a real impact on shear capacity at a given crack due to aggregate interlock; yet, it may be more important to know how that crack got there, and what stresses are acting on and around it. The beams of this investigation, when shear failure was observed, failed away from flexural cracked regions. This research has given valuable insight into SCC behavior, and shown that SCC should not be readily discarded as a construction material. Because of the limited practicality of rectangular cross-sections for prestressed concrete beams and girders, additional research of SCC tested in differing geometrical and scalar cross-sections should be carried out.

8. SUMMARY, CONCLUSIONS, AND RECOMMENDATIONS

8.1 SUMMARY

The purpose of this report was to investigate the ability of SCC to resist shear forces relative to CC at normal and high strengths. That objective was accomplished by performing a sequence of activities that were believed to contribute to the whole picture of how SCC behaves in shear as compared to CC.

First, a literature review was undertaken. The literature review surveyed relevant and necessary information available that would contribute to understanding SCC and how it behaves in the plastic and hardened state, with emphasis on shear behavior. Plastic concrete behavior and mechanics, current industry recognized guidelines and recommended practices for achieving robust SCC, and plastic concrete test procedures were identified. Hardened concrete behavior and predictive models were reviewed along with hardened concrete standardized mechanical test procedures. Fundamental shear theory, specifics about the aggregate interlock shear mechanism, and widely recognized shear predictive models were reviewed and analyzed. Small scale concrete shear tests were surveyed, and one, the push-off test, was selected for use in investigating the aggregate interlock mechanism of shear resistance for this study. Precast prestressed beam studies were also reviewed for behavior in shear; researchers that had investigated beam shear with SCC were also found.

Next, before any physical work could be accomplished, the concrete batch proportions to be tested had to be determined. The determination of concrete mixtures to test was achieved by the aid of MoDOT and Missouri precast concrete suppliers through

responses to a survey inquiring about SCC batch proportions in use at the time of this study. It should be noted that precast concrete suppliers in Missouri are using SCC for structural and non-structural applications for building construction; yet only non-structural members are permitted to be cast using SCC for MoDOT infrastrucutre. MoDOT gave guidelines for determining the control (normal density conventional concrete), and the survey responses gave typical Missouri precast SCC. The survey was also sent to Missouri ready-mix suppliers as well as AASHTO members from each of the fifty states; no responses were received from the ready-mix suppliers, but useful information was gathered about the prevalence and robustness of SCC across the US.

The constituent materials used throughout this study were investigated. There are limitations on the physical properties of the materials used in concrete; these properties were measured and were confirmed to be acceptable for use. The tested properties included absorption, bulk specific gravity, moisture content, and gradation. The measurement of the physical properties also enables proportioning of materials according to the standard volumetric method. Once the constituent materials were characterized and the batch proportions to be tested were obtained as described above, fresh concrete was mixed. The fresh concrete behavior was also measured using standard and non-standard methodologies. The L-box and other, newly developed or narrowly used SCC test procedures have not yet been accepted by standards associations. The tested fresh properties include slump, slump-flow, T_{20}, VSI, J-ring, L-box, segregation column, unit weight, and air percentage by the pressure method.

Next, hardened concrete behavior was tested. Hardened properties tests included the concrete compressive strength, Young's Modulus, and splitting tensile strength.

These hardened properties are very important for correlation to member behavior under load. These properties have real impacts on concrete performance, and are all commonly present in mechanistic failure models of all kinds, including the failure mode of interest to this investigator – shear.

Shear behavior was monitored by two major test regiments. First, the small scale push-off test was used to investigate the aggregate interlock mechanism contribution to shear resistance. The test schedule consisted of testing CC and SCC at two separate strength levels, with two distinct C.A. types, and the SCC had three variations of C.A. volumetric fraction of the aggregate portion. Additional mixtures were tested because the test was relatively simple and low cost. The additional batch proportions tested included a companion push-off specimen of the shear beams tested (to be discussed shortly), specimens for a third strength level of limestone aggregate mixtures, and two specimens from concrete produced by another active researcher at Missouri S&T. Post-failure imaging of the cross-section was performed to give added insight into segregation and aggregate contribution. Next, shear behavior was also explored through testing precast prestressed concrete beams. The beams were selected to be precast prestressed because of increased compatibility with real-world applications; however, the beams were not full-scale and were of simple rectangular geometry. The beams could not comprise the entire cost of this research; therefore, four economical beams were constructed that permitted testing on both ends resulting in eight shear beam test results.

With the details of the materials, tests, and theory gathered, work commenced. Batch proportions were determined from a practical means and reflect current industry practice. Fresh and hardened concrete properties were tested and recorded for correlation

to shear test results. Shear was investigated through two avenues; one looked at the specifics of relative behavior of SCC and CC when subject to aggregate interlock, the other looked at the macroscopic behavior of a shear beam. All of these tasks, results, and analyses contribute to the ability to compare and contrast CC and SCC. The investigation was able to accomplish the objective of characterizing SCC relative to CC and enabled the statement of the following conclusions.

8.2 FINDINGS AND CONCLUSIONS

The following findings and conclusions are supported by the review of literature and the observed behavior and test results from this investigation:

- National SCC studies have produced guidelines for developing fresh property test programs to develop robust mix designs and reliable QA/QC programs.
- There exist standardized test procedures for testing “fresh” or plastic SCC.
- The majority of AASHTO survey respondents report less than 25% of all projects utilizing SCC with first use occurring within the last 7 years; few respondents report a majority of projects using SCC with more than 10 years of experience.
- The increased rate and higher ultimate strength development of SCC compared to CC observed by other researchers was also observed in this investigation.
- The decreased MOE for SCC compared to CC noted by others was not exhibited by the concrete batch proportions tested in this study.

- Researchers have reported conflicting results regarding the relative tensile strength of SCC to CC; this researcher witnessed improved tensile strength of SCC with respect to CC.
- The concrete batch proportions containing river gravel exhibited improved hardened mechanical properties of increased compressive strength, increased MOE, and increased STS despite their decreased surface roughness compared to limestone aggregates tested.
- Vertical push-off specimen fabrication was effective in resembling actual member fabrication and adequately controlled geometrical tolerances for superior stress propagation and improved test results.
- Software imaging of post-failure cross-sections indicate segregation was not a significant issue and that tested specimens closely match calculated material proportions.
- The precrack test result analysis indicates that initial crack widths are highly controllable by increasing the initial clamping force.
- Precrack load was found to be proportional to concrete compressive strength, tensile strength, and initial clamping force.
- Push-off test results indicate decreasing aggregate interlock with increasing concrete compressive strength, a trend noted by other researchers and supported by theory.
- For the concrete batch proportions tested, river gravel exhibited superior aggregate interlock capability when compared to the limestone; this was the

variable that had the largest effect on shear resistance of the concrete specimens and variables tested within this study.

- Despite other researchers findings and theoretical conflict, the SCC did not appear to resist shear through aggregate interlock in a manner distinguishable from CC; the effect of C.A. percentage was not detectable for the tests performed in this investigation.
- The E-value that other researchers have proposed and relied on for push-off analysis was discussed and discarded as the highly sensitive analysis tool it has been proposed to be. The E-value does examine shear and normal stress, crack width, and crack opening; however, it effectively averages and smears important incremental information.
- The increased rate of strength gain for SCC relative to CC was also noted for the shear beams; increased SCC strength at the time of release may be important to elastic prestress loss as well as losses over time.
- The tested shear beams exhibited similar flexural stiffness in the elastic range, this is supported by the consistent MOE of SCC and CC discussed above.
- SCC shear beams demonstrate increased deflections at increased shear strengths over comparable CC beams in this study. Other researchers have seen mixed results when comparing shear strength of SCC and CC beams.
- The beams of this study were tested once on each end. All secondary tests had increased shear strength and deflections over the virgin test indicating increased ductility.

- At failure, the SCC beams displayed crushing in their top fibers, the CC beams failed explosively in a shear plane extending from support to load point, away from developing flexural shear cracks.

These conclusions are drawn from the testing performed throughout this investigation. Other researcher's findings were incorporated into the conclusions when possible, their findings either support or deviate from the findings of this study.

8.3 RECOMMENDATIONS

It is recommended that an SCC be designed and developed following the guidelines from the NCHRP report 628 to become familiar with the issues and sensitivities of fresh SCC. Subsequent to SCC batch proportioning, it would be useful to conduct a QA/QC study across numerous Missouri precast and possibly ready-mix suppliers to ensure that adequate control of the material is ensured with the fast and simple fresh tests of slump-flow and J-ring. This process would familiarize all parties involved with the concerns of creating robust SCC, as well as help to establish practical and acceptable limits on the filling capacity and stability of subsequently developed SCC batch proportions.

No concerns were identified in this investigation with regard to hardened mechanical testing of SCC relative to CC. Strength development and tensile strength was identified to be improved for SCC over similar CC. MOE was consistent between SCC and CC; other researchers have noted decreased MOE for SCC, but have also seen that the lower bound predictive models are still conservative.

Additional shear testing of SCC would be useful. Push-off tests conducted throughout this investigation proved to be economical and quick, once familiar with the fabrication and testing procedures. Additional push-off testing, with some standardization and improvements to the test suggested by this researcher, would be useful in refining the results of this study as well as investigating additional variables. Push-off testing would be most useful for lower strength concrete batch proportions where the impact of aggregate interlock is greater than at higher strengths. Variables that could be investigated could include maximum aggregate size, C.A. gradation, C.A. surface roughness and angularity, C.A. hardness, mineral and chemical admixtures, as well as the variables tested in this investigation. A broad push-off test program may identify additional or compounding effects that have not been previously identified. It would also be valuable to conduct additional shear beam testing. As with CC, it was identified that SCC shear beams have been tested in third point loading, but not commonly with distributed loading. Larger scale and more practical geometries of beams and girders should be tested in shear to compare to trends identified in this study. A beam with web-shear cracking may exhibit completely different behavior from the rectangular beams tested in this study that produced flexural-shear cracks and failed in a plane away from these developing cracks. Full-scale beam testing with complete stress-strain instrumentation should be undertaken. Given that SCC has already seen consistent public use, ongoing monitoring of a conservatively designed SCC beam used by the public may also be deemed acceptable.

(This Page Intentionally Left Blank)

REFERENCES

American Association of State Highway and Transportation Officials (AASHTO) Load and Resistance Factor Design (LRFD) (2004). Bridge design specifications and commentary, AASHTO, Washington, D.C.

AASHTO "Subcommittee on Materials." <http://www.materials.transportation.org> (Jan. 16. 2011).

American Concrete Institute (ACI) Committee 237 (2007). "Self-consolidating concrete." American Concrete Institute, Farmington Hills, Michigan.

ACI Committee 318 (2011). "Building Code Requirements for Structural Concrete (ACI 318-08) and Commentary." American Concrete Institute, Farmington Hills, Michigan.

ACI Committee 363 (2010). "Report on High-Strength Concrete." American Concrete Institute, Farmington Hills, Michigan.

ACI – ASCE Committee 426 (1973). "The Shear Strength of Reinforced Concrete Members – Chapters 1 to 4," Proceeds ASCE, J. of the Structural Division, 99 (6), 1091-1187.

American Society for Testing and Materials (ASTM) C127 (2007). "Standard Test Method for Density, Relative Density (Specific Gravity), and Absorption of Coarse Aggregate." Annual book of ASTM standards, ASTM, West Conshohocken, Pennsylvania.

ASTM C128 (2007). “ Standard Test Method for Density, Relative Density (Specific Gravity), and Absorption of Fine Aggregate.” Annual book of ASTM standards, ASTM, West Conshohocken, Pennsylvania.

ASTM C136 (2006). “Standard Test Method for Sieve Analysis of Fine and Coarse Aggregates.”Annual book of ASTM standards, ASTM, West Conshohocken, Pennsylvania.

ASTM C138 (2010). “Standard Test Method for Density (Unit Weight), Yield, and Air Content (Gravimetric) of Concrete.” Annual book of ASTM standards, ASTM, West Conshohocken, Pennsylvania.

ASTM C143 (2010). “Standard Test Method for Slump of Hydraulic-Cement Concrete.” Annual book of ASTM standards, ASTM, West Conshohocken, Pennsylvania.

ASTM C192 (2007). “Standard Practice for Making and Curing Concrete Test Specimens in the Laboratory.” Annual book of ASTM standards, ASTM, West Conshohocken, Pennsylvania.

ASTM C231 (2010). “Standard Test Method for Air Content of Freshly Mixed Concrete by the Pressure Method.” Annual book of ASTM standards, ASTM, West Conshohocken, Pennsylvania.

ASTM C469 (2010). “Standard Test Method for Static Modulus of Elasticity and Poisson’s Ratio of Concrete in Compression.” Annual book of ASTM standards, ASTM, West Conshohocken, Pennsylvania.

ASTM C496 (2011). “Standard Test Method for Splitting Tensile Strength of Cylindrical Concrete Specimens.” Annual book of ASTM standards, ASTM, West Conshohocken, Pennsylvania.

ASTM C566 (2004). “Standard Test Method for Total Evaporable Moisture Content of Aggregate by Drying.” Annual book of ASTM standards, ASTM, West Conshohocken, Pennsylvania.

ASTM C1231 (2010). “Standard Practice for Use of Unbonded Caps in Determination of Compressive Strength of Concrete Cylinders.” Annual book of ASTM standards, ASTM, West Conshohocken, Pennsylvania.

ASTM C1611 (2009). “Standard Test Method for Slump Flow of Self-Consolidating Concrete.” Annual book of ASTM standards, ASTM, West Conshohocken, Pennsylvania.

ASTM C1621 (2009). “Standard Test Method for Passing Ability of Self-Consolidating Concrete by J-Ring.” Annual book of ASTM standards, ASTM, West Conshohocken, Pennsylvania.

Albajar, J. S. (2008). “The Influence of Aggregate Fracture on the Shear Strength of Reinforced Concrete Beams.” Doctoral Thesis, Imperial College London, London, United Kingdom.

Barragan, B., Gettu, R., Agullo, L. and Zerbino, R. (2006). “Shear failure of steel fiber-reinforced concrete based on push-off tests.” ACI Mater. J., 103 (4), 251-257.

BASF (2010). “Glenium 7700 Data Sheet.” <http://www.basf-admixtures.com> (March 15. 2011).

BASF (2011). “MB-AE-90 Data Sheet.” <http://www.basf-admixtures.com> (March 15. 2011).

Bentz, E. C., Vecchio, F. J., and Collins, M. P. (2006). “Simplified Modified Compression Field Theory for Calculating Shear of Reinforced Concrete Elements.” ACI Struct. J., 103(4), 614-624.

DIYMAPS (2011). “Do It Yourself Color-Coded State, US, Canada and Mexico Maps.” <http://diymaps.net> (Aug. 19. 2011).

EFNARC (2005). “The European Guidelines for Self-compacting Concrete.” <http://www.efnarc.org> (Jan. 21. 2012).

EFNARC (2006). “Guidelines for Viscosity Modifying Admixtures for Concrete.” <http:www.efnarc.org> (Jan. 28. 2012).

FHWA (2005). “Advances in Self-consolidating Concrete.” Focus, <http://www.fhwa.dot.gov> (Dec. 15. 2011).

Ghezal, A., and Khayat, K. H. (2002). “Optimizing self-consolidating concrete with limestone filler by using statistical factorial design methods.” ACI Mater. J., 99(3), 264-272.

Hwang, S., Khayat, K. H., and Bonneau, O. (2006). “Performance-Based Specifications of Self-Consolidating Concrete use in Structural Applications.” ACI Mater. J., 103(2), 121-129.

Khayat, K. H., and Assaad, J. (2002). “Air-Void Stability in Self-Consolidating Concrete.” ACI Mater. J., 99(4), 408-416.

Kim, Y. H. (2008). “Characterization of Self-Consolidating Concrete for the Design of Precast, Pretensioned Bridge Superstructure Elements.” Doctoral Dissertation, Texas A&M University, College Station, Texas.

Mattock, A. H., Hawkins, N. M. (1972). “Shear Transfer in Reinforced Concrete – Recent Research.” PCI J., 17(2), 55-75.

Mattock, A. H., Hofbeck, J. A., and Ibrahim, I. O. (1969). “Shear Transfer in Reinforced Concrete.” ACI J., 66(2), 119-128.

Mindess, S., Young, J. F., Darwin, D. (2003). “Concrete – Second Edition.” Prentice Hall, Upper Saddle River, New Jersey.

Missouri Department of Transportation (MoDOT) (2012). “Missouri Standard Specifications for Highway Construction.” MoDOT, Jefferson City, MO.

Myers, J. J., Carrasquillo, R. L. (1999). “The Production and Quality Control of High Performance Concrete in Texas Bridge Structures.” Center for Transportation Researcher, Research Report 580/589-1, The University of Texas at Austin.

Naito, C.J., Parent, G., and Brunn, G. (2006). “Performance of Bulb-T Girders Made with Self-Consolidating Concrete.” PCI J., 51(6), 72-85.

National Cooperative Highway Research Program (NCHRP) (2009). “Report 628 – Self-Consolidating Concrete for Precast, Prestressed Concrete Bridge Elements.” Transportation Research Board, Washington, D.C.

National Institute of Health (NIH) (2004). “ImageJ.” Image Processing and Analysis in Java, <http://rsbweb.nih.gov/ij/> (Nov. 6, 2011).

Nawy, E. G. (2010). “Prestressed Concrete - A Fundamental Approach - Fifth Edition Update.” Prentice Hall, Upper Saddle River, New Jersey.

Nowak, A., Morcous, G., Kaszynska, M., Tuan, C., Paczkowski, P., Akhnoukh, A., Lutomirski, T., and Kozikowski, M. (2007). “Development of a Guide for Cast-

in-Place Applications of Self-Consolidating Concrete." Nebraska Department of Roads (NDOR), Lincoln, Nebraska.

Sika (2003). "Sikatop® 122 Plus – Product Data Sheet." Products and Solutions – Concrete Restoration, <http://usa.sika.com/en/group.html> (Jan. 20, 2012).

Vecchio, F. J., and Collins, M. P. (1986). "The Modified Compression Field Theory for Reinforced Concrete Elements Subjected to Shear." ACI Struct. J., 83(2), 219-231.

Vecchio, F. J., and Lai, D. (2004). "Crack Shear-Slip in Reinforced Concrete Elements." J. of Advanced Concrete Technology, 2(3), 289-300.

Walraven, J. C. (1981). "Fundamental analysis of aggregate interlock." J. Struct. Div., ASCE, 107(11), 2245-2270.

Walraven, J. C., and Reinhardt, H. W. (1981). "Theory and Experiments on Mechanical Behavior of Cracks in Plain and Reinforced Concrete Subjected to Shear Loading." Heron, 26(1A), 68.

Walraven, J. C., and Stroband, J. (1994). "Shear Friction in High-Strength Concrete." SP-149, Proc., American Concrete Institute Int. Conf., Singapore, 311-330.

APPENDIX A

MATERIAL DATA SHEETS

BASF
The Chemical Company

3 | 03 30 00 Cast-in-Place Concrete | 03 40 00 Precast Concrete | Product Data

Glenium® 7700

High–Range Water-Reducing Admixture

Description

Glenium 7700 ready-to-use high-range water-reducing admixture is based on the next generation of polycarboxylate technology found in all of the Glenium 7000 series products. This technology combines state-of-the-art molecular design with a precise understanding of regional cements to provide specific and exceptional value to all phases of the concrete construction process.

Glenium 7700 is particularly effective in improving the day to day consistency of concrete mixtures. This is accomplished by providing unparalleled slump retention without compromising early compressive strength development and setting time. Workability retention helps to maintain more consistent performance from batch to batch, thereby improving operational efficiencies. Glenium 7700 meets ASTM C 494 compliance requirements for Type A, water-reducing, and Type F, high-range water-reducing, admixtures.

Applications

Recommended for use in:

- Concrete requiring high-early compressive strength development
- Applications requiring workability retention without retardation
- Concrete where high flowability, increased stability and durability are needed
- Production of Self-Consolidating Concrete (SCC) mixtures
- Concrete with varying water reduction requirements (5-40%)

Features

- Superior slump retention
- Excellent early strength development
- High ultimate strengths
- Optimum setting time
- Consistent air entrainment
- Dosage flexibility

Benefits

- Consistency in placement operations
- Optimized mixture costs
- Reduction in patching costs
- Ability to attain difficult combinations of high-early and late-age compressive strengths
- Increased productivity
- Improved operational efficiencies
- Less QC support
- Fewer rejected loads
- Faster form turnover
- Workability retention without retardation

Performance Characteristics

Slump Retention: Concrete produced with Glenium 7700 admixture maintains slump significantly longer than concrete mixtures containing naphthalene, melamine, and first generation polycarboxylate high-range water-reducing admixtures. This slump retention is achieved without affecting rate of hardening or early age compressive strength development.

Mixture Data: Figure 1 represents average slump retention performance across multiple field trials throughout North America. Figure 2 represents average compressive strength results from these same field trials. Materials were all different as were starting consistencies. The reference admixture in this graph represents the first generation of high-early strength polycarboxylate technology.

Figure 1. Average Slump Retention Performance

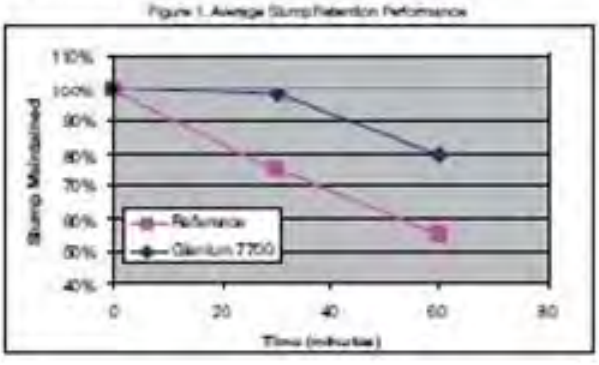

Master Builders

Product Data: Glenium® 7700

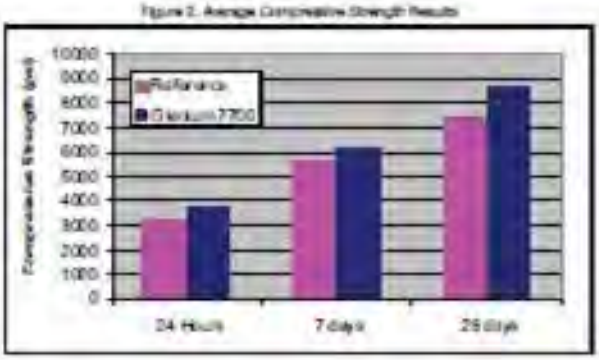

Guidelines for Use

Dosage: Glenium 7700 has a recommended dosage range of 2-15 fl oz/cwt (150-975 mL/100 kg) of cementitious materials. For most applications, dosages in the range of 2-12 fl oz/cwt (130-780 mL/100 kg) will provide excellent performance. For very high performance and Rheodynamic® Self-Consolidating concrete mixtures, up to 15 fl oz/cwt (975 mL/100 kg) of cementitious materials can be utilized. Because of variations in concrete materials, job site conditions and/or applications, dosages outside of the recommended range may be required. In such cases, contact your local sales representative.

Mixing: Glenium 7700 admixture can be added with the initial batch water or as a delayed addition. However, optimum water reduction is generally obtained with a delayed addition.

Product Notes

Corrosivity – Non-Chloride, Non-Corrosive: Glenium 7700 admixture will neither initiate nor promote corrosion of reinforcing steel embedded in concrete, prestressing steel or of galvanized steel floor and roof systems. Neither calcium chloride nor other chloride-based ingredients are used in the manufacture of Glenium 7700 admixture.

Compatibility: Glenium 7700 admixture is compatible with most admixtures used in the production of quality concrete, including normal, mid-range and high-range water-reducing admixtures, accelerators, retarders, extended set control admixtures, air-entrainers, corrosion inhibitors, and shrinkage reducers.

Do not use Glenium 7700 admixture with admixtures containing beta-naphthalene sulfonate. Erratic behaviors in slump, workability retention and pumpability may be experienced.

Storage and Handling

Storage Temperature: Glenium 7700 admixture must be stored at temperatures above 40 °F (5 °C). If Glenium 7700 admixture freezes, thaw and reconstitute by mechanical agitation. **Do not use pressurized air for agitation without consulting technical support.**

Shelf Life: Glenium 7700 admixture has a minimum shelf life of 6 months. Depending on storage conditions, the shelf life may be greater than stated. To ensure the longest shelf life potential, recirculation is recommended. Please contact your local sales representative regarding suitability for use and dosage recommendations if the shelf life of Glenium 7700 admixture has been exceeded.

Packaging

Glenium 7700 admixture is supplied in 55 gal (208 L) drums, 275 gal (1040 L) totes and by bulk delivery.

Related Documents

Material Safety Data Sheets: Glenium 7700 admixture

Additional Information

For additional information on Glenium 7700 admixture or its use in developing concrete mixtures with special performance characteristics, contact your local sales representative.

The Admixture Systems business of BASF's Construction Chemicals division is a leading provider of innovative admixtures for specialty concrete used in the ready-mixed, precast, manufactured concrete products, underground construction and paving markets throughout the North American region. The Company's respected Master Builders brand products are used to improve the placing, pumping, finishing, appearance and performance characteristics of concrete.

BASF Corporation
Admixture Systems
www.masterbuilders.com
United States: 23700 Chagrin Boulevard, Cleveland, Ohio 44122-5544 • Tel. 800 628-9990 • Fax: 216 839-8821
Canada: 1600 Clark Boulevard, Brampton, Ontario L6T 4M7 • Tel: 800 387-5862 • Fax: 905 792-0651

Master Builders

BASF
The Chemical Company

MB-AE™ 90

Air-Entraining Admixture

Description

MB-AE 90 air-entraining admixture is for use in concrete mixtures. It meets the requirements of ASTM C 260, AASHTO M 154 and CRD-C 13.

Applications

Recommended for use in:

- Concrete exposed to cyclic freezing and thawing
- Production of high-quality normal or lightweight concrete (heavyweight concrete normally does not contain entrained air)
- All paving-related concrete exposed to freezing and thawing cycles

Features

- Ready-to-use in the proper concentration for rapid, accurate dispensing

Benefits

- Improved resistance to damage from cyclic freezing and thawing
- Improved resistance to scaling from deicing salts
- Improved plasticity and workability
- Reduced permeability – increased watertightness
- Reduced segregation and bleeding

Performance Characteristics

Concrete durability research has established that the best protection for concrete from the adverse effects of freezing and thawing cycles and deicing salts results from: proper air content in the hardened concrete, a suitable air-void system in terms of bubble size and spacing, and adequate concrete strength, assuming the use of sound aggregates and proper mixing, transporting, placing, consolidation, finishing and curing techniques. MB-AE 90 admixture can be used to obtain adequate freeze-thaw durability in a properly proportioned concrete mixture, if standard industry practices are followed.

Air Content Determination: The total air content of normal weight concrete should be measured in strict accordance with ASTM C 231, "Standard Test Method for Air Content of Freshly Mixed Concrete by the Pressure Method" or ASTM C 173/C 173M, "Standard Test Method for Air Content of Freshly Mixed Concrete by the Volumetric Method." The air content of lightweight concrete should only be determined using the Volumetric Method. The air content should be verified by calculating the gravimetric air content in accordance with ASTM C 138/C 138M, "Standard Test Method for Density (Unit Weight), Yield, and Air Content (Gravimetric) of Concrete." If the total air content, as measured by the Pressure Method or Volumetric Method and as verified by the Gravimetric Method, deviates by more than 1-1/2%, the cause should be determined and corrected through equipment calibration or by whatever process is deemed necessary.

Guidelines for Use

Dosage: There is no standard dosage for MB-AE 90 admixture. The exact quantity of air-entraining admixture needed for a given air content of concrete varies because of differences in concrete-making materials and ambient conditions. Typical factors that might influence the amount of air entrained include: temperature, cementitious materials, sand gradation, sand-aggregate ratio, mixture proportions, slump, means of conveying and placement, consolidation and finishing technique.The amount of MB-AE 90 admixture used will depend upon the amount of entrained air required under actual job conditions. In a trial mixture, use 1/4 to 4 fl oz/cwt (16-260 mL/100 kg) of cementitious material. Measure the air content of the trial mixture, and, if needed, either increase or decrease the quantity of MB-AE 90 admixture to obtain the desired air content.

In mixtures containing water-reducing or set-control admixtures, the amount of MB-AE 90 admixture needed may be somewhat less than the amount required in plain concrete.

Master Builders

Product Data: MB-AE™ 90

Due to possible changes in the factors that can affect the dosage of MB-AE 90 admixture, frequent air content checks should be made during the course of the work. Adjustments to the dosage should be based on the amount of entrained air required in the mixture at the point of placement.

If an unusually high or low dosage of MB-AE 90 admixture is required to obtain the desired air content, consult your Local sales representative. In such cases, it may be necessary to determine that, in addition to a proper air content in the fresh concrete, a suitable air-void system is achieved in the hardened concrete.

Dispensing and Mixing: Add MB-AE 90 admixture to the concrete mixture using a dispenser designed for air-entraining admixtures, or add manually using a suitable measuring device that ensures accuracy within plus or minus 3% of the required amount.

For optimum, consistent performance, the air-entraining admixture should be dispensed on damp, fine aggregate. If the concrete mixture contains fine lightweight aggregate, field evaluations should be conducted to determine the best method to dispense the air-entraining admixture.

Precaution

In a 2005 publication from the Portland Cement Association (PCA R&D Serial No. 2789), it was reported that problematic air-void clustering that can potentially lead to above normal decreases in strength was found to coincide with late additions of water to air-entrained concretes. Late additions of water include the conventional practice of holding back water during batching for addition at the jobsite. Therefore, caution should be exercised with delayed additions of water to air-entrained concrete. Furthermore, an air content check should be performed after any post-batching addition to an air-entrained concrete mixture.

Product Notes

Corrosivity – Non-Chloride, Non-Corrosive: MB-AE 90 admixture will neither initiate nor promote corrosion of reinforcing and prestressing steel embedded in concrete, or of galvanized floor and roof systems. No calcium chloride or other chloride-based ingredients are used in the manufacture of this admixture.

Compatibility: MB-AE 90 admixture may be used in combination with any BASF admixture, unless stated otherwise on the data sheet for the other product. When used in conjunction with other admixtures, each admixture must be dispensed separately
into the concrete mixture.

Storage and Handling

Storage Temperature: MB-AE 90 admixture should be stored and dispensed at 31 °F (-0.5 °C) or higher. Although freezing does not harm this product, precautions should be taken to protect it from freezing. If MB-AE 90 admixture freezes, thaw at 35 °F (2 °C) or above and completely reconstitute by mild mechanical agitation. ***Do not use pressurized air for agitation.***

Shelf Life: MB-AE 90 admixture has a minimum shelf life of 18 months. Depending on storage conditions, the shelf life may be greater than stated. Please contact your Local sales representative regarding suitability for use and dosage recommendations if the shelf life of MB-AE 90 admixture has been exceeded.

Safety: Chemical goggles and gloves are recommended when transferring or handling this material.

Packaging

MB-AE 90 admixture is supplied in 55 gal (208 L) drums, 275 gal (1040 L) totes and by bulk delivery.

Related Documents

Material Safety Data Sheets: MB-AE 90 admixture.

Additional Information

For additional information on MB-AE 90 admixture, or its use in developing a concrete mixture with special peformance characteristics, contact your Local sales representative.

The Admixture Systems business of BASF's Construction Chemicals division is a leading provider of innovative admixtures for specialty concrete used in the ready-mixed, precast, manufactured concrete products, underground construction and paving markets throughout the North American region. The Company's respected Master Builders brand products are used to improve the placing, pumping, finishing, appearance and performance characteristics of concrete.

BASF Corporation
Admixture Systems

www.masterbuilders.com
United States 23700 Chagrin Boulevard, Cleveland, Ohio 44122-5544 • Tel. 800 628-9990 • Fax: 216 839-8821
Canada 1800 Clark Boulevard, Brampton, Ontario L6T 4M7 • Tel: 800 387-5862 • Fax: 905 792-0651

Master Builders

SIKATOP® 122 PLUS

Two-component, polymer-modified, cementitious, trowel-grade mortar plus FerroGard 901 penetrating corrosion inhibitor

Description

SikaTop 122 PLUS is a two-component, polymer-modified, portland-cement, fast-setting, trowel-grade mortar. It is a high performance repair mortar for horizontal and vertical surfaces and offers the additional benefit of FerroGard 901, a penetrating corrosion inhibitor.

Where to Use

- On grade, above, and below grade on concrete and mortar.
- On horizontal surfaces.
- As a structural repair material for parking structures, industrial plants, walkways, bridges, tunnels, dams, and ramps.
- To level concrete surfaces.
- As an overlay system for topping/resurfacing concrete.
- Overlay in cathodic protection systems.

Advantages

- High compressive and flexural strengths.
- High early strengths. Opens to traffic fast: foot in 4-6 hours, pneumatic tire in 8-12 hours.
- High abrasion resistance.
- Increased freeze/thaw durability and resistance to deicing salts.
- Compatible with coefficient of thermal expansion of concrete - Passes ASTM C-884 (modified).
- Increased density - improved carbon dioxide resistance (carbonation) without adversely affecting water vapor transmission (not a vapor barrier).
- Enhanced with FerroGard 901, a penetrating corrosion inhibitor - reduces corrosion even in the adjacent concrete.
- Not flammable, non-toxic.
- Conforms to ECA/USPHS standards for surface contact with potable water.
- USDA approved for food industry.
- ANSI/NSF Standard 61 potable water approved.

Yield

0.51 cu. ft./ unit mortar; 0.75 cu. ft./unit concrete; (SikaTop 122 + 42 lbs. 3/8 pea gravel)

Packaging

Component 'A' - 1-gal. plastic jug; 4/carton.
Component 'B' - 61.5-lb. multi-wall bag.

Typical Data

(Material and curing conditions @ 73°F (23°C) and 50% R.H.)

Shelf Life

One year in original, unopened packaging.

Storage Conditions

Store dry at 40°-95°F (4°-35°C). Condition material to 65°-75°F before using. Protect Component 'A' from freezing; if frozen, discard.

Color

Concrete gray when mixed.

Mixing Ratio

Plant-proportioned kit. Mix entire unit.

Application

Approximately 30 minutes.

Time

Application time is dependent on temperature and relative humidity.

Finishing Time

50-120 minutes (***Note:*** All times start after adding Component 'B' to Component 'A' and are highly affected by temperature, relative humidity, substrate temperature, wind, sun and other job site conditions.)

Density (wet mix)

136 lbs./cu. ft. (2.18 kg./l)

Flexural Strength (ASTM C-293)

28 days 2,000 psi (13.8 MPa)

Splitting Tensile strength (ASTM C-496)

28 days 750 psi (5.2 MPa)

Bond Strength* (ASTM C-882 modified)

28 days 2,200 psi (15.2 MPa)

Bond Strength Pull-Out Test Compressive Strength (ASTM C-109)

1 day 1,250 psi (8.6 MPa)
7 days 5,000 psi (34.5 MPa)
28 days 6,000 psi (41.4 MPa)

Permeability (AASHTO T-277)

28 days Approximately 500 Coulombs

Freeze/Thaw Resistance (ASTM C-666)

300 cycles 98%

Corrosion Testing for ferrogard 901 Cracked Beam Corrosion Tests:

Reduced corrosion rates 63% versus control specimens. ASTM G109 modified after 400 days.

* Mortar scrubbed into substrate.

How to Use

Substrate

Concrete, mortar, and masonry products.

Surface Preparation: Concrete/Mortar: Remove all deteriorated concrete, dirt, oil, grease, and all bond-inhibiting materials from surface. Be sure repair area is not less than 1/8 inch in depth. Preparation work should be done by high pressure water blast, scabbler, or other appropriate mechanical means to obtain an exposed aggregate surface with a minimum surface profile of ±1/16 inch (CSP-5). Saturate surface with clean water. Substrate should be saturated surface dry (SSD) with no standing water during application.

SIKATOP® 122 PLUS

Two-component, polymer-modified, cementitious, trowel-grade mortar plus FerroGard 901 penetrating corrosion inhibitor

Reinforcing Steel: Steel reinforcement should be thoroughly prepared by mechanical cleaning to remove all traces of rust. Where corrosion has occurred due to the presence of chlorides, the steel should be high-pressure washed with clean water after mechanical cleaning. For priming of reinforcing steel use Sika Armatec 110 EpoCem (consult Technical Data Sheet).

Priming

Concrete Substrate: Prime the prepared substrate with a brush or sprayed applied coat of Sika Armatec 110 Epo-Cem (consult Technical Data Sheet). Alternately, a scrub coat of SikaTop 122 Plus can be applied prior to placement of the mortar. The repair mortar has to be applied into the wet scrub coat before it dries.

Mixing

Pour approximately 7/8 of Component 'A' into the mixing container. Add Component 'B' (powder) while mixing continuously. Mix mechanically with a low-speed drill (400-600 rpm) and mixing paddle or mortar mixer. Add remaining Component 'A' (liquid) to mix if a more loose consistency is desired. Mix to a uniform consistency, maximum 3 minutes. Thorough mixing and proper proportioning of the two components is necessary. For SikaTop 122 PLUS concrete: Pour all of Component 'A' into mixing container. Add all of Component 'B' while mixing, then introduce 3/8 inch coarse aggregate at desired quantity. Mix to uniform consistency, maximum 3 minutes. Addition rate is 42 lbs. per bag (approx. 3.0 to 3.5 gal. by loose volume). The aggregate must be non-reactive (reference ASTMC1260, C227 and C289), clean, wellgraded, saturated surface dry, have low absorption and high density, and comply with ASTM C 33 size number 8 per Table 2. Note: Variances in the quality of the aggregate will affect the physical properties of SikaTop 122 PLUS. The yield is increased to 0.75 cu. ft./unit with the addition of the aggregate (42 lbs.). Do not use limestone aggregate.

Application & Finish

SikaTop 122 PLUS must be scrubbed into the substrate, filling all pores and voids. Force material against edge of repair, working toward center. After filling repair, consolidate, then screed. Allow mortar or concrete to set to desired stiffness, then finish with wood or sponge float for a smooth surface, or broom or burlap-drag for a rough finish.

Curing

As per ACI recommendations for portland cement concrete, curing is required. Moist cure with wet burlap and polyethylene, a fine mist of water or a water based* compatible curing compound. Curing compounds adversely affect the adhesion of following layers of mortar, leveling mortar or protective coatings. Moist curing should commence immediately after finishing. Protect newly applied material from direct sunlight, wind, rain and frost. *Pretesting of curing compound is recommended.

Limitations

Application thickness:	Min.	Max. in one lift
Neat	1/8 inch (3 mm)	1 inch (25 mm)
Extended	1 inch (25 mm)	4 inches (100 mm)

- Minimum ambient and surface temperatures 45°F (7°C) and rising at time of application.
- Addition of coarse aggregates may result in variations of the physical properties of the mortar.
- Do not use solvent-based curing compound.
- Size, shape and depth of repair must be carefully considered and consistent with practices recommended by ACI. For additional information, contact Technical Service.
- For additional information on substrate preparation, refer to ICRI Guideline No.03732 Coatings, and Polymer Overlays.
- If aggressive means of substrate preparation is employed, substrate strength should be tested in accordance with ACI 503 Appendix A prior to the repair application.
- As with all cement based materials, avoid contact with aluminum to prevent adverse chemical reaction and possible product failure. Insulate potential areas of contact by coating aluminum bars, rails, posts etc. with an appropriate epoxy such as Sikadur Hi-Mod 32.

Caution

Component 'A' - Irritant - May cause skin/eye/respiratory irritation. Avoid breathing vapors. Use with adequate ventilation. Avoid skin and eye contact. Safety goggles and rubber gloves are recommended.

Component 'B' - Irritant; suspect carcinogen - Contains portland cement and sand (crystalline silica). Skin and eye irritant. Avoid contact. Dust may cause respiratory tract irritation. Avoid breathing dust. Use only with adequate ventilation. May cause delayed lung injury (silicosis). IARC lists crystalline silica as having sufficient evidence of carcinogenicity in laboratory animals and limited evidence of carcinogenicity in humans. NTP also lists crystalline silica as a suspect carcinogen. Use of safety goggles and chemical resistant gloves is recommended. If PELs are exceeded, an appropriate, NIOSH approved respirator is required. Remove contaminated clothing.

First Aid

In case of skin contact, wash thoroughly with soap and water. For eye contact, flush immediately with plenty of water for at least 15 minutes, and contact a physician. For respiratory problems, remove person to fresh air.

Clean Up

In case of spillage, scoop or vacuum into appropriate container, and dispose of in accordance with current, applicable local, state and federal regulations. Keep container tightly closed and in an upright position to prevent spillage and leakage. Mixed components: Uncured material can be removed with water. Cured material can only be removed mechanically.

Chemical analysis, MRT Labadie, Silo C, sample date 3/4/11, sample ID # 11MRSM037								
	Class C	Method		Analysis:				
Silicon Dioxide	33.46	ICP		Sam Marshall				
Aluminum Oxide	19.53	ICP						
Ferric Oxide	6.28	ICP						
Calcium Oxide	26.28	ICP						
Magnesium Oxide	5.54	ICP						
Sulfur Trioxide	2.40	LECO						
Loss on Ignition	0.34	C311						
Moisture	0.15	C311						
Potassium Oxide	0.45	ICP						
Phosphorus Pentoxide	1.30	ICP						
Titanium Dioxide	1.48	ICP						
Sodium Oxide	1.728	ICP						
Manganic Oxide	0.041	ICP						
Zinc Oxide	0.019	ICP						
Chromium Oxide	0.011	ICP						
Barium Oxide	0.841	ICP						
Strontium Oxide	0.397	ICP						
Sum Oxides (Si+Al+Fe)	59.270	C618						
Available alkalies								
TOTALS	98.86		0.00	0.00				

APPENDIX B

SAMPLE SURVEY QUESTIONNAIRE

Dear Valued Partner,

The Missouri University of Science and Technology (Missouri S&T), in association with the Missouri Department of Transportation (MoDOT), is conducting research in the use of Self-Consolidating Concrete (SCC) for bridge structural elements. The research is focused on testing mixes and aggregates likely to be used in Missouri, because previous research has shown SCC to be sensitive to the materials used.

Dr. John Myers and Graduate Research Assistant Eric Sells with Missouri S&T has developed a SCC survey, and we would appreciate valuable input from industry leading companies such as your own. We understand your business is built upon the quality mix designs your company has developed; therefore, all survey responses will be kept strictly confidential and only seen by the research team and limited technical contacts within MoDOT. With these safeguards in place, we respectfully request that you complete the SCC survey.

We appreciate your valuable input. If you have any questions regarding the integrity of this research please contact Jen Harper at (573)526-3636 or Jennifer.harper@modot.gov. If you experience any problems with the survey itself, please contact Eric Sells at (417)298-4932 or ebsn87@mail.mst.edu

1. What is your Contact information?
(a) What is your name?_____
(b) What is your position?_____
(c) How long have you had this position?_____
(d) What is your Phone number?_____
(e) What is your email address?_____

2. Does your company use Self-Consolidating Concrete (SCC)? (highlight one) Yes No
(a) If Not, Why:_____
_____
_____
(b) If So, When did you first begin producing SCC mixes?_____

3. About what percentage of your current projects use SCC?_____%

4. For what Applications have you used SCC mixes? (highlight)

Architectural Panels	Shear Walls	Structural Beams/Girders	Reinforced Slabs
Pipes/Culverts	Retaining Walls	Bridge Deck Panels	Columns

Other:_____

5. What has been the range of strengths achieved?
(a) At time of release:_____
(b) Design Strength (28 day):_____

6. What types of coarse aggregates have been used? (highlight)
River Gravel Dolomitic Limestone Calcitic Limestone Quartz

Blast Furnace Slag Chert Expanded Shale or Slate

Other:_____

7. What maximum aggregate size was used?_____

8. What fraction (by weight) of coarse aggregate was used?_____%

9. What has been typical mix designs used? (Please list specific mixes used, ranges of typically used mixes, or both)
Cement Type (I-V) _____.
Cement Dosage (lb/cy) _____.
Coarse Agg. Type _____.
Coarse Dosage (lb/cy) _____.
Fine Agg. Type _____.
Fine Agg. Dosage (lb/cy) _____.
Mineral Admixtures Type _____.
Mineral Admix. Dosage (lb/cy) _____.
Chemical Admix. Type (air) _____.
Dosage (oz/cwt) _____.
Chem. Admix. Type (WR/HRWRA)_____.
Dosage (oz/cwt) _____.
Chem. Admix. Type (VMA) _____.
Dosage (oz/cwt) _____.

10. Who is/are your aggregate/materials supplier(s)?_____
_____
(This will be used to determine index properties of the raw materials)

11. Who is/are your chemical admixture supplier(s)?_____
_____
(This will be used to determine admixture alternatives and market base for these types of chemicals)

12. May we contact you for additional information if a trend is realized through the survey responses, research results, or for clarifying information? (highlight one) Yes No

13. Preferred Contact Method? (highlight) Phone E-mail

APPENDIX C

SAMPLE BATCH WEIGHT AND FRESH PROPERTY RESULT SPREADSHEETS

w/Cm	0.37
Batch (ft^3)	3.35
F.A. % (of Agg. Portion)	42%
Air Dosage (oz/cwt)	0.7
HRWRA Dosage (oz/cwt)	3.1

Batch ID	C6-58L (8/3/2011)	
Addmixtures (mL)		
Air	MB-AE-90	19
HRWRA	Glenium 7700	85

Material	Weight ,W (lb)	Specific Gravity, G (lb/ft^3)	Unit Weight Water, γ_w (lb/ft^3)	Abs. Volume (ft^3)	Agg. Water Correction (lb)	Agg. Batch Correction	Final Batch Weights
Cement	750.00	3.15	62.4	3.82	---	---	93.1
Water	277.50	1.00	62.4	4.45	---	---	39.8
Air	0.06	0.00		1.62	---	---	0.0
C.A.	1610.7	2.60	62.4	9.93	-44.4	1614.6	200.3
F.A.	1166.3	2.60	62.4	7.19	1.5	1176.1	145.9

$TMC_{C.A.}$	0.243	$Absorption_{C.A.}$	3	$SM_{C.A.}$	-2.757
$TMC_{F.A.}$	0.831	$Absorption_{F.A.}$	0.7	$SM_{F.A.}$	0.131

Record:

Batch Time	Before HRWRA	After HRWRA	Measured Air Content	Temp.	Unit Weight

Note Any Abnormalities:

Yellow Cells – Input cells which may vary from batch proportion to batch proportion
Blue Cells – Output cells which vary depending upon input cells

Figure C.1 – Sample Batch Weight Spreadsheet

Static Segregation ASTM C1610 Batch ID S1-36L (8/1/2011)

		(Less than A + 2 min)	(B + 15min +/- 1 min)	To nearest .1 lb		(Less than C + 20 min)	2(E-D)/(E+D) in %
	A	B	C	D	E	F	G
Batch ID	Time Begin	Time finished	Time after Standing	OD +#4 sieve of top	OD +#4 sieve of bottom	Time finished	Static Seg.
S1-36L							
S1-36L							

Slump Flow and T_{50} ASTM C1611

	Largest dia.	Perp. Dia. (nearest .25in)	(A+B)/2 (nearest .5in)	Time to 20 in (nearest .2sec)	See Appendix of ASTM for guidance
	A	B	C	D	E
Batch ID	d_1	d_2	Slump Flow	T_{50}	VSI
S1-36L					
S1-36L					

J-Ring ASTM C1621

	Largest dia.	Perp. Dia. (.25in)	(A+B)/2 (.5in)	See Tbl 1 of ASTM for guidance
	A	B	C	D
Batch ID	j_1	j_2	J-Ring Flow	Blocking Assessment
S1-36L				
S1-36L				

L-Box Non-standard

	Height Gate	Height End	(B/A)
	A	B	D
Batch ID	h1	h2	Filling Ability
S1-36L			
S1-36L			

Note: some brief instruction to ensure consistency with associated ASTM test standards.

Figure C.2 – Sample Fresh Property Spreadsheet (Unpopulated)

APPENDIX D

SHEAR BEAM DESIGN AID

X-Section Details		
h	16	in
yt	8	in
yb	8	in
b	8	in
A	128	in^2
I	2731	in^4
L	17	ft
f'ci	4000	psi

Tendon Details								
		g (in)						
Line	# Tendons	North End	Mid	South End	Area (in^2)			
1	2	2	2	2	0.153	fpu	270000	
2	2	4	4	4	0.153	fpi	189000	
3	0	6	6	6	0.153	fse	170100	-----> 0.63 fpu
Tot	4							
	e	5	5	5				

Fiber Stresses							
	End			Mid			
	Calc.	Limit	Accept?	Calc.	Limit	Accept?	
f^t	711.6293	379.4733	N.G.	542.2934	189.7367	N.G.	-----> Can Reinforce
f_b	-2338.21	-2800	OK	-2168.87	-2400	OK	

6ksi	
Flexural Capacity	
fps	251.8
a	3.78
Mn	1712.5
Shear Capacity	
Pu	53.5
Vu	35.7
Vc	24.6
	69%

10ksi	
Flexural Capacity	
fps	257.4
a	2.32
Mn	1865.6
Shear Capacity	
Pu	58.3
Vu	38.9
Vc	26.0
	67%

Yellow – Indicates percentage of predicted concrete shear capacity relative to ultimate shear produced at the predicted flexural capacity

Figure D.1 – Shear Beam Design Aid Spreadsheet